

AMERICAN UNIVERSITY OF BEIRUT

ALGINATE/POLYCAPROLACTONE NANOPARTICLES FOR
DRUG DELIVERY AND WOUND HEALING APPLICATIONS

by
BATOUL IBRAHIM MAATOUK

A thesis
submitted in partial fulfillment of the requirements
for the degree of Master of Science
to the Biomedical Engineering Program
of the Maroun Semaan Faculty Engineering and Architecture and Faculty of Medicine
at the American University of Beirut

Beirut, Lebanon
September 2019

AMERICAN UNIVERSITY OF BEIRUT

ALGINATE/POLYCAPROLACTONE NANOPARTICLES FOR
DRUG DELIVERY AND WOUND HEALING APPLICATIONS

by
BATOUL IBRAHIM MAATOUK

Approved by:

[Dr. Rami Mhanna, Assistant Professor]
[Biomedical Engineering Program]
Maroun Semaan Faculty of Engineering and Architecture



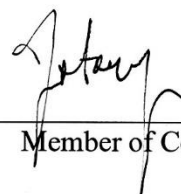
Advisor

[Dr. Ayad Jaffa, Assistant Dean, Chairperson and Professor]
[Department of Biochemistry and Molecular Genetics]
Faculty of Medicine



Co-advisor

[Dr. Jason Ammatoury, Assistant Professor]
[Biomedical Engineering Program]
Maroun Semaan Faculty of Engineering and Architecture



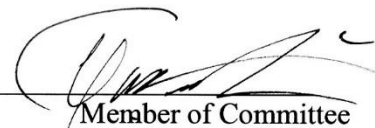
Member of Committee

[Dr. Ali Tehrani, Associate Professor]
[Bahaa and Walid Bassatne Department of Chemical Engineering and Advanced Energy]
Maroun Semaan Faculty of Engineering and Architecture

Ali Tehrani

Member of Committee

[Dr. Yousef Mubarak, Visiting Associate Professor]
[Bahaa and Walid Bassatne Department of Chemical Engineering and Advanced Energy]
Maroun Semaan Faculty of Engineering and Architecture



Member of Committee

Date of thesis/dissertation defense: [September 12, 2019]

AMERICAN UNIVERSITY OF BEIRUT

THESIS, DISSERTATION, PROJECT RELEASE FORM

Student Name: Maatauk Bataul Ibrahim
Last First Middle

Master's Thesis Master's Project Doctoral Dissertation

I authorize the American University of Beirut to: (a) reproduce hard or electronic copies of my thesis, dissertation, or project; (b) include such copies in the archives and digital repositories of the University; and (c) make freely available such copies to third parties for research or educational purposes.

I authorize the American University of Beirut, to: (a) reproduce hard or electronic copies of it; (b) include such copies in the archives and digital repositories of the University; and (c) make freely available such copies to third parties for research or educational purposes after: **One --- year from the date of submission of my thesis, dissertation, or project.**
Two --- years from the date of submission of my thesis, dissertation, or project.
Three --- years from the date of submission of my thesis, dissertation, or project.

بتول 16/9/2019

Signature

Date

This form is signed when submitting the thesis, dissertation, or project to the University Libraries

ACKNOWLEDGEMENTS

First and foremost, I would like to thank Allah for his blessings and making countless things possible. I profound my gratitude to my advisor Dr. Rami Mhanna for granting me the opportunity to explore this field and for his guidance and support on many aspects inside and outside the scope of the project.

I would like to thank my co-advisor Dr. Ayad Jaffa for his guiding and introducing me to biological concepts that made such an interdisciplinary research feasible and most importantly for giving the chance to work in his lab.

A word of appreciation goes out to all my colleagues at Dr.Jaffa's lab especially Wared and Mia for their help in the experiments and Maryam and Duaa for making it a fun experience, and to Dr. Rami's team members especially Zeina and Waddah for answering many of my endless questions.

I would like to thank the Dr. Ali Tehrani, Dr. Yousef Mubarak , and Dr.Jason Ammatoury for serving as committee members for this thesis, Dr. Houssam AlRassy for letting us use the sonicator located in his lab, Dr. Ali Tehrani again for the PLGA, Dr. Miran Jaffa for her help in statistics, and Dr. Aida Abdulkareem for the Rho-a inhibitors.

Finally, I'm very grateful to my family and friends for their continuous and infinite support during the whole journey.

AN ABSTRACT OF THE THESIS OF

Batoul Ibrahim Maatouk

for Master of Science
Major: Biomedical Engineering

Title: Alginate/Polycaprolactone Nanoparticles for Drug Delivery and Wound Healing Applications

Diabetic foot ulcers (DFUs) that are not effectively treated might ultimately lead to partial or complete lower limb amputations; such losses take place every 30 seconds worldwide. DFU's and related amputations together pose an annual economic burden of up to \$15 billion on the global healthcare system. The lack of connective tissue growth factor (CTGF) and insulin-like growth factor (IGF-I) in DFU results in limited matrix deposition and consequently limited tissue repair. In the current thesis, we sought to address the lack of growth factors in DFUs by engineering double emulsion polymeric nanoparticles (NPs) with high affinity and sustained release of CTGF and IGF and study the effect of the synthesized growth factor (GF)-loaded NPs on DFU healing. The double emulsion NPs were made of an alginate (Alg) or the heparin-mimetic alginate sulfate (AlgSulf) core and a polycaprolactone (PCL) shell. The optimal NPs formulation was determined by investigating the effects of sonication time and amplitude, organic solvent evaporation rate and processed volume on the morphology, size, and polydispersity of the NPs using scanning electron microscopy (SEM) and dynamic light scattering (DLS). The protein encapsulation efficiency (EE) and release profile were assessed using bovine serum albumin (BSA) as a model drug via the Lowry protein assay. Toxicity of the synthesized NPs and their effect on signaling pathways were evaluated using trypan blue, MTT and immunoblotting assays. Finally, the effect of NPs on wound healing and the role of RhoA signaling were evaluated using a scratch assay.

The results showed that an increase in the sonication time and amplitude which correspond to an increase in the total delivered energy, significantly reduced the NPs diameter to a minimum of 235.5 ± 25 nm. Similarly, increasing the organic solvent evaporation rate by which particles solidify or decreasing the total processed volume caused a significant decrease in the NPs diameter ($P=0.002$). The highest BSA (EE) based on Alg or AlgSulf in the inner core combined with PCL or poly(lactic-co-glycolic) (PLGA) in the shell was attained with PCL/AlgSulf (94.6 %, $P=0.028$). The unloaded PCL/Alg NPs showed no cytotoxic effect for concentrations below $100 \mu\text{g/ml}$ after 72hr ($P>0.213$) as shown by trypan blue and including $100 \mu\text{g/ml}$ by MTT ($P=0.436$), and immunoblotting ($P>0.646$)

assays. Moreover, the treatment that caused the most rapid wound closure was the combination of CTGF (250 ng/ml) and highly sulfated AlgSulf (10 μ g/ml). Finally, western blot analysis of the wound healing assay after 72 hr showed that cells treated with alginates bound or unbound to GFs, expressed fibronectin unlike all other conditions which expressed it only for 24 hr implying that alginates prevented fibronectin degradation with time. Therefore, NPs based on heparin-mimetic sulfated alginates and loaded with CTGF represent a novel approach which can significantly enhance diabetic wound healing. The developed nanoparticles may also be tailored for the delivery of various drugs and growth factors especially given the known high affinity of AlgSulf to all heparin-binding GFs.

CONTENTS

ACKNOWLEDGEMENTS	v
AN ABSTRACT OF THE THESIS OF	vi
CONTENTS	viii
ILLUSTRATIONS	xi
TABLES	xiv
ABBREVIATIONS	xv
Chapter	
1. INTRODUCTION	1
1.1 Drug delivery	1
1.1.1 Controlled Release	2
1.1.2 Nanotechnology	4
1.2 Drug Carriers	5
1.2.1 Liposomes	5
1.2.2 Polymeric Micelles	6
1.2.3 Polyelectrolyte Multilayers	6
1.2.4 Nanoparticles	7
1.3 Polymeric NPs	7
1.3.1 Biodegradable NPs	8
1.3.2 Poly (Caprolactone)	9
1.3.4 Poly (Vinyl Alcohol)	11
1.3.5 Alginate	11
1.4 Emulsions	13
1.4.1 Double Emulsions	15
1.4.2 Energy Source	16
1.4.3 Emulsification parameters	17
1.5 Sulfated glycosaminoglycans mimetics	18
1.5.1 Heparin/Heparan Sulfate	19
1.5.2 Alginate Sulfate	20

1.6 Wound Healing	21
1.6.1 GAGs and GFs in Wound Healing	22
1.6.2 Chronic and Diabetic Wounds	22
1.7 Research Objective and Specific Aims	23
1.7.1 Aim 1: Synthesis and characterization of PCL/Alg double emulsion NPs.....	24
1.7.2 Aim2 Measuring the EE and studying the drug release profile from different NPs formulations.	25
1.8 References	26
2. MATERIALS AND METHODS	33
2.1 Materials	33
2.2 Methods	34
2.2.1 Synthesis of Alginate and PCL NPs	34
2.2.2 Physical Characterization of the NPs.....	36
2.2.3 Modeling the Effect of Energy, Time, Amplitude, and Volume on the Size of the NPs.....	37
2.2.4 Encapsulation and Release.....	38
2.2.5 Stability of NPs.....	40
2.2.6 Cell Culture.....	40
2.2.7 Nanoparticles cytotoxicity	41
2.2.8 Statistical analysis.....	44
2.3 References	45
3. SYNTHESIS AND CHARACTERIZATION OF NPs.....	46
3.1 Optimization of nanoparticles	46
3.1.1 Effect of sonication time and sonication amplitude.....	46
3.1.2 Effect of organic solvent evaporation rate	50
3.1.3 Effect of ratio of the outer aqueous phase	52
3.1.4 Effect of the processed volume.....	54
3.1.5 Effect of using sulfated alginates as the inner core	55
3.2 Modeling	57
3.2.1 Effect of energy	57
3.2.2 Effect of sonication time, amplitude, and processing volume	61
3.3 Effect of loading different amounts of BSA on size	63

3.4 Encapsulation Efficiency	65
3.5 <i>In Vitro</i> Release Studies	68
3.6 Thermal and Colloidal Stability of the Nanoparticles.....	71
3.7 Cytotoxicity studies.....	73
3.7.1 Trypan-Blue exclusion assay	73
3.7.2 MTT assay	74
3.7.3 Immunoblotting	75
3.8 References	77
4. IN VITRO ASSESSMENT OF ALGINATES AND GROWTH FACTORS ON WOUND HEALING.....	79
4.1 Introduction	79
4.1.1 Growth factors and cytokines	79
4.1.2 Wound dressing	81
4.1.3 Objective.....	82
4.2 Materials and Methods	
4.2.1 Measurement of cell migration in vitro	83
4.2.2 Bioactivity assay for CTGF	84
4.2.3 Role of Rho-GTPase signaling in the effects of CTGF, IGF, and alginates on HaCat cells	85
4.2.4 Role of Alginates in protecting FN from degradation	85
4.4 Results and Discussion.....	86
4.4.1 Effect of Alginates and Growth Factors on HaCat Cells Migration <i>in Vitro</i>	86
4.4.2 Effect of CTGF and AlgSulf on Cellular Activity and Proliferation.....	90
4.4.3 RhoA is involved in the cellular migration during wound healing.....	92
4.4.4 Alginates protects matrix proteins from degradation	94
4.5 References	96
5. CONCLUSION.....	99
6. APPENDIX.....	102

ILLUSTRATIONS

Figure 1 The therapeutic index of drugs [2].	2
Figure 2 Drug release profile [7].	3
Figure 3 Schematic diagram of the ionic gelation of Alg that generates the egg-box model [44].	13
Figure 4 Schematic representation of the steps involved in the EEM [27].	15
Figure 5 Schematic of the double emulsion.	16
Figure 6 Graphical representation of the cavitation process due to alternation between high and low pressure [53].	17
Figure 7 Chemical structure of heparan sulfate and heparin [58].	20
Figure 8 Methods for chemical sulfation of Algs [62].	21
Figure 9 Effect of sonication exposure time in the second emulsification step.	47
Figure 10 Effect of sonication amplitude in the second emulsification step.	49
Figure 11 Effect of evaporation rate.	51
Figure 12 Effect of the volume of the outer aqueous phase on the particles.	53
Figure 13 Effect of total processing volume on the average hydrodynamic size.	55
Figure 14 AlgSulf2.0 instead of pure Alg in the inner aqueous phase.	56
Figure 16 Effect of sonication energy released when processing time and amplitude were varied on the average hydrodynamic size based on actual data.	59

Figure 17 Curve-fitting based on the relation between the average hydrodynamic size and sonication energy.	60
Figure 18 Modeling of the average hydrodynamic size based on second step sonication time.	61
Figure 19 Modeling of the average hydrodynamic size based on second step amplitude.	62
Figure 20 Modeling of the average hydrodynamic size based on total processing volume while keep phase ration constant.	63
Figure 21 Effect of BSA amount in the inner aqueous phase on the average hydrodynamic size of the particles.	64
Figure 22 Comparing the encapsulation efficiency and the burst release of the different formulations.	67
Figure 23 Cumulative release profile of BSA from the three different formulations, 2% Alg PCL, 2% AlgSulf2.0 PCL, and 2% Alg PLGA.	70
Figure 24 Cumulative release profile of BSA from the 2% AlgSulf2.0 with or without shaking during incubation.	71
Figure 25 NP's thermal and colloidal stability studies.	72
Figure 26 % Viability of HaCaT cells using Trypan Blue as a function of NP's concentration.	74
Figure 27 % Activity of HaCaT cells using MTT assay as a function of NP's concentration.	75
Figure 28 Regulation of ERK and AKT signaling by NP's in HaCat cells.	76
Figure 29 The in vitro wound healing upon the application of CTGF and IGF at a concentration of 250ng/ml.	89

Figure 30 The effect of different treatments on the activity of the cells.90

Figure 31 Comparison between the effect of AlgSulf and heparin with and without CTGF at different concentrations.) 91

Figure 32 RhoA signal transduction involved in cell migration. (-) indicates the absence of the GTPase inhibitor (n=3).93

Figure 33 Immunoblotting results after the scratch assay (24 and 72 hr).....95

TABLES

Table 1 Conversion in concentration from $\mu\text{g/ml}$ to $\mu\text{g/cm}^2$	42
Table 2 Energy allocated for disrupting the spheres by eliminating heat losses.	58
Table 3 The average size, PDI and zeta potential of the three different formulations	66
Table 4 Summary of the longitudinal statistical analysis with the P-values of each treatment against the control. (ns: not significant).....	86

ABBREVIATIONS

GF: growth factor

DDS: drug delivery system

EPR: enhanced permeability and retention

NPs: nanoparticles

PLGA: poly (lactide-co-glycolide)

PVA: poly (vinyl alcohol)

PCL: polycaprolactone

EEM: emulsification solvent evaporation

O/W: oil in water

W/O: water in oil

ECM: extracellular matrix

GAGs: glycosaminoglycans

Alg:Alginate

AlgSulf: sulfated alginates

AlgSulf_{2.0}: sulfated alginates with a degree of sulfation: 2

HBGF: heparin-binding growth factor

FN: fibronectin

CTGF: connective tissue growth factor

IGF-I: insulin-like growth factor

BSA: bovine serum albumin

DMEM: Dulbecco's Modified Eagle Medium

FBS: fetal bovine serum

DDW: double distilled water

DCM: dichloromethane

MTT: 3-(4,5-dimethylthiazol-2-yl)-2,5-diphenyltetrazolium bromide

HaCat cells: human immortal keratinocyte cell line

Chapter I

INTRODUCTION

1.1 Drug delivery

Discovering a drug and introducing it into the market is a laborious and expensive process where approximately one out of a pool of thousand compounds gets considered. Based on data from pharmaceutical companies, it was shown that these complications are attributed mostly to poor pharmacokinetics which is affected by drug adsorption, distribution, metabolism, and excretion. Other reasons that can cause failure include the lack of clinical efficacy, toxicity, and adverse effects of the drug. Regardless of the drug administration route, delivering drug molecules to the targeted tissues while maintaining maximum activity and minimum toxicity, i.e. keeping the concentration within the therapeutic window (Fig.1), remains a challenging task. For instance, one of the traditional methods of administering drugs is orally using pills or capsules; such delivery systems have low bioavailability. That is, they are eliminated by the body either intact or after being bio-transformed by enzymatic or acid-catalysis before reaching the systemic circulation or due to insufficient intestinal absorption. Another conventional route is through injection into blood stream directly to increase bioavailability. However, the drug gets cleared as well especially if it has a short half-life such as proteins and growth factors (GFs), and it might pose toxic effects on healthy tissues. Therefore, the drugs are usually administered at a relatively higher doses compared to their therapeutic indices. Due to these limitations, the

idea of controlled delivery emerged to enhance the pharmacokinetics and increase the clinical efficacy of the drugs [1-6].

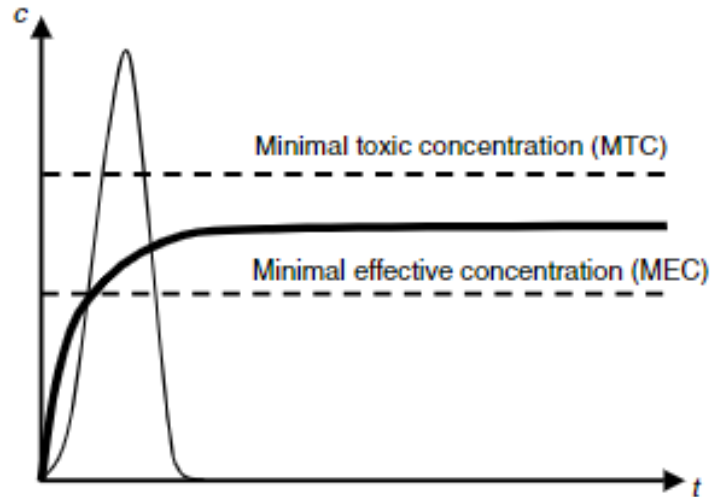


Figure 1 The therapeutic index of drugs [2].

1.1.1 Controlled Release

When the drug is administered freely, its concentration in the blood increases initially until it reaches a peak and then drops down. To overcome this, controlled delivery is utilized by either adjusting the release rate of the drug over time or transporting the drug to the target tissue. The release rate is decreased to ensure sustained release over time or increased in the case of non-soluble drugs; thus, the concentration of the drugs will be maintained within the therapeutic range for a longer time. This can be implemented by conjugating the drug to natural or synthetic carriers to stabilize it [1,7].

Most drug delivery systems (DDS) including reservoir and matrix systems follow the release profile (Fig.2). It begins by a burst release based on diffusion followed by a zero-order controlled release governed by diffusion, erosion, and solubility. The burst effect

is desired in certain systems like targeted DDS; on the other hand, drugs that might cause toxicity at high concentrations or have short half-lives must be encapsulated in carriers that have lower porosity, i.e. better surface crosslinking, to mitigate the initial released amount [7-8].

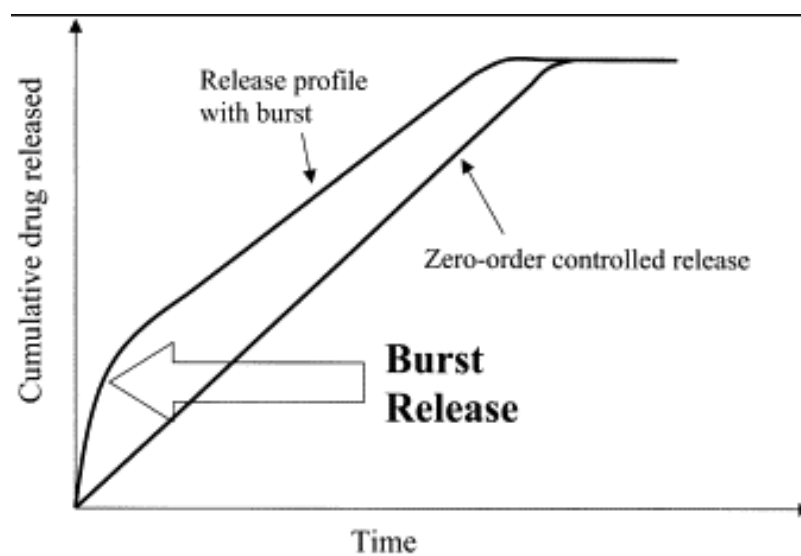


Figure 2 Drug release profile [7].

The other mode of controlled release is the targeted delivery where the drug is released in the desired tissue either at once (triggered- release) or in a sustained fashion. For instance, targeting could be passive by relying on the physical structure of the target tissue and the properties of the carrier. The size of the carriers can be tuned to target different organs based on their membrane's type, pore size, and the dimension of fenestrations. For instance, the enhanced permeability and retention (EPR) effect where blood vessels become leaky close to the cancerous tissue allows carriers to exit the blood stream into the tumor. Then the drug can be released by employing internal or external stimuli where the

responses can be precipitation, degradation, swelling, change in shape, etc... Internal triggers include the biological environment such as pH levels, redox potential, or temperature in case of infection. For example, the local pH in cancerous tissues is 7.2-6.5, in chronic wounds is approximately 8.0, and in lysosomes is 4.5-5.0; hence, pH responsive carriers can be used. As for the external stimuli, ultrasound irradiation can be used to manipulate the properties of the carrier by increasing its permeability by which the drug can diffuse. On the other hand, active targeting requires transporting the carrier using a biological moiety such as specific receptors on target cells or by the aid of an external magnetic field that can direct iron-containing carrier within the body [8-10]. Another advantage of using drug carriers is to circumvent the biological barriers in the body such the skin or the blood brain barrier by exploiting lipid carriers or adsorbing chemical permeability enhancers [11].

1.1.2 Nanotechnology

“Nano” is a Greek term that mean “dwarf”, and “Nanotechnology” is an umbrella under which many of the leading investigated materials are found. Intensive efforts are being invested to translate the technology into real-life applications in numerous fields including engineering, physics, chemistry, and medicine. One attractive field is nanotechnology in biomedical applications. It arises from the fact that most biological functions take place at a nanoscale. In addition, it can be employed in a wide range of applications such as therapy, diagnosis, and imaging. In therapeutics, for instance, microspheres have been used to treat millions of patients annually; however, they lack the

ability to enter the blood vessels after interstitial injections or to be taken-up by the cells due to their relatively large size. Therefore, nano -drug carriers that have a size ranging from 10 to 1000 nm can be utilized to overcome these limitations. Besides, this grants them the property of large surface to volume ratio for improved release. Furthermore, nanoparticles (NPs) can substitute polymerase chain reaction (PCR) that is used to identify a target in a sample by coating the particles with ligands and then using nuclear magnetic resonance. They are also being developed for imaging applications by adding fluorescent agents [1, 8, 11-13].

1.2 Drug Carriers

There exists a plethora of drug carriers which vary in material, structure, type of the entrapped drug, and the method of formation depending on the intended application. Utilizing these particles will aid in overcoming many limitations of conventional drug delivery. Their advantages include, but not limited to, controlled release, targeting, and rapid intracellular delivery [14-16]. These DDSs include liposomes, polymeric micelles, polyelectrolyte layers, and NPs.

1.2.1 Liposomes

Liposomes are one of the most studied DDSs; they are spherical phospholipid molecules consisting of hydrophilic heads and hydrophobic tails mimicking the lipid bilayer of the cell membrane. They already exist in the market as a cancer treatment such as Doxil that encapsulates Doxorubicin, a chemotherapeutic agent. Such systems can be

modified to achieve controlled delivery either by active or passive targeting where the release can then be stimulated. Their properties including size, charge, and rigidity can be manipulated by the selection of the lipid composition and the formation conditions. In addition, the size can range between 100nm to several micrometers and the circulation time can be enhanced by coating its surface to circumvent the immune system. Due to its unique structure, it can contain both hydrophilic and hydrophobic drugs. However, they have some drawbacks that include low solubility, short half-life, and leakage of drug [8, 13, 17-18].

1.2.2 Polymeric Micelles

Like liposomes, polymeric micelles also contain hydrophilic and hydrophobic parts with an inner core and an outer shell. Accordingly, they form instantaneously when placed in an aqueous medium. Furthermore, they can conjugate different types of drugs with a higher ability to incorporate large amounts of hydrophobic drugs due to their relatively bigger core. Despite these advantages, release from polymeric micelles is based on the critical micelle concentration, concentration at which aggregates are formed, where drugs can escape the system once diluted in blood stream [8,19].

1.2.3 Polyelectrolyte Multilayers

The layer by layer (LBL) system was introduced initially by Decher in 1990's. This technique is based on building a highly stable film of alternating opposite charges where selecting the charge of the terminal layer depends on the application. Different shapes and sizes can be created by binding consecutive layers electrostatically. Furthermore, both

loading and release of the drug can be controlled by optimizing the number of layers. In addition, in each individual layer, fusogenic or stimuli responsive materials can be embedded to control delivery and release. Therefore, the carrier can be rendered multifunctional by blending different substances and encapsulating more than one drug to be released in a synergistic manner [20-23]. However, the number of generated layers poses a tradeoff between cytotoxicity and stability and the amount of the integrated drug.

1.2.4 Nanoparticles

Nanotechnology is divided into two main domains, nanodevices and nanomaterials. NPs belong to the nanomaterials class and are already exploited in myriad applications such as solar cells, sensors, optics, food, cosmetics, and, remarkably, drug delivery. Besides, they can be categorized into polymeric and non-polymeric NPs. That is, they can be produced from polymers, metals, or silica. The selection of the materials to be used in the generation of the NPs is based on a chain of factors. It depends primarily on the application that dictates the necessary factors such as biodegradability, drug release profile, solubility, size, and permeability [24-26].

1.3 Polymeric NPs

The versatility of polymeric NPs owes back to the fact that they can be developed from various types of polymers with different physical and chemical properties. For instance, they are classified into natural or synthetic, biodegradable or non-biodegradable, hydrophilic or hydrophobic, crystalline or amorphous, etc.... Furthermore, NPs can be

formed through diverse approaches. They can be prepared based on the physiochemical properties of the polymer or using chemical reactions. The first approach is attempted by using hydrophilic or water-insoluble hydrophilic polymers, while the second requires polymerization or polycondensation. The third method, which is favored over the two other methods due to its simplicity and ease of tuning, is the formation of nanoemulsions. Their formation can be implemented via three processes. They can be produced by single emulsion solvent evaporation, double emulsion solvent evaporation, or by emulsion solvent displacement. Emulsions are also preferred because they can serve as the building block for many designed advanced materials and employs readily prepared polymers with specific molecular weights. Therefore, it does not require polymerization reactions and, thus, it lacks the presence of any impurities including monomers, unreacted agents, or catalysts [8,25,27-28].

1.3.1 Biodegradable NPs

Polymers in general, despite their chemical structure, undergo degradation in adequate conditions. However, polymers exploited in temporary biomedical systems, such as in drug delivery, orthopedic fixation, tissue engineering, and wound dressings, must be biodegradable. In other words, they are required to have hydrolytically or enzymatically labile bonds that will break and show a triggered functionality placed in a physiological environment. Such reactions take place by hydrolyzing the ester backbone through which the chains are cleaved forming oligomers or even smaller units of monomers, smaller chains of polymers. Additionally, the resulting byproducts are ought to be biocompatible,

that is, they do not cause immune responses or inflammation by the body. Moreover, biodegradable polymers are either naturally, synthetic, or a modified version of both, semisynthetic. Polymers which are naturally occurring and readily exist in the nanotechnology applications include proteins and polysaccharides like alginate (Alg), chitosan, hyaluronic acid, albumin, and collagen. On the other hand, synthetic polymers include but not limited to polylactic acid, polyglycolic acid, poly(lactide-co-glycolide) (PLGA), poly(orthoester), poly (vinyl alcohol) (PVA), and poly(caprolactone) (PCL). Alternatively, a blend of more than one can be used to optimize the properties of the NPs. Utilizing biodegradable NPS does not only assist the body in disposing the material after it is no longer needed, but also provides control over the release rate due to tunable biodegradation rate [27-31].

1.3.2 Poly (Caprolactone)

PCL is a biocompatible, biodegradable, and a nontoxic synthetic polymer based on hexanoate repeat units that belongs to the aliphatic polyesters' family. It has a semi-crystalline structure, i.e. rubbery, at room and body temperatures with a glass and melting temperatures of -60 and 60 °C, respectively. This property leads to a slower degradation rate compared to polymers with amorphous structure such as PLGA. In addition, its structure contains a low number of ester bonds; consequently, enzymatic degradation by esterase or lipase enzymes takes a longer time. It can also be degraded by hydrolysis in a self-catalyzed process through which water molecules attack the ester bonds and the resulting carboxylic groups speed the reaction. Therefore, it is usually used for prolonged

drug delivery where it exhibits sustained release properties. It is typically produced by ring opening polymerization of ϵ -caprolactone and crystallinity depends on the molecular weight attained. The higher the molecular weight the lower the crystallinity and the longer the chains. As a result of the long chains, the possibility of the chain to be attacked by water molecules or enzymes increases causing faster biodegradation. When PCL is degraded, it releases carboxylic groups that increase the pH of the environment that becomes basic in chronic wounds. Furthermore, PCL is already approved by the Food and Drug Administration (FDA) to be used in biomedical applications. Besides, it has been used already in generating films, electro-spun mats, scaffolds, and NPs [30-37].

1.3.3 Poly (lactic-co-glycolic acid)

Like PCL, PLGA is a biocompatible biodegradable polymer that has ester bond linkages and belongs to the polyester family. It is produced by ring opening polymerization and is composed of two polymers, lactic and glycolic acids. The ratio of these two polymers affects the physical and chemical properties of the copolymer. For instance, higher amount of lactic compared to glycolic acid results in a more crystalline polymer with a slower degradation rate. PLGA is biologically degraded by hydrolysis to release its monomers, lactic and glycolic acids, which have existing excretion pathways in the body. It is already FDA approved to be used in biomedical applications and can be utilized in constructing scaffolds, membranes, NPs, etc... As mentioned earlier, because its structure is less crystalline compared to that of PCL, it has a higher biodegradability rate and, thus, the release rate of the encapsulated drugs is accelerated [32,37].

1.3.4 Poly (Vinyl Alcohol)

PVA is a linear synthetic polymer that is biocompatible, nontoxic, and non-carcinogenic. It is also a hydrophilic polymer that can improve biodegradation with a glass and melting temperatures of 80 and 100 °C, respectively. Like PCL, PVA is also approved by FDA and is already used in various biomedical applications inside and outside the body. Although it does not undergo chemical or enzymatic degradation, but it gets depleted by erosion via dissolution into the medium. Besides its hydrophilic nature, it has a high-water capacity and retention which makes it suitable for wound healing applications. Owing to its high pH and temperature stability it is commonly used to stabilize NPs when applied as a protective coating. Accordingly, PVA renders NPs stable despite the harsh environment in freeze-drying. It is also used as a surfactant in forming double emulsion due to its resistance to organic solvents [30,38-42].

1.3.5 Alginate

Unlike PCL and PVA, Alg is a naturally occurring and highly abundant polysaccharides that can be extracted from brown seaweed or formed in bacteria. It has a linear polymer structure consisting of a series of linked α -L-galuronic acid (G) and β -D-mannuronic acid (M) residues; where the galuronic acid makes the polymer absorbent and the mannuronic acids softens it. Besides, the sequence of these residues influences the properties of Alg. In addition, it is an anionic polymer that can be gelled by chemical and physical crosslinks. It can be gelled by using multivalent cations such as calcium chloride generating what is known as egg-box model (Fig. 3). One of its crucial properties is

biodegradability which enables it to be used in biomedical applications. Another essential feature is absorbance where it can absorb 200 to 300 of its original weight. Its degradability depends on time, pH, and temperature and occurs by proton catalyzed hydrolysis. For instance, at low pH levels the gel becomes very viscous which slows down the degradation. Based on the attractive properties of Alg, it has been utilized in various biomedical applications since 1980 and has been approved by FDA. It is already used as an emulsifier in the pharmaceutical products. It is also used in wound dressing where sodium leaching from the wound can exchange ions with calcium in the matrix which solubilizes it. One of the main drawbacks accompanied by natural polymers is the high heterogeneity and poor reproducibility. However, its gentle gelling properties allow it to encapsulate sensitive molecules. Furthermore, because crosslinking can take place at mild conditions, these fragile materials such as drugs and proteins can be easily encapsulated by using external gelling via dipping the Alg in a cationic bath for crosslinking to take place [43-46].

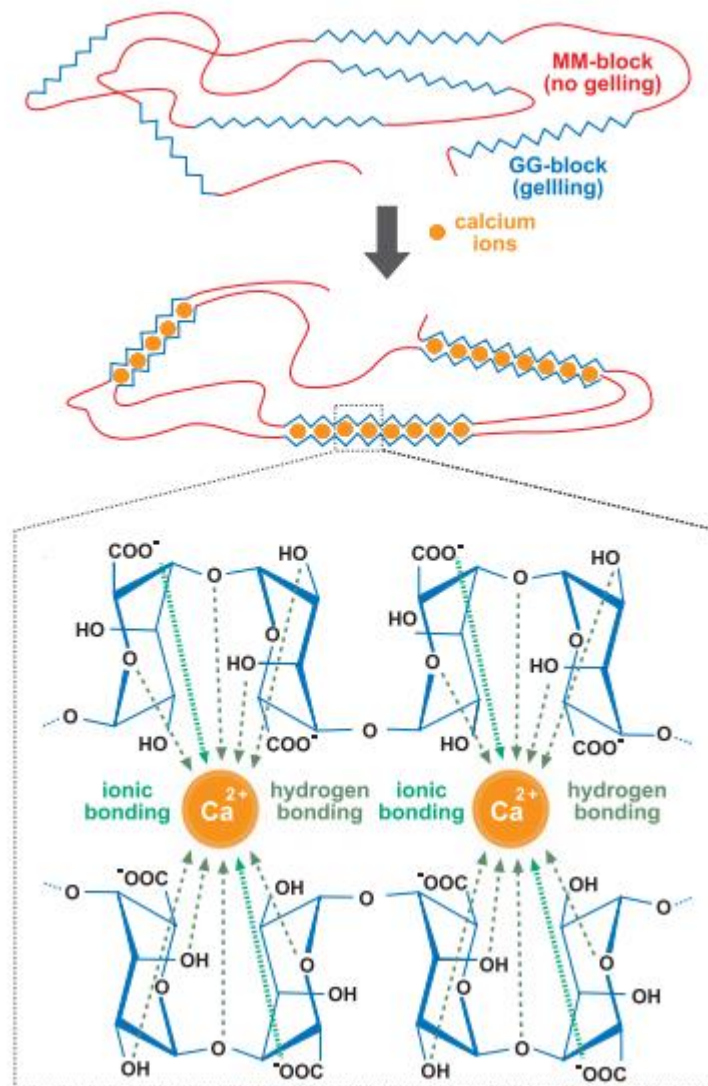


Figure 3 Schematic diagram of the ionic gelation of Alg that generates the egg-box model [44].

1.4 Emulsions

Creating emulsions, despite the methodology followed, represents an approach to form polymeric NPs. It is a heterogeneous system where the process involves two

immiscible phases where one is continuous and the other is dispersed and both can contain different types of polymers, natural or synthetic, depending on their solubility. The two main approaches employed are emulsification-solvent replacement and emulsification solvent-evaporation methods (EEM). Although solvent replacement is considered as a low energy process, but it requires large amounts of solvents to induce the aggregation of NPs as they move from the internal to the external phase; accordingly, the process becomes uneconomic and hard to scale-up. On the other hand, EEM requires a relatively higher energy input, but delivers competent results with respect to size distribution, versatility, and ability to be scaled up beyond the laboratory. This method was created by Vanderhoff in the 1970; since then, prodigious efforts have been invested by researchers to amend the process. Basically, it requires an aqueous phase, organic phase, a surfactant, and an energy source (Fig.4). Firstly, the two phases are mixed together to form large emulsions which endure high pressure by a mechanical homogenizer or acoustic waves by a sonicator through which they are broken down into smaller emulsion, micro or nano. Then, the organic phase is left to evaporate on a stirrer leaving porous NPs to solidify. Finally, the NPs are washed and collected and can be further freeze-dried to be stored for a long period of time. Nevertheless, single emulsions merely permit the encapsulation of hydrophobic drugs. To circumvent this limitation, double emulsions are utilized to contain hydrophilic and water-soluble drugs such as proteins, DNA, and GFs [25,27,36, 47-48].

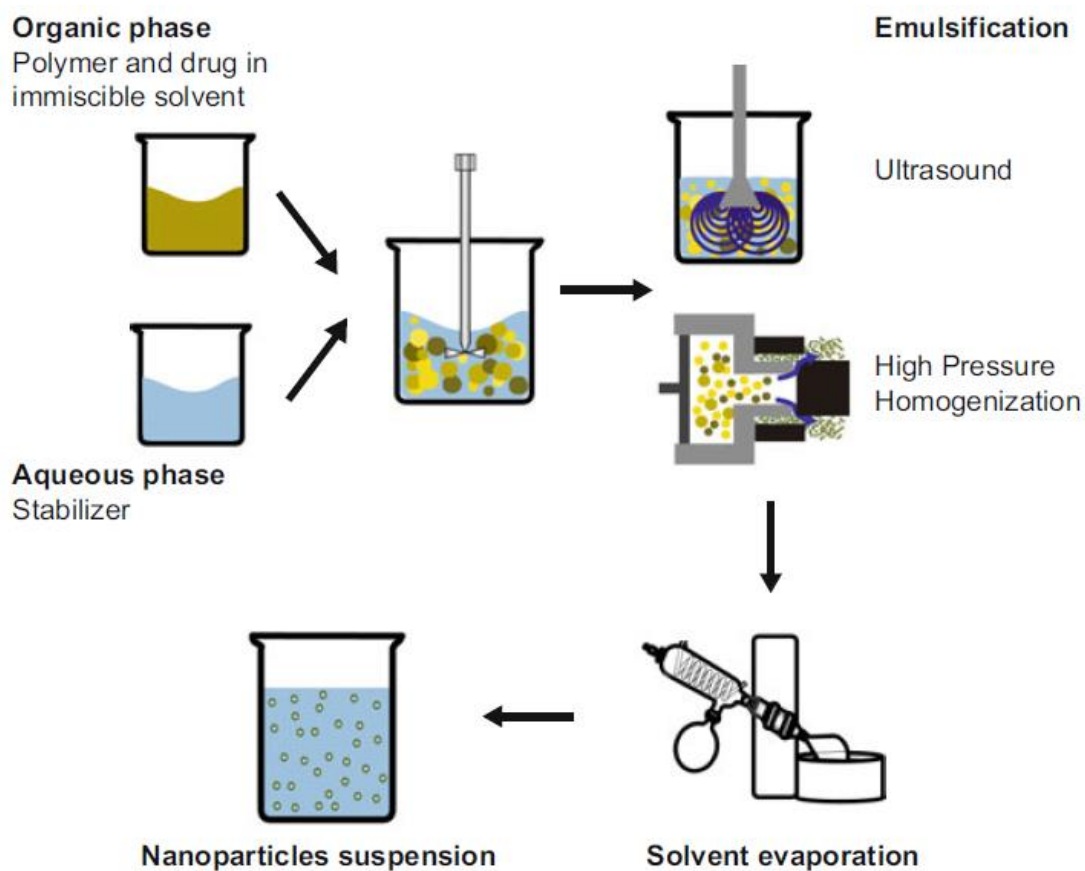


Figure 4 Schematic representation of the steps involved in the EEM [27].

1.4.1 Double Emulsions

An emulsion is a well-studied system, however, it lacks the ability to encapsulate hydrophilic drugs. Therefore, double emulsions were developed by William Seifriz in 1925 to overcome the limitations of single emulsions. They go through the same steps implemented in the single emulsion solvent evaporation method, yet an extra stage is added through which an inner aqueous core is developed. That is, the emulsification step is applied twice resulting in the formation of three layers an aqueous core, oil intermediate

layer, and an outer aqueous coating (Fig. 5). Accordingly, the hydrophilic drugs can be encapsulated in the inner core [25,27,36, 47-50].

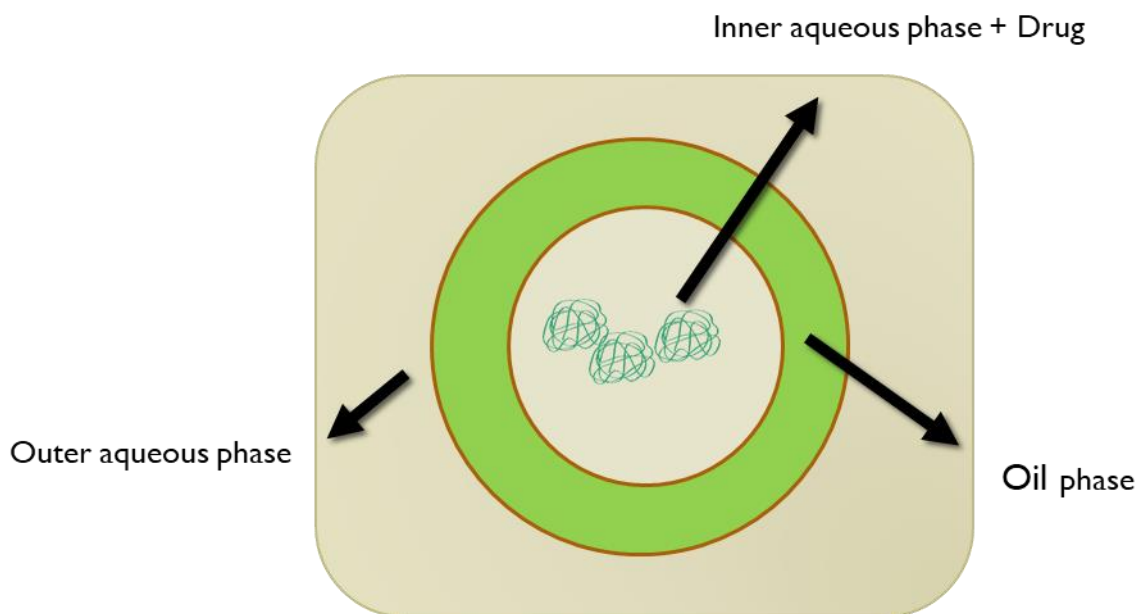


Figure 5 Schematic of the double emulsion.

1.4.2 Energy Source

The preparation procedure of double emulsion requires an energy source to emulsify the immiscible phases and break the macro-emulsions into micro- and nano-emulsions. This energy can be transmitted to the solution by the means of a high-pressure homogenizer or an ultrasonicator. The first one generates pressure and stress in the particles to break them apart. On the other hand, the ultrasonicator delivers acoustic waves which leads to the nucleation, growth and then collapse of bubbles. This cavitation will not take place until a certain threshold is reached. The continuous cyclic process between high and low pressures cavitation and explosion of the bubbles takes place respectively will break

the large agglomerates into smaller particles (Fig.6). Both energy sources are used in the field of double emulsions; however, sonication has several advantages over the other. For instance, it leads to the formation of small droplets with narrow size distribution, requires less surfactant, enhances drug loading, and is more energy efficient [35, 51-53].

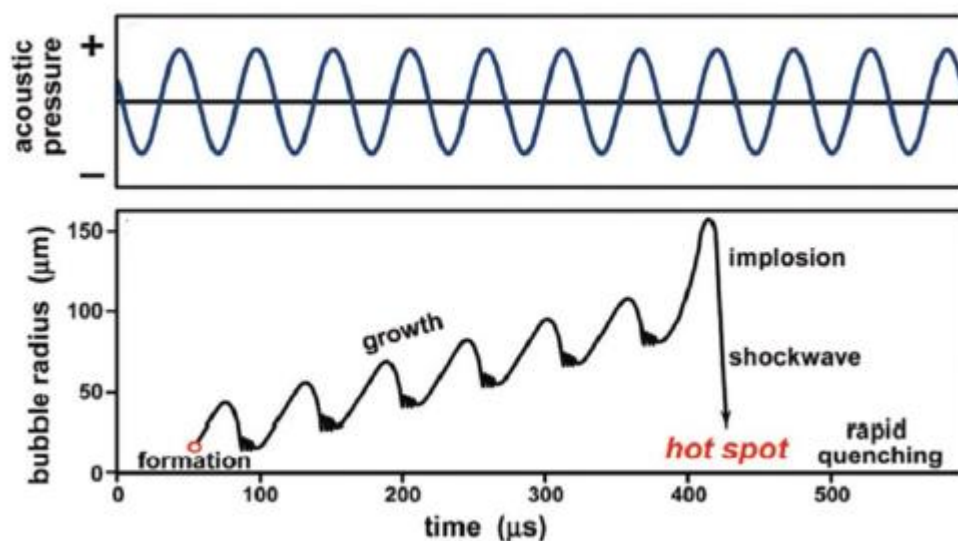


Figure 6 Graphical representation of the cavitation process due to alternation between high and low pressure [53].

1.4.3 Emulsification parameters

Due to the wide range of applications of double emulsions, it is crucial to optimize the emulsification process. The size and morphology of the resulting NPs depend considerably on the various process parameters. In a probe sonicator unlike bath sonicator, the horn is the element that delivers ultrasonic waves to the liquid. The tip of the horn moves up and down during operation, and the distance covered by the tip during expansion

and compression is represented by the amplitude. The distance and the amplitude are measured in μm and percentage (%), respectively. However, the value of the amplitude that can be set by the user corresponds to a specified distance found on a calibration curve of the operation manual of different sonicators. Varying the amplitude affects the intensity of cavitation. Therefore, both sonication time and amplitude are responsible of the energy delivered to the solution. In addition, the volumes of the aqueous and oil phases, their ratios, and the type of emulsifier dictate the type of resulting emulsions, i.e. oil in water (O/W) or water in oil (W/O) and can affect their size. In addition, the volume of the solution on which the sonication energy is distributed is also an affecting parameter. The energy delivered to the particles cannot be set by the user but rather depends on the volume of the solution, sonication time and amplitude, and physical properties of the solution. Besides, this energy based on amplitude is not similar for different sonicators, thus, calibration curves can be generated for each device individually. Finally, the evaporation of the organic solvent is a critical step in the technique, during which the particles solidify, thus its rate can influence their formation [35,36,49-54].

1.5 Sulfated glycosaminoglycans mimetics

Different tissues in the body are surrounded by a highly dynamic niche microenvironment defined as the extracellular matrix (ECM). It provides a physical architecture and biochemical cues for the cells; hence, it has a role in regulating cellular functions. The ECM is composed of water and macromolecules including proteins and polysaccharides. Glycosaminoglycans (GAGs) are carbohydrates composed of repeating

disaccharides units of uronic acid and amino sugars that play a vital role in development of mammalian tissues. They are negatively charged due to the sulfate groups and have different heterogeneous sulfation patterns except for hyaluronan that is negative to presence of glucuronic acid (GlcA). They act as a reservoir by binding to GFs, proteins, chemokines, and cytokines via electrostatic interactions that highly depend on the degree of sulfation [55-57].

1.5.1 Heparin/Heparan Sulfate

Heparin or heparan sulfate are sulfated GAGs with alternating α 1,4 GlcNAc and β 1,4 GlcA units (Fig.7). They activate different signaling pathways when bound to GFs by inducing the dimerization of their receptors. Although both share the same monomeric subunits, however, heparin has more sulfated groups. They regulate cell-to-cell and cell-to-ECM interactions to play a role in cell proliferation, differentiation, and angiogenesis. Molecules that bind to heparin are called heparin-binding proteins and include but not limited to fibroblast growth factor (FGF), insulin-like growth factor (IGF), connective tissue growth factor (CTGF), platelet derived growth factor (PDGF), Interleukin 8, fibronectins, and Annexin V. This affinity protects them from degradation and makes them available for the cells. Heparin is the GAG with the highest degree of sulfation and is a very potent anticoagulant. Although it has many biological roles and can be involved in many biomedical applications, but it cannot be administered at high doses because it can be associated with excessive bleeding. Furthermore, it is usually derived from animal sources, hence it poses safety issues. In addition, due to its heterogeneous structure, customizing it

as a drug becomes complex. Therefore, the demand for finding or engineering a heparin analogue arises [58-60].

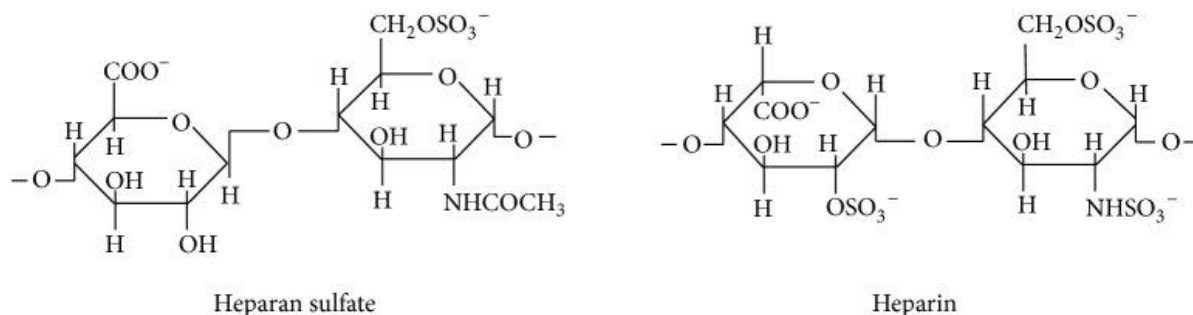


Figure 7 Chemical structure of heparan sulfate and heparin [58].

1.5.2 Alginate Sulfate

Algs share structural features with heparin which nominates it to be a suitable analogue; they both are copolymers based on uronans. Chemical sulfation of Algs can be implemented by various reactions (Fig.8). When sulfated by the esterification of their hydroxyl groups, Algs exhibit mucoadhesive properties and tend to mimic heparin, HS, and chondroitin sulfate since it is basically a polysaccharide that contains a sulfate group to which GFs can bind. Sulfated Algs (AlgSulf) also show anticoagulation and antifouling properties like that in heparin. Accordingly, AlgSulf can be employed in various biomedical application including hydrogels or NPs for cellular and drug encapsulation, respectively. Heparin-binding growth factors (HB-gf) show a high affinity towards heparin mimetic polysaccharides such as AlgSulf. Fibroblast gf (fgf-2) has been reported to bind strongly to AlgSulf [60-63].

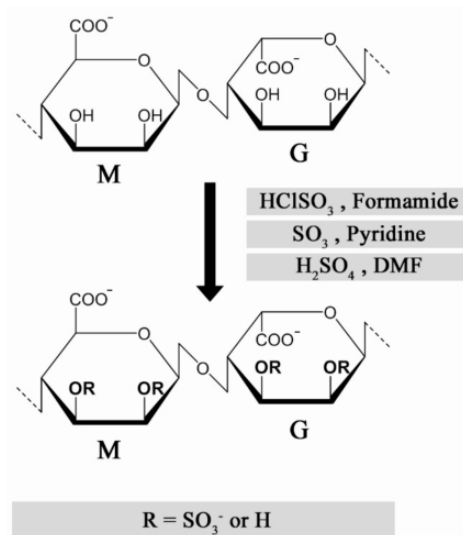


Figure 8 Methods for chemical sulfation of Algs [62].

1.6 Wound Healing

Wound healing is a highly dynamic orchestrated process that is initiated by homeostasis upon injury. It coordinates biochemical pathways and sequential interaction cell-to-cell and cell-to-ECM interactions. It involves many types of cells including blood, epithelial, connective tissue and inflammatory cells along with other soluble factors. The process starts by hemostasis to recruit platelets and initiate the coagulation. Then inflammation by the immune system takes place via neutrophils and macrophages. Macrophages release critical factors such as vascular endothelial growth factor (VEGF), Transforming growth factor beta (TGF- β), and platelet derived growth factor (PDGF). Healing also requires cellular proliferation achieved by fibroblasts that produce a collagen matrix, migration of epidermal cells such as keratinocytes, and formation of new blood vessels. Finally, wound closure is implemented by contraction of the edges due to matrix deposition and myofibroblasts. These phases may overlap or occur consecutively [64-67].

1.6.1 GAGs and GFs in Wound Healing

Chronic wounds lead to extensive losses of the dermal matrix that consequently requires repair. The ECM synthesis and deposition are crucial for the implementation of the dynamic healing process. That is, it serves mainly as a reservoir for multiple molecules that play an integral role in healing. These molecules include structural proteins such as collagens, multidomain adhesive glycoproteins such as fibronectin (FN), GAGs, and matricellular proteins. The ECM constituents control the sequestration and release of growth factors through which they turn into tetrameric complexes and their receptors get stabilized. Accordingly, their activity is prolonged, they are protected from degradation and denaturation, and the variation in sensitivity is regulated. GAGs play a vital role in wound healing since they are primary constituents of the ECM. They regulate many of the inter and intracellular signaling pathways. Therefore, the levels of heparin were found to be elevated in wounds as they can provide both scaffold support and a storage for the necessary molecules. These molecules include heparin binding GF's proteolytic enzymes and protease inhibitors. Heparin also contribute to the recruitment of inflammatory cells. In addition, it binds to matrix proteins such FN and laminin [66-68].

1.6.2 Chronic and Diabetic Wounds

Diabetes mellitus is a group of chronic metabolic diseases characterized by hyperglycemia that is either due to lack of insulin production (type 1) or its resistance where cells fail to respond normally to insulin (type 2). In 2017, the number of people suffering from diabetes was estimated to be 425 million and expected to reach 629 million

by 2045. A high glucose level in blood might be accompanied by multiples complications including cardiovascular diseases, neuropathy, nephropathy, and retinopathy. The chronic diabetes neuropathy affects 15% to 25% of diabetic patients and occurs due to a decreased blood flow and high glyceic levels. Accordingly, the peripheral nerve fibers are lost, and the nerve tissue is damaged; hence, ulceration might occur. Therefore, chronic wounds and prolonged inflammation are more prevalent in diabetic patients. This is because the wound healing processes compromising of the overlapping events of homeostasis, inflammation, proliferation, and remodeling get halted in one or more of the phases or due to lack of certain matricellular proteins such as the connective tissue growth factor (CTGF), GFs such as IGF-1, and cytokines like tumor necrosis factor alpha (TNF- α) Diabetic foot ulcers (DFU) that are not treated effectively might ultimately lead to part or whole lower limb amputation; such losses take place every 30 seconds worldwide due to diabetes. Both DFU's and related amputations pose an annual economic burden reaching up to \$13 to \$15 billion to the healthcare system. Wound healing can be enhanced either passively by merely using wound dressing or actively by delivering bioactive substances such as peptides or GF's [69-73].

1.7 Research Objective and Specific Aims

Chronic wounds, specifically the ones developed in diabetic patients, are associated with a dysregulation in the production of endogenous healing stimulants such as GFs, cytokines, and other matrix molecules which result in slowed or failed wound repair. GFs, including CTGF and IGF, which are the most potent stimulants have a short half-life and

can be easily damaged by varying the microenvironmental conditions including temperature, pH, ions concentrations. Therefore, the controlled delivery of exogenous GFs may improve the speed and enhance the quality of the repaired tissues. One approach would be through using encapsulating them in biodegradable polymers to form NPs that have a higher stability and ability to permeate biological barriers compared to larger particles. These NPs can be prepared by the EEM technique, namely, a W/O/W emulsion where the water-soluble GFs can be embedded in the aqueous core and protected by a hydrophobic layer. Accordingly, they can be protected from the biological microenvironment prolonging their half-life and their release from the carrier. Moreover, heparin is known to have a high affinity to GFs and can thus help prolong its release when incorporated in matrices and particles [57-58]. Alg sulfates have been proposed by our lab as well as other laboratories as heparin mimetic polysaccharides that exhibit high affinity to most heparin binding growth factors [58,63]. Therefore, combining PCL and Alg or AlgSulf to form NPs and generate a hydrocolloid system where GFs are embedded can lead to the development of an effective wound dressing.

1.7.1 Aim 1: Synthesis and characterization of PCL/Alg double emulsion NPs

Synthesis and characterization of double emulsion NPs prepared using Alg, PCL, and PVA as depicted in Fig.14. Subsequently, measurement of cytotoxic effects of the NPs on HaCaT cell line, an immortalized keratinocyte cell line established from adult human skin cells.

Hypothesis: Factors including sonication time, sonication intensity, evaporation rate, oil phase to aqueous phase volume ratio, and polysaccharide in the inner core, and polymer in

the intermediate phase influence the chemical and physical properties of the NPs. The constituents of the NPs are all proven to be biocompatible, however, at high concentrations they might pose stresses on the cells which in turn decreases their viability. Cytotoxic studies aid in identifying the concentration threshold after which NPs become unsafe.

1.7.2 Aim2 Measuring the EE and studying the drug release profile from different NPs formulations.

Encapsulating Bovine Serum Albumin (BSA) as a model drug in different NPs formulations and measuring their encapsulation efficiency, burst release, and the overall release profile.

Hypothesis: Utilizing different materials in the core, pure or sulfated Algs, or in the outer layer, PCL or PLGA, affects the drug-carrier interactions and the properties of the NPs. Accordingly, the total amount of drug that can be encapsulated and its release with time are affected as well.

1.8 References

- [1] M. J. Rathbone *et al*, *Modified-Release Drug Delivery Technology*. 2003;2002;126.
- [2] T. N. Tozer and M. Rowland, *Introduction to Pharmacokinetics and Pharmacodynamics: The Quantitative Basis of Drug Therapy*. Baltimore MD: Lippincott Williams & Wilkins, 2006.
- [3] L. Shargel, S. Wu-Pong and A. B. C. Yu, *Applied Biopharmaceutics & Pharmacokinetics*. (6th ed.) 2012
- [4] A. Bhattacharyya *et al*, "Development of pH sensitive polyurethane–alginate nanoparticles for safe and efficient oral insulin delivery in animal models," *RSC Advances*, vol. 6, (48), pp. 41835-41846, 2016.
- [5] C. Liu *et al*, "A novel ligand conjugated nanoparticles for oral insulin delivery," *Drug Delivery*, vol. 23, (6), pp. 2015-2025, 2016.
- [6] X. Zhu *et al*, "Penetratin derivative-based nanocomplexes for enhanced intestinal insulin delivery," *Molecular Pharmaceutics*, vol. 11, (1), pp. 317-328, 2014.
- [7] X. Huang and C. S. Brazel, "On the importance and mechanisms of burst release in matrix-controlled drug delivery systems," *Journal of Controlled Release : Official Journal of the Controlled Release Society*, vol. 73, (2-3), pp. 121, 2001.
- [8] Anonymous *Carrier-Based Drug Delivery*. United States: 2004.
- [9] D. Schmaljohann, "Thermo- and pH-responsive polymers in drug delivery," *Advanced Drug Delivery Reviews*, vol. 58, (15), pp. 1655-1670, 2006.
- [10] M. Alsaggar and D. Liu, "Organ-based drug delivery," *Journal of Drug Targeting*, vol. 26, (5-6), pp. 385-397, 2018.
- [11] R. Yang *et al*, "Getting Drugs Across Biological Barriers," *Advanced Materials*, vol. 29, (37), pp. 1606596-n/a, 2017.
- [12] B. Rogers, J. Adams and S. Pennathur, *Nanotechnology: The Whole Story*. Boca Raton, Fla: CRC Press, 2013.
- [13] F. Hadeif and A. Otmani, "mechanical alloying/milling," in Anonymous Weinheim, Germany: Wiley-VCH Verlag GmbH & Co. KGaA, 2015, pp. 263-276.

- [14] C. Mattu *et al*, "Comparative evaluation of novel biodegradable nanoparticles for the drug targeting to breast cancer cells," *European Journal of Pharmaceutics and Biopharmaceutics*, vol. 85, (3), pp. 463-472, 2013
- [15] C. Gómez-Gaete *et al*, "Optimization of rhein-loaded polymeric nanoparticles using a factorial design and evaluation of the cytotoxic and anti-inflammatory effects," *Drug Development and Industrial Pharmacy*, vol. 44, (8), pp. 1285-1294, 2018.
- [16] T. Repenko *et al*, "Bio-degradable highly fluorescent conjugated polymer nanoparticles for bio-medical imaging applications," *Nature Communications*, vol. 8, (1), pp. 1-8, 2017.
- [17] A. Akbarzadeh *et al*, "Liposome: classification, preparation, and applications," *Nanoscale Research Letters*, vol. 8, (1), pp. 1-9, 2013.
- [18] V. P. Torchilin, "Recent advances with liposomes as pharmaceutical carriers," *Nature Reviews Drug Discovery*, vol. 4, (2), pp. 145-160, 2005.
- [19] M. Yokoyama, "Polymeric micelles as drug carriers: their lights and shadows," *Journal of Drug Targeting*, vol. 22, (7), pp. 576-583, 2014.
- [20] C. A. Holmes and M. Tabrizian, "Substrate-mediated gene delivery from glycol-chitosan/hyaluronic acid polyelectrolyte multilayer films," *ACS Applied Materials & Interfaces*, vol. 5, (3), pp. 524-531, 2013. [21] P. Li *et al*, "A pH-sensitive multifunctional gene carrier assembled via layer-by-layer technique for efficient gene delivery," *International Journal of Nanomedicine*, vol. 7, pp. 925, 2012.
- [22] M. Möhwald *et al*, "Aspherical, Nanostructured Microparticles for Targeted Gene Delivery to Alveolar Macrophages," *Advanced Healthcare Materials*, vol. 6, (20), pp. 1700478-n/a, 2017.
- [23] Z. J. Deng *et al*, "Layer-by-layer nanoparticles for systemic codelivery of an anticancer drug and siRNA for potential triple-negative breast cancer treatment," *ACS Nano*, vol. 7, (11), pp. 9571-9584, 2013.
- [24] B. Kong *et al*, "Experimental considerations on the cytotoxicity of nanoparticles," *Nanomedicine*, vol. 6, (5), pp. 929-941, 2011.
- [25] E. Malikmammadov *et al*, "PCL and PCL-based materials in biomedical applications," *Journal of Biomaterials Science, Polymer Edition*, vol. 29, (7-9), pp. 863-893, 2018.

- [26] H. Liang *et al*, "Cytotoxicity of silica nanoparticles on HaCaT cells," *Journal of Applied Toxicology*, vol. 34, (4), pp. 367-372, 2014.
- [27] C. Vauthier, G. Ponchel and SpringerLink (Online service), *Polymer Nanoparticles for Nanomedicines: A Guide for their Design, Preparation and Development*. 2016;2017;. DOI: 10.1007/978-3-319-41421-8.
- [28] X. Han and J. Pan, "A model for simultaneous crystallisation and biodegradation of biodegradable polymers," *Biomaterials*, vol. 30, (3), pp. 423-430, 2008.
- [29] J. Karlsson, H. J. Vaughan and J. J. Green, "Biodegradable Polymeric Nanoparticles for Therapeutic Cancer Treatments," *Annual Review of Chemical and Biomolecular Engineering*, vol. 9, (1), pp. 105-127, 2018.
- [30] C. Bouaoud *et al*, "Development of biodegradable polymeric nanoparticles for encapsulation, delivery, and improved antifungal performance of natamycin," *Journal of Applied Polymer Science*, vol. 133, (31), pp. n/a, 2016.
- [31] C. X. Lam, S. H. Teoh and D. W. Hutmacher, "Comparison of the degradation of polycaprolactone and polycaprolactone-(β -tricalcium phosphate) scaffolds in alkaline medium," *Polymer International*, vol. 56, (6), pp. 718-728, 2007.
- [32] N. Kamaly *et al*, "Degradable Controlled-Release Polymers and Polymeric Nanoparticles: Mechanisms of Controlling Drug Release," *Chemical Reviews*, vol. 116, (4), pp. 2602-2663, 2016.
- [33] Y. Tokiwa and B. P. Calabia, "Biodegradability and Biodegradation of Polyesters," *Journal of Polymers and the Environment*, vol. 15, (4), pp. 259-267, 2007.
- [34] N. Tuancharoensri *et al*, "Ternary blend nanofibres of poly(lactic acid), polycaprolactone and cellulose acetate butyrate for skin tissue scaffolds: influence of blend ratio and polycaprolactone molecular mass on miscibility, morphology, crystallinity and thermal properties," *Polymer International*, vol. 66, (11), pp. 1463-1472, 2017.
- [35] M. Iqbal *et al*, "Preparation of biodegradable PCL particles via double emulsion evaporation method using ultrasound technique," *Colloid and Polymer Science*, vol. 293, (3), pp. 861-873, 2015.
- [36] N. Ahmed *et al*, "Modified double emulsion process as a new route to prepare submicron biodegradable magnetic/polycaprolactone particles for in vivo theranostics," *Soft Matter*, vol. 8, (8), pp. 2554-2564, 2012.

- [37] X. S. Wu and N. Wang, "Synthesis, characterization, biodegradation, and drug delivery application of biodegradable lactic/glycolic acid polymers. Part II: Biodegradation," *Journal of Biomaterials Science, Polymer Edition*, vol. 12, (1), pp. 21-34, 2001.
- [38] L. I. F. Moura *et al*, "Recent advances on the development of wound dressings for diabetic foot ulcer treatment—A review," *Acta Biomaterialia*, vol. 9, (7), pp. 7093-7114, 2013.
- [39] A. W. Du and M. H. Stenzel, "Drug carriers for the delivery of therapeutic peptides," *Biomacromolecules*, vol. 15, (4), pp. 1097-1114, 2014.
- [40] K. Pal, A. K. Banthia and D. K. Majumdar, "Preparation and characterization of polyvinyl alcohol-gelatin hydrogel membranes for biomedical applications," *Aaps Pharmscitech*, vol. 8, (1), pp. E142-E146, 2007.
- [41] M. I. Baker *et al*, "A review of polyvinyl alcohol and its uses in cartilage and orthopedic applications," *Journal of Biomedical Materials Research Part B: Applied Biomaterials*, vol. 100B, (5), pp. 1451-1457, 2012.
- [42] B. Ellis *et al*, *Polymers: A Property Database*. (2nd ed.) 2009;2008;.
- [43] J. P. Paques *et al*, "Preparation methods of alginate nanoparticles," *Advances in Colloid and Interface Science*, vol. 209, pp. 163-171, 2014.
- [44] B. H. A. Rehm, M. F. Moradali and SpringerLink (Online service), *Alginates and their Biomedical Applications*. 2018;2017;11.
- [45] M. Rafienia, A. Saberi and E. Poorazizi, "A novel fabrication of PVA/Alginate-Bioglass electrospun for biomedical engineering application," *Nanomedicine Journal*, vol. 4, (3), pp. 152-163, 2017.
- [46] D. Jain and D. Bar-Shalom, "Alginate drug delivery systems: application in context of pharmaceutical and biomedical research," *Drug Development and Industrial Pharmacy*, vol. 40, (12), pp. 1576-1584, 2014.
- [47] U. Bilati, E. Allémann and E. Doelker, "Sonication Parameters for the Preparation of Biodegradable Nanocapsules of Controlled Size by the Double Emulsion Method: RESEARCH ARTICLE," *Pharmaceutical Development and Technology*, vol. 8, (1), pp. 1-9, 2003.

- [48] U. Bilati, E. Allémann and E. Doelker, "Nanoprecipitation versus emulsion-based techniques for the encapsulation of proteins into biodegradable nanoparticles and process-related stability issues," *Aaps Pharmscitech*, vol. 6, (4), pp. E594-E604, 2005.
- [49] S. Ding et al , "Double emulsions prepared by two–step emulsification: History, state-of-the-art and perspective," *Journal of Controlled Release*, vol. 295, no. ISSN 0168-3659, pp. 31-49, 2019.
- [50] R. H. Staff *et al*, "Particle Formation in the Emulsion-Solvent Evaporation Process," *Small*, vol. 9, (20), pp. 3514-3522, 2013.
- [51] T. S. H. Leong *et al*, "The formation of double emulsions in skim milk using minimal food-grade emulsifiers – A comparison between ultrasonic and high pressure homogenisation efficiencies," *Journal of Food Engineering*, vol. 219, pp. 81-92, 2018.
- [52] R. H. Staff *et al*, "Particle Formation in the Emulsion-Solvent Evaporation Process," *Small*, vol. 9, (20), pp. 3514-3522, 2013.
- [53] J. J. Hinman and K. S. Suslick, "Nanostructured Materials Synthesis Using Ultrasound," *Topics in Current Chemistry*, vol. 375, (1), pp. 1-36, 2017.
- [54] J. S. Taurozzi, V. A. Hackley and M. R. Wiesner, "Ultrasonic dispersion of nanoparticles for environmental, health and safety assessment - issues and recommendations," *Nanotoxicology*, vol. 5, (4), pp. 711-729, 2011.
- [55] C. Frantz, K. M. Stewart and V. M. Weaver, "The extracellular matrix at a glance," *Journal of Cell Science*, vol. 123, (Pt 24), pp. 4195, 2010.
- [56] N. S. Gandhi and R. L. Mancera, "The Structure of Glycosaminoglycans and their Interactions with Proteins," *Chemical Biology & Drug Design*, vol. 72, (6), pp. 455-482, 2008.
- [57] R. Mammadov *et al*, "Growth factor binding on heparin mimetic peptide nanofibers," *Biomacromolecules*, vol. 13, (10), pp. 3311-3319, 2012.
- [58] I. Freeman, A. Kedem and S. Cohen, "The effect of sulfation of alginate hydrogels on the specific binding and controlled release of heparin-binding proteins," *Biomaterials*, vol. 29, (22), pp. 3260-3268, 2008.
- [59] P. Olczyk, Ł. Mencner and K. Komosinska-Vassev, "Diverse Roles of Heparan Sulfate and Heparin in Wound Repair," *BioMed Research International*, vol. 2015, pp. 549417-7, 2015.

- [60] E. M. Muñoz and R. J. Linhardt, "Heparin-Binding Domains in Vascular Biology," *Arteriosclerosis, Thrombosis, and Vascular Biology*, vol. 24, (9), pp. 1549-1557, 2004.
- [61] D. Soares da Costa, R. L. Reis and I. Pashkuleva, "Sulfation of Glycosaminoglycans and Its Implications in Human Health and Disorders," *Annual Review of Biomedical Engineering*, vol. 19, (1), pp. 1-26, 2017.
- [62] Ø. Arlov and G. Skjåk-Bræk, "Sulfated Alginates as Heparin Analogues: A Review of Chemical and Functional Properties," *Molecules (Basel, Switzerland)*, vol. 22, (5), pp. 778, 2017.
- [63] R. Mhanna *et al*, "Sulfated Alginate as a Mimic of Sulfated Glycosaminoglycans: Binding of Growth Factors and Effect on Stem Cell Behavior," *Advanced Biosystems*, vol. 1, (7), pp. 1700043-n/a, 2017.
- [64] L. I. F. Moura *et al*, "Recent advances on the development of wound dressings for diabetic foot ulcer treatment—A review," *Acta Biomaterialia*, vol. 9, (7), pp. 7093-7114, 2013.
- [65] M. A. Fonder BS *et al*, "Treating the chronic wound: A practical approach to the care of nonhealing wounds and wound care dressings," *Journal of the American Academy of Dermatology*, vol. 58, (2), pp. 185-206, 2008.
- [66] S. Ghatak *et al*, "Roles of Proteoglycans and Glycosaminoglycans in Wound Healing and Fibrosis," *International Journal of Cell Biology*, vol. 2015, pp. 834893-20, 2015.
- [67] P. Olczyk, Ł. Mencner and K. Komosinska-Vassev, "Diverse Roles of Heparan Sulfate and Heparin in Wound Repair," *BioMed Research International*, vol. 2015, pp. 549417-7, 2015.
- [68] Diabetesatlas.org. (2017). IDF diabetes atlas - Home. [online] Available at:<http://www.diabetesatlas.org/> [Accessed 29 Nov. 2018].
- [69] [2] G. S. Schultz and A. Wysocki, "Interactions between extracellular matrix and growth factors in wound healing," *Wound Repair and Regeneration : Official Publication of the Wound Healing Society [and] the European Tissue Repair Society*, vol. 17, (2), pp. 153-162, 2009.
- [70] F. R. Henshaw *et al*, "Topically Applied Connective Tissue Growth Factor/CCN2 Improves Diabetic Preclinical Cutaneous Wound Healing: Potential Role for CTGF in Human Diabetic Foot Ulcer Healing," *Journal of Diabetes Research*, vol. 2015, pp. 1-10, 2015.

[71] W. Yan et al, "Acellular dermal matrix scaffolds coated with connective tissue growth factor accelerate diabetic wound healing by increasing fibronectin through PKC signalling pathway," *Journal of Tissue Engineering and Regenerative Medicine*, vol. 12, (3), pp. e1461-e1473, 2018.

[72] R. Gary Sibbald and K. Y. Woo, "The biology of chronic foot ulcers in persons with diabetes," *Diabetes/Metabolism Research and Reviews*, vol. 24, (S1), pp. S25-S30, 2008.

[73] S. Patel, S. Srivastava, M. R. Singh, and D. Singh, "Mechanistic insight into diabetic wounds: Pathogenesis, molecular targets and treatment strategies to pace wound healing," *Biomedicine & Pharmacotherapy*, vol. 112, p. 108615, 2019.

CHAPTER II

MATERIALS AND METHODS

2.1 Materials

Sodium alginate (Sigma-Aldrich, W201502), Poly(vinyl alcohol) (Mw 13,000-23,000, 87%-89% hydrolyzed, Sigma-Aldrich), Polycaprolactone (average Mn 80,000 Sigma-Aldrich), Poly(lactic-co-glycolic acid) (Mw 362,000 PURASORB® PLG 8523, Corbion), Dichloromethane (DCM, Sigma-Aldrich), Calcium Chloride (CaCl₂, Anhydrous, Fisher Scientific), Sulfated Alginate (AlgSulf_{2.0}, Novamatrix), Acyl 12:0 NBD PC (1-acyl-2-{ 12-[(7-nitro-2-1,3-benzoxadiazol-4-yl)amino]dodecanoyl}-*sn*-glycero-3-phosphocholine, Recombinant Human CTGF (Peprotech), Recombinant Human IGF-1 (Peprotech), Antibodies: p44/42 MAPK (Erk1/2) Rabbit (Cell Signaling), Phospho-Akt (Cell signaling), and Rb pAB to β Actin (Abcam), Dulbecco's Modified Eagle's Medium - high glucose (Sigma), Fetal Bovine Serum (FBS, Sigma), Penicillin-Streptomycin (Sigma), Sodium Pyruvate (Lonza), Trypsin Solution 10X (Sigma Aldrich), and Phosphate Buffered Saline 10x (PBS, Sigma).

2.2 Methods

2.2.2 Synthesis of Alginate and PCL NPs

Preparation of Solvents

Alg and PCL NPs were prepared using the double-emulsion solvent evaporation technique. Briefly, 40 mg of PCL were dissolved in DCM to form a clear solution at a concentration of 10 mg/ml. Sodium Alg and PVA were mixed in double-deionized water (DDW) at a concentration of 1% and 3% by weight, respectively, at 60°C until they dissolved completely. The solution was then filtered through a 220nm syringe filter (corning), unless specified otherwise. Another aqueous phase containing PVA and CaCl₂ at 1% and 2% weight, respectively, was prepared in DDW.

Formation of NPs

The primary emulsion (W1/O) was formed by dispersing 1ml of the Alg and PVA solution in 4 ml of the PCL solution. Then, the mixture was homogenized using ultrasonic homogenizer “Q 700 Sonica” at a frequency of 20 KHz and an amplitude of 50% for 5 minutes. To form the secondary emulsion (W1/O/W2), the second aqueous phase containing PVA and CaCl₂ was added dropwise into the primary emulsion solution. This mixture was homogenized at an amplitude of 65% for 10 minutes. Then it was left on the stirrer for a minimum of 3 hours for the organic solvent to evaporate in a container with a surface area of 2463mm² at room temperature and atmospheric pressure. Afterwards, the particles were collected by centrifugation at a speed of 14,800 RPM for 20 minutes at 4°C and washed with DDW to remove any PVA or DCM residues. Then the particles were

placed at -80°C for a minimum of 30 minutes to be dried in the lyophilizer (Labnconco) for 48 hours. When freeze-dried, the particles can be stored at 4°C for up to year.

Sonication Parameters

The reference emulsion sample was prepared according to the parameters mentioned in the earlier section. The effect of varying multiple process parameters on the size and morphology of the NPs was investigated by altering one parameter at a time while keeping the others constant. The parameters include:

1. Second emulsion sonication time (5, 10, 15 and 20 minutes) for both filtered and non-filtered aqueous inner phase containing Alg and PVA.
2. Second emulsion sonication amplitude (65, 80, and 95%) for both filtered and non-filtered aqueous phase containing Alg and PVA.
3. Organic solvent (DCM) evaporation rate where the mixture, after processing, was stirred in containers having different surface areas (452.39, 1661.9, 2463, and 3848.45 mm²), thus, affecting the rate of evaporation.
4. Volume of outer aqueous phase (5, 10, and 20 ml).
5. Total processed volume (7.5, 15, and 30 ml), while keeping the phases' ratio constant.
6. AlgSulf_{2.0}, instead of pure sodium Alg, in the inner aqueous phase.

2.2.2 Physical Characterization of the NPs

Average Hydrodynamic Size and Zeta-Potential

After synthesizing the particles, their average hydrodynamic diameter, polydispersity index (PDI), and zeta potential were measured by dynamic light scattering using NanoPlus HD® DLS. The samples were prepared by adding 10 µl of particulate dispersion to 990 µl DDW and then placed in a plastic cell to be analyzed at 25°C. As for the zeta potential, the samples were prepared in a similar manner and then inserted into a flow cell for analysis.

$$PDI = \frac{\sigma^2}{Z_D^2}$$

Where PDI is the measurement of size distribution

σ is the standard deviation

Z_D is the average size

Morphology

To study the morphology of the particles, scanning electron microscopy (SEM) was performed by “MIRA 3 TESCAN”. After freeze-drying the collected particles, samples were mounted on metallic stubs using conductive double coated carbon tape. The particles were then sputter coated with a 20nm thick layer of conductive metal such as gold, chromium, or platinum using Quorum 150V Plus.

2.2.3 Modeling the Effect of Energy, Time, Amplitude, and Volume on the Size of the NPs

The energy delivered based on the sonication time and amplitude varies from one sonicator to another and thus leads to diverging results, thus, the following calculations aids in creating a calibration curve based on the energy. The acoustic energy delivered into the processed volume is not totally allocated for homogenizing the solution as part of the energy is lost as heat. Therefore, the heat released during the process was quantified by measuring the temperature of the liquid before and after sonication. Due to the relatively low volume of the oil phase compared to the aqueous phase and the minor change in temperature, the heat capacity of DCM was assumed to be constant (C_p at 25°C). The energy released as heat was calculated by the following equations:

$$\text{DCM: } C_{p\text{DCM}}(25^\circ\text{C}) = 24 \text{ Cal/mol}\cdot^\circ\text{C}, \rho_{\text{DCM}}(25^\circ\text{C}) = 1.322 \text{ g/ml [1]}$$

$$\text{Water: } C_{p\text{H}_2\text{O}} = \int_{T_1}^{T_2} (75.4 \times 10^{-3}) dT \left(\frac{\text{KJ}}{\text{mol}\cdot^\circ\text{C}} \right), \rho_{\text{H}_2\text{O}}(25^\circ\text{C}) = 0.997 \text{ g/ml [2]}$$

$$Q = nC_p\Delta T$$

Where

Q is the Heat Energy (J)

n is the number of moles (mol)

C_p is the heat capacity depending on the material (Cal/mol. $^\circ$ C or KJ/ mol. $^\circ$ C)

$\Delta T = (T_2 - T_1)$ is the difference between the temperature of the mixture before and after sonication

The calculated energy from heat was then subtracted from the total energy to find the magnitude of energy employed merely for disruption of the particles. This procedure was applied twice, during both sonication time and sonication amplitude variation. Accordingly,

the effect of the rate of the delivered energy on the ultimate results can be investigated. Model-fitting was performed in both cases as a relation between energy and size. The size was evaluated through the two generated equations at different magnitudes of energy then the paired T-test was applied to compare results.

2.2.4 Encapsulation and Release

For encapsulation and release studies, Bovine Serum Albumin (BSA, Sigma) was used as a model drug. Different amounts of BSA (1, 5, 10 mg) were dissolved into the first aqueous phase containing Alg and PVA to be encapsulated in the inner hydrophilic core of the nanoparticles. Several alterations were introduced to the preparation protocol described earlier. The changes include reducing the primary emulsification step to 1 minute, processing the solutions over ice to protect the BSA, and adding 15 ml of 1% PVA solution to the particle dispersion before stirring to further stabilize emulsions. In addition, to compare the properties of the NPs developed in this research to the others that were studied earlier [3], PLGA was used instead of PCL in one of the formulations.

After the optimization based on the size and zeta potential, the constituents of the particles were varied to investigate their influence on encapsulation efficiency and release profile. The conditions were: (1) 1% pure Alg coated with PCL, (2) 2% pure Alg coated with PCL, (3) 2% AlgSulf_{2.0} coated with PCL, and (4) 2% pure Alg coated with PLGA.

Encapsulation Efficiency

The NPs suspension was centrifuged at 4°C and 14,800 RPM, then the collected particles were washed by DDW. The amount of drug loaded was determined by analyzing the amount of BSA present in the supernatant. The amount of BSA was quantified by using Lowry protein assay. The encapsulation efficiency (EE%) was calculated using the following formula:

$$\%EE = \frac{\text{Total BSA} - \text{Free BSA}}{\text{Total BSA}} \times 100$$

Release Rate

10 mg of the different types of NPs described earlier in this section were incubated in 1 ml PBS (pH 7.2) in eppendorfs and placed in the shaker at 37°C and 200 RPM. At each time point (0, 1, 2, 4, 24, 48, 168, 336, and 504 hours), the samples were centrifuged at 14,800 RPM for 20 minutes and the supernatants were collected. Samples were then resuspended in 1 ml of fresh PBS and incubated again. To study the effect of shaking on the release rate, particles containing BSA composed of 2% AlgSulf_{2.0} coated with PCL were kept in the incubator at 37°C without shaking. In addition, to simulate the chronic wound environment in terms of pH levels, particles containing BSA composed of 2% pure Alg coated with PLGA were incubated with PBS (pH 8.0) in the shaker at 37°C and 200 RPM (Appendix). The supernatants of these two samples were also collected at similar time points. All removed supernatants were stored at -20°C until quantified using Lowry protein assay. A control with no BSA of each sample was used to correct for the effect of the degradation on the assay. All samples were run in triplicates.

2.2.5 Stability of NPs

Fresh aliquots of the NPs prepared at an amplitude of 65% for 10 minutes in the second sonication step were dispersed in 1 ml DDW. The centrifuge tubes containing the particles were incubated at 37°C. They were collected after different time points (0,1,3,5, and 7 days) to measure the size and PDI in order to evaluate their thermal stability.

Furthermore, to investigate their colloidal stability in different biological environments, aliquots were added to cell culture media and their size and PDI were measured.

2.2.6 Cell Culture

The HaCat cell-line was used to perform the in vitro experiments. The cells were cultured in DMEM supplemented with 10% FBS, 1% sodium pyruvate, 1% penicillin-streptomycin, 0.2% kanamycin at 37°C and 5% CO₂. The cells were cultured in T-75 flasks and subcultured when they reached 100% confluency. Cells were prepared for experiments by removing the medium then washing them with PBS to remove any traces of medium. Trypsin-EDTA solution was added to cover the whole surface. Then the flasks were incubated for 10 minutes at 37 °C for cells to detach completely. A minimum amount of about double the trypsin volume of complete medium is added to deactivate it after which the mixture is collected in 15 ml conical tube. The cells were collected by centrifugation at 1200 RPM for 5 minutes to be counted. Accordingly, the cells were prepared with cell culture medium at the desired density to be seeded in 6, 12, 24, or 96-well plates depending on the experiment.

2.2.7 Nanoparticles cytotoxicity

Trypan-blue exclusion assay

To evaluate the cytotoxicity of the Alg/PCL nanoparticles, HaCat cells were seeded at a density of 50,000 cells/well in a 24-well plate. The cells were cultured until they reached 40% confluency. The culture medium was then replaced with fresh medium containing nanoparticles at different concentrations (0, 5, 25, 50, and 100 µg/ml) in triplicates. The cells were incubated with the particles for 24, 48 and 72 hours and then the viability was measured at each time point. The cells were trypsinized and stained with trypan blue, a diazo dye that is absorbed by viable cells with intact membrane. The % viability at each condition was then calculated by the following equation:

$$\%viability = \frac{\text{number of viable cells}}{\text{(Total number of cells)}} \times 100$$

and then normalized against the control (0 µg/ml).

MTT assay

In vitro cytotoxicity was also evaluated using tetrazolium dye (MTT) colorimetric cell proliferation assay. The 3-(4,5-dimethyl-2-yl)-2,5-diphenyl tetrazolium bromide is converted by the mitochondrial NAD(P)H-dependent cellular oxidoreductase enzymes into a purple insoluble formazan [4]. The converted amount is directly related to the activity of the cells which can be linked to the number of viable cells. HaCat cells were seeded at a density of 50,000 cells/well in 96-well plate. However, in order to eliminate any discrepancy between the trypan blue exclusion assay and this assay, the concentrations of

the NPs were adjusted based on the surface area of the wells as the particles tend to settle with time [4]. The modified concentrations are shown in Table 2.1:

24 Well-plate: Area= 1.9 cm²/ well

96 Well-plate: Area=0.32 cm²/ well

Concentration (µg/ml)	5	25	50	100
Concentration (µg/cm ²)	2.6	13	26	53

Table 1 Conversion in concentration from µg/ml to µg/cm².

After culturing the cells for 24 hours, the culture medium was removed, and the cells were incubated with the particles for 24 hours. After incubation, 90 µl of fresh media and 10 µl of the MTT solution were added to each well and reincubated for 3 hours at 37 °C for formazan crystals to form. To dissolve the crystals, 150 µl of MTT stop solution containing Iso-propanol, tritonX-100 and 37% HCl was added to each well. Then the solutions from each well were transferred to a new plate to ensure that the settled particles will not interfere with the assay. The new plate was read at an absorbance of 595 nm using a microplate reader. Cell grown in particle-free medium was used as a reference (100% viability). The % activity of the cells was calculated by the following equation:

$$\% \text{ Activity} = \frac{(\text{SampleOD} - \text{blank})}{(\text{controlOD} - \text{blank})} \times 100$$

Immunoblotting

Protein extraction

To test if the nanoparticles activate any survival or proliferative pathway, ERK and AKT activation due to nanoparticles was measured by western blot. HaCat cells were seeded in 12-well plates at a density of 250,000 cells/well and treated after 24 hours with nanoparticles at different concentrations (0, 5, 25, 50, and 100 $\mu\text{g/ml}$) for 15 minutes. Cells were washed with PBS and then harvested to be lysed with using 1X RIPA buffer including a cocktail of protease inhibitors to prevent protein degradation. The lysates were centrifuged at 13,800xg for 10 minutes at 4°C. The total protein concentration in each sample was determined by Lowry assay.

Protein migration and transfer

Protein samples were prepared with DDW based on the concentration measurement to load equal amounts at all conditions (40 μg of proteins in a total of 30 μl and 10 μl of 4X laemmli buffer to trace and preserve proteins during migration). Subsequently, the samples were loaded into 10% SDS-PAGE gels. After migration (100v), the proteins were transferred (150 v, 350 mAmp, 1.5 hours) onto nitrocellulose membranes (0.45 μm). The membranes were probed with anti-ERK and anti-AKT primary antibodies. Horseradish secondary antibodies and enhanced chemiluminescence (ECL) were used to detect the proteins on the membranes through Biorad Chemidoc. Finally, the apparent bands were quantified using ImageJ software and normalized against the amount of T-ERK and T-AKT.

2.2.8 Statistical analysis

All statistical tests were performed using SPSS software. In case of comparing two groups, T-test was used for parametric data and Mann–Whitney U test for non-parametric data. As for more than two groups One-Way ANOVA was used for parametric data and Kruskal Wallis for non-parametric data. Two-Way ANOVA was used when groups were studied against two variables. All P-values less than 0.05 were considered significant.

2.3 References

[1] "Methylene chloride," *Methylene chloride*. [Online]. Available:

<https://webbook.nist.gov/cgi/cbook.cgi?ID=C75092&Mask=1&Type=JANAFG&Table=on>

[2] "Water," *Water*. [Online]. Available:

<https://webbook.nist.gov/cgi/cbook.cgi?ID=C7732185&Type=JANAFL&Plot=on>.

[3] G. Gainza *et al*, "rhEGF-loaded PLGA-Alginate microspheres enhance the healing of full-thickness excisional wounds in diabetised Wistar rats," *European Journal of Pharmaceutical Sciences*, vol. 50, (3-4), pp. 243-252, 2013.

[4] B. Kong *et al*, "Experimental considerations on the cytotoxicity of nanoparticles," *Nanomedicine*, vol. 6, (5), pp. 929-941, 2011.

CHAPTER III

SYNTHESIS AND CHARACTERIZATION OF NPs

3.1 Optimization of nanoparticles

The morphology the NP's comprising their size, PDI, and morphological stability besides their colloidal stability can be affected by several factors.

3.1.1 Effect of sonication time and sonication amplitude

The NP's preparation approach explained earlier is based on the ultrasonic energy. Therefore, the magnitude of the acoustic energy delivered to the suspension considerably affects the final size of the emulsions. This energy is controlled by two main parameters, the ultrasonic exposure time and amplitude.

Firstly, the effect of time was investigated in the secondary sonication step since the ultimate size of the particles does not depend on the exposure time of the first emulsion [1]. Therefore, the first emulsification step was performed at an amplitude of 50% for 5 minutes in all the samples of the optimization process. However, in this experiment, the secondary emulsion was processed for 5, 10, 15, and 20 minutes at an amplitude of 65%. In addition, the processing parameters were applied for both filtered and non-filtered inner aqueous phase. It was observed that as the exposure time increased, the average hydrodynamic size of the particles decreased until reaching a minimum of 247.6 and 355.6 nm for filtered and non-filtered, respectively, at 15 minutes (Fig. 9).

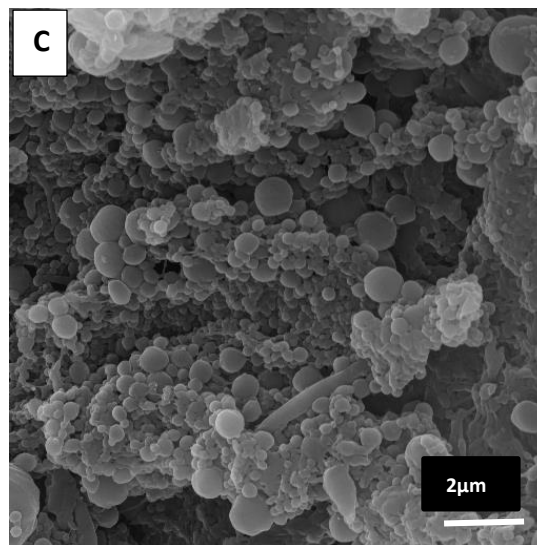
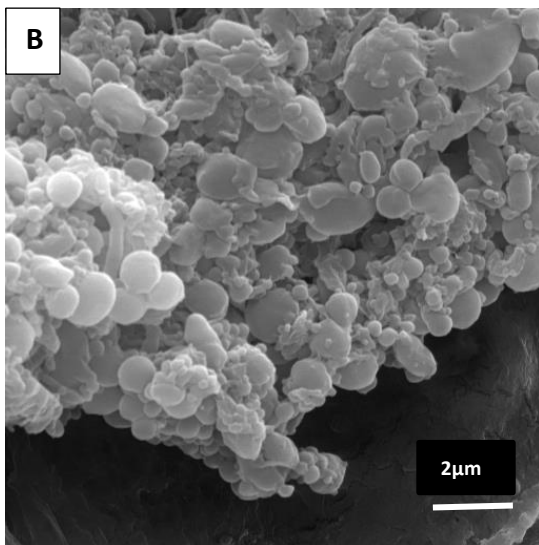
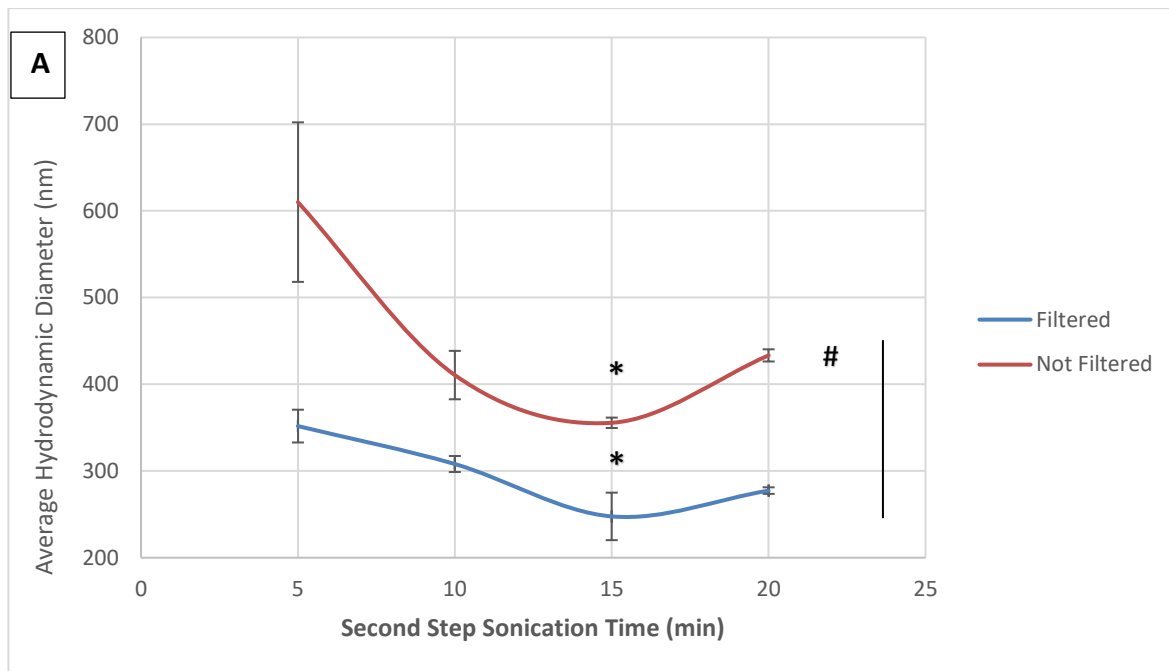


Figure 9 Effect of sonication exposure time in the second emulsification step. (A) The relation between the average hydrodynamic diameter and second step sonication time for both filtered and non-filtered inner aqueous phases [* ($P < 0.05$ vs. 5 min., # ($P < 0.001$) between filtered and non-filtered)] . The size was measured by DLS. The data is reported as mean \pm SEM ($n=3$). SEM images of (B) Double emulsions processed for 10 minutes with a non-filtered inner core. (C) Double emulsions processed for 10 minutes with a filtered inner core. The other parameters were kept constant. (Scale-bar = $2\mu\text{m}$).

Unexpectedly, the size started to increase after that threshold when sufficient energy to disrupt the particles was supplied. This can be either due to the excessive energy that renders the particles unstable or the result of increased foaming, or both. As for the filtration effect, filtering the inner aqueous phase resulted in significantly ($P < 0.001$) lower diameters compared to non-filtered. Filtration aided in taking care of the undissolved PVA or Algs that might have acted as impurities in the process.

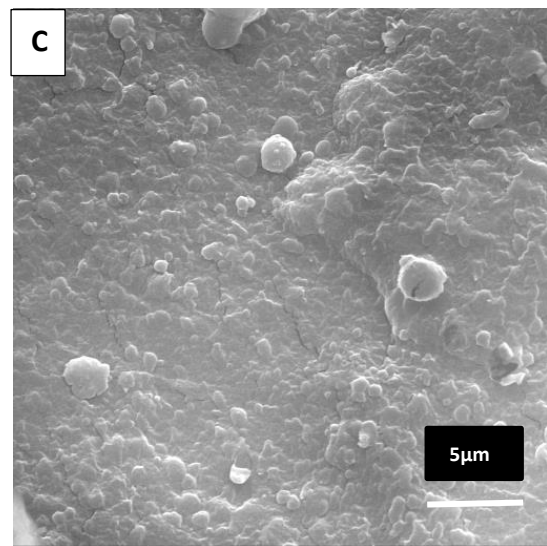
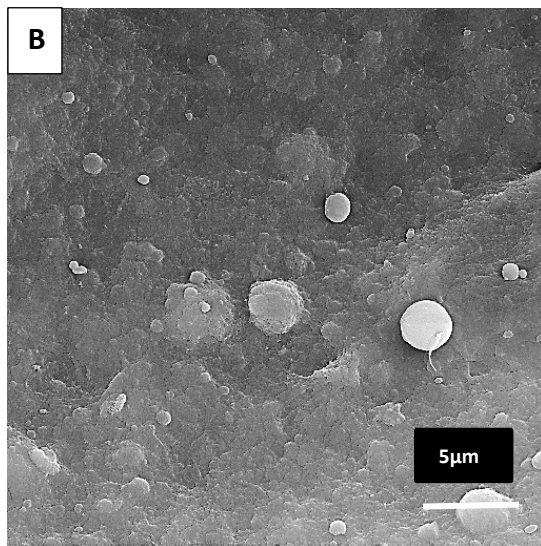
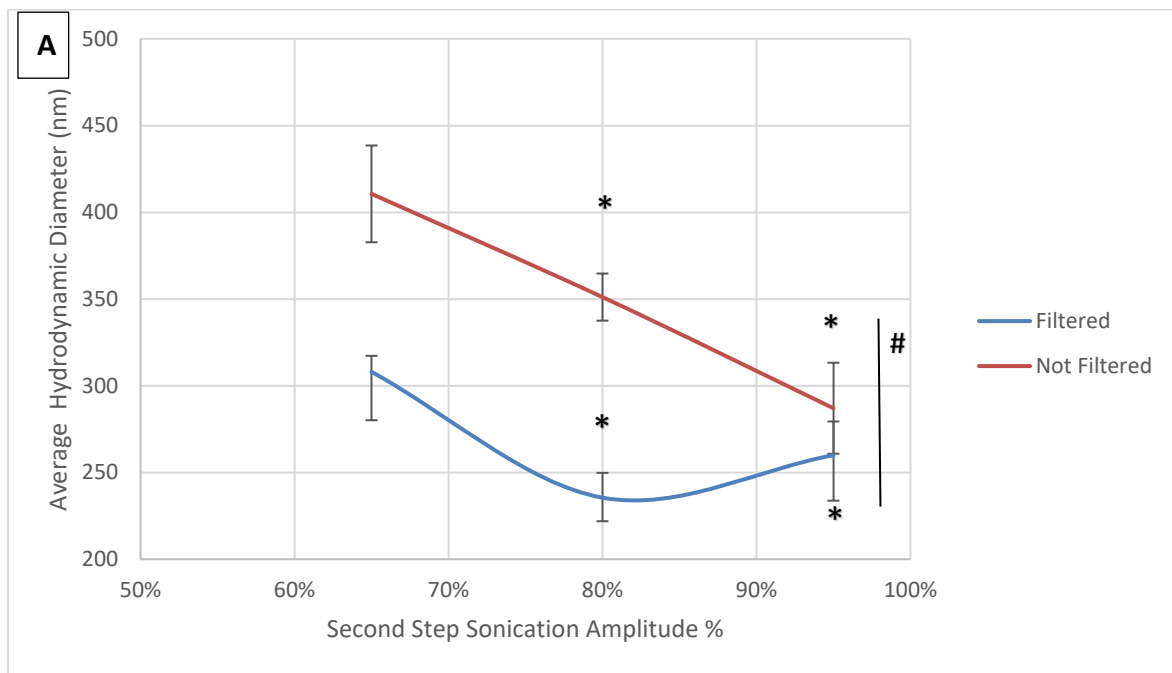


Figure 10 Effect of sonication amplitude in the second emulsification step. (A) The relation between the average hydrodynamic diameter and second step sonication amplitude for both filtered and non-filtered inner aqueous phases [$*(P<0.05)$ vs. 65%, $\#(P<0.001)$ between filtered and non-filtered]. The size was measured by DLS. The data is reported as mean \pm SEM (n=3). SEM images of (B) Double emulsions processed an amplitude of 80% with a filtered inner core. (C) Double emulsions processed at 95% with a filtered inner core. The other parameters were kept constant. (Scale-bar = 5 μ m).

Secondly, the sonication amplitude corresponds to the intensity of cavitation. That is, as the amplitude increases, the alternation frequency between high and low pressure increases, thus, dissipating a high energy. This factor was also investigated based on the second sonication step by setting the amplitude at 65, 80, and 95%. Accordingly, the size was affected in a similar manner compared to the exposure time. It decreased with increasing the amplitude until reaching a minimum of 235.5 nm at 80% and 287.1 nm at 95% for filtered and non-filtered, respectively (Fig.10). In this case, the non-filtered samples did not reach the minimum size threshold that might have been reached if more energy was supplied by sonicating it for a longer time for agglomeration can take place. As for the effect of filtration, the difference in size between samples with filtered and non-filtered inner core was significant ($P=0.000$). This can be attributed to the absence of impurities as mentioned before.

3.1.2 Effect of organic solvent evaporation rate

Organic solvent evaporation is the following step after sonication during which the NP's solidify. The volatile organic solvent escapes through the walls of the polymer creating pores. To study the effect of evaporation rate on the morphology of the particles, containers with different internal diameters were used to simulate varying evaporation rates. The different surface areas were 452.4, 1661.9, and 2463 mm². As depicted in (Fig.11), the larger the surface area (i.e. faster evaporation rate) the smaller the size of the NP's. This is because when the solvent evaporates rapidly, the particles solidify immediately before they fuse again and reaggregate. On the other hand, when the particles

are left for a longer time in suspension, they coalesce due to the disruption of the liquid film between the particles forming larger ones. The relationship constructed between the two variables is linear ($R^2=0.9977$) with a significant difference ($P<0.05$) between the three evaporation conditions.

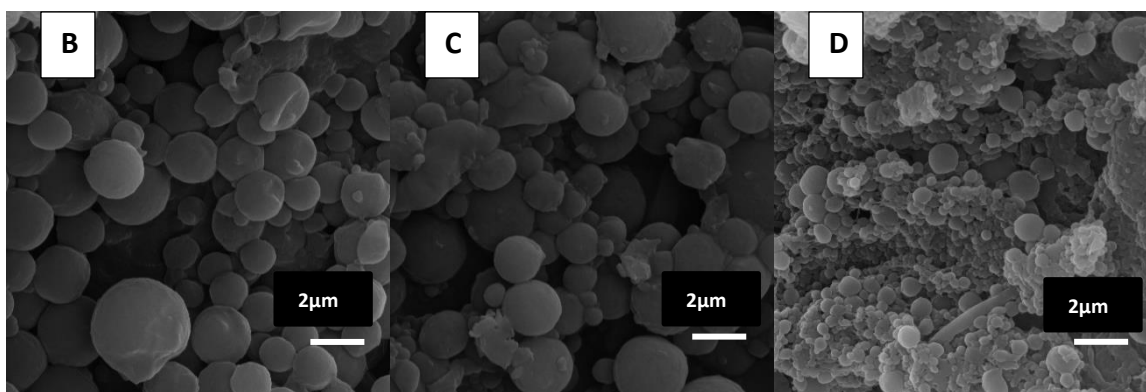
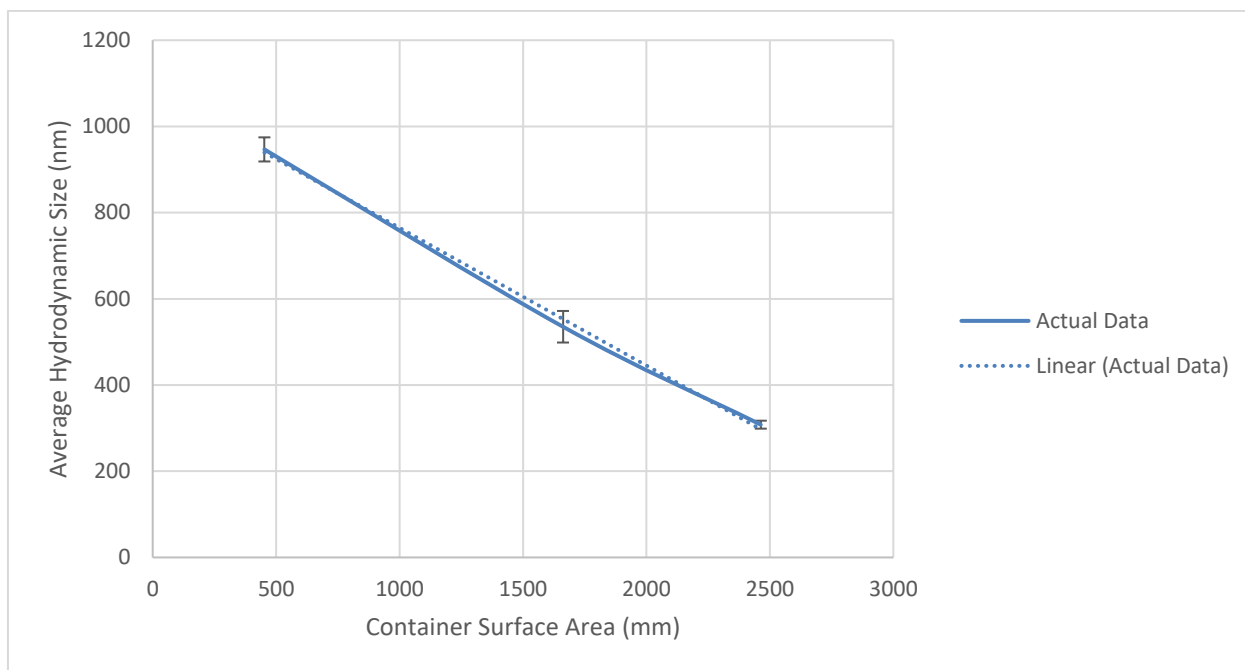


Figure 11 Effect of evaporation rate. (A) Relation between the evaporation rate and the average hydrodynamic size of the particles ($P<0.05$ between the three samples). The size was measured by DLS. The data is reported as mean \pm SEM ($n=3$). SEM images of particles of solutions that underwent (B) evaporation in a 452 mm² container (C) evaporation in a 1661 mm² container, and (D) evaporation in a 2463 mm² container.

3.1.3 Effect of ratio of the outer aqueous phase

Dispersing the primary emulsion solution into the outer aqueous phase transforms them into double emulsions. This third layer is composed of 1% PVA as a stabilizer and 2% CaCl₂ as a crosslinker of the Algs. In order to study the effect of varying the volume of the outer phase, the primary emulsion solution was dispersed into half and double the volume used in the reference sample (5 and 20 ml). As shown in the Fig.12, when the volume increased, the size of the particles increased which agrees with literature [2-3]. This can be attributed to the fact that the delivered energy is distributed on a larger volume delivering less energy per unit volume. In addition, increasing the aqueous phase volume decreases the bulk viscosity; hence, mitigating the energy delivered from the sonicator. The energy supplied by the sonicator depends on the viscosity of the processed volume besides other parameters. Although increased aqueous volume can enhance rate of organic solvent extraction that influences its evaporation, but the apparently the particles were already large due to sonication limitations. However, this led to elimination of fibrous structures that were evident sometimes in the reference sample. Therefore, to exploit the advantage of stability without the side-effect of the increase in diameter, an additional aqueous phase containing PVA as a stabilizer can be added after emulsification and before the evaporation step to avoid interference of the increased volume with energy. On the hand, when the volume was halved, double emulsions did not successfully form (Fig.12 C).

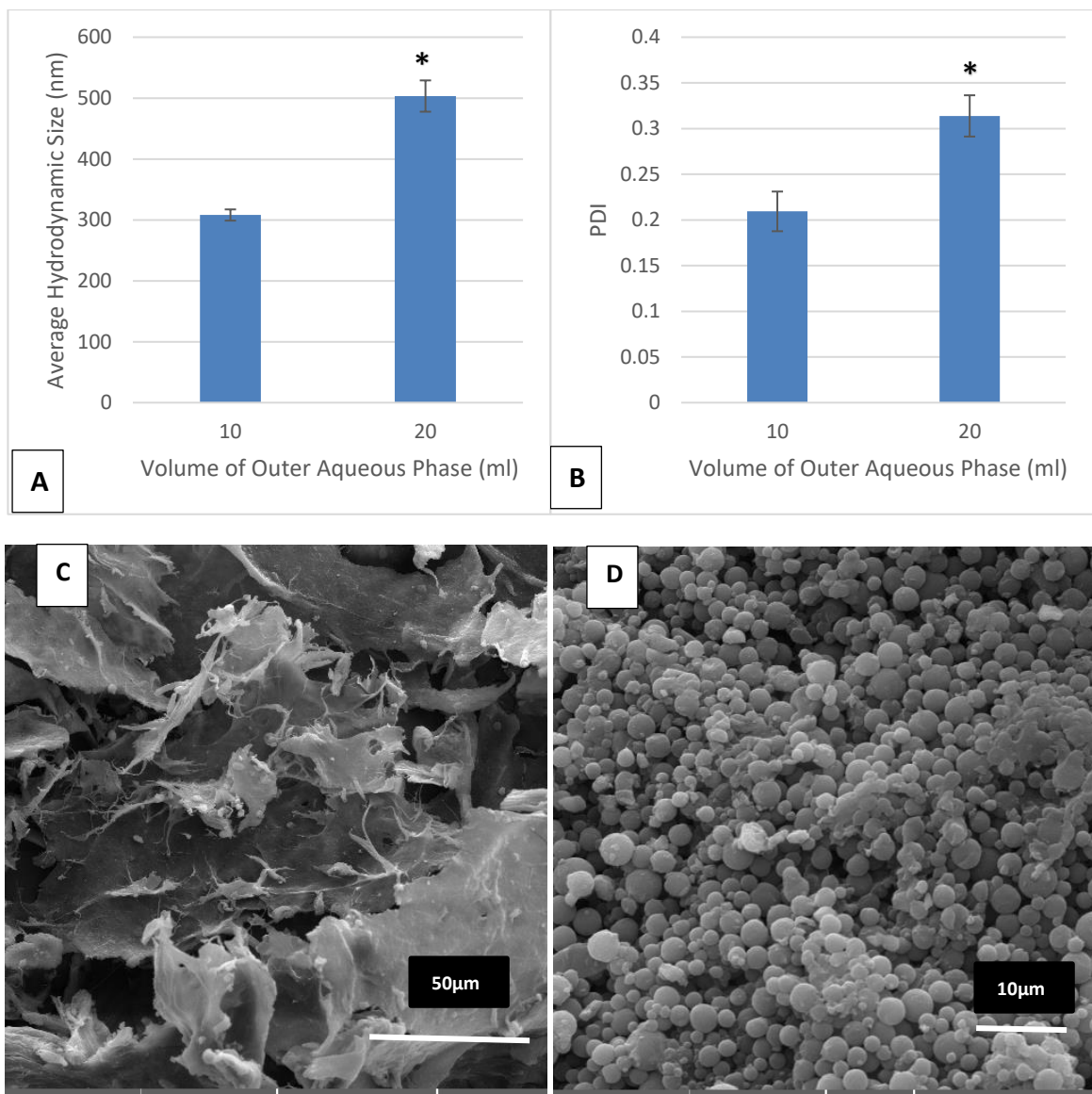


Figure 12 Effect of the volume of the outer aqueous phase on the particles. (A) The average hydrodynamic diameter vs. the volume of the outer aqueous phase ($P < 0.05$). (B) PDI vs. the volume of the outer aqueous phase ($*P < 0.05$). The size and PDI were measured by DLS. The data is reported as mean \pm SEM ($n=3$). SEM images of (C) sample with 5ml outer aqueous phase particles did not form (Scale bar = 50 μm), and (D) sample with 10 ml outer aqueous phase (Scale bar = 10 μm).

3.1.4 Effect of the processed volume

This study was implemented to verify the ability of scaling-up this process and to investigate the effect of the total processing volume on the size. The total volume of the reference sample was first halved and then doubled while keeping the phase ratio constant. As evident in Fig.13, there is a positive relationship between size and total volume. This could be explained by the situation described earlier regarding the distribution of energy on a larger volume and, thus, decreasing the intensity per unit volume. The difference was not significant when the volume increased from 7.5 to 15 ml; however, it became significant when it reached 30 ml. Furthermore, the relation between the size and the volume is linear indicating the ease of scaling-up the process into an industrial scale or lowering the volume based on the desired drug to be loaded.

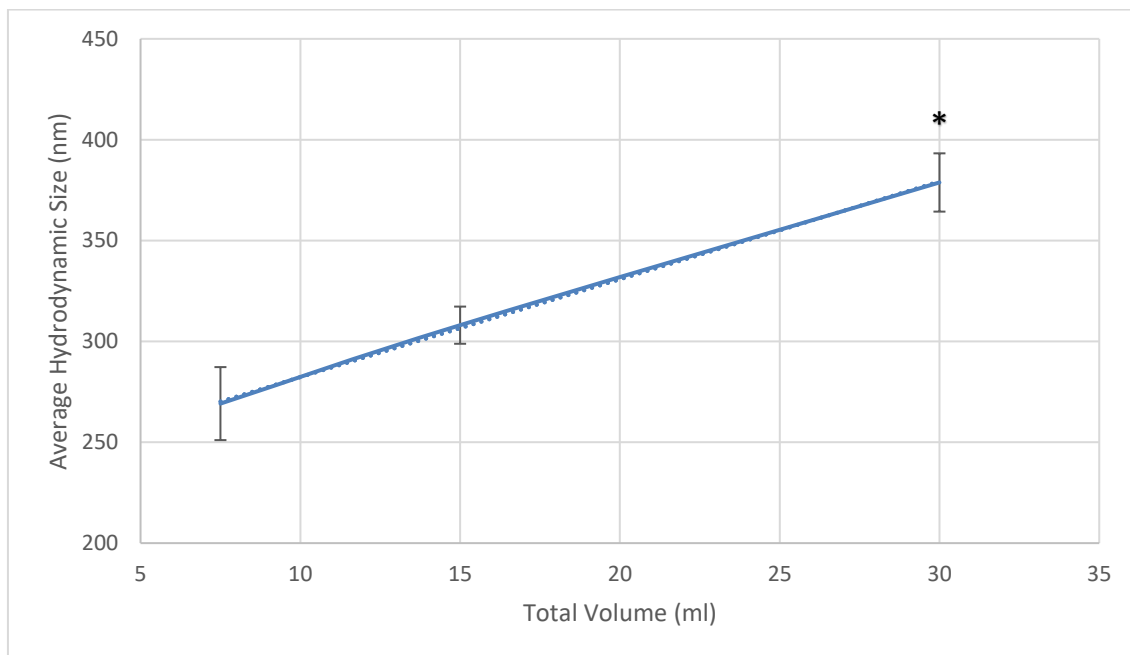


Figure 13 Effect of total processing volume on the average hydrodynamic size while keeping the phase ratio constant (* $P < 0.05$ vs. 7.5 ml and 15 ml). The size was measured by DLS. The data is reported as mean \pm SEM (n=3).

3.1.5 Effect of using sulfated alginates as the inner core

Algs with a degree of sulfation 2.0 were dissolved in the inner aqueous phase instead of pure Algs compared to the reference sample. It was shown that including AlgSulf_{2.0} led to significant reduction in and size and lower PDI (Fig.14). The smaller NP's resulted from the softer nature of the AlgSulf compared to the pure ones since they have much lower molecular weights (11KDa) compared to the pure ones (900KDa). In other words, introducing sulfate moieties diminishes the storage modulus due to lower crosslinking density [4].

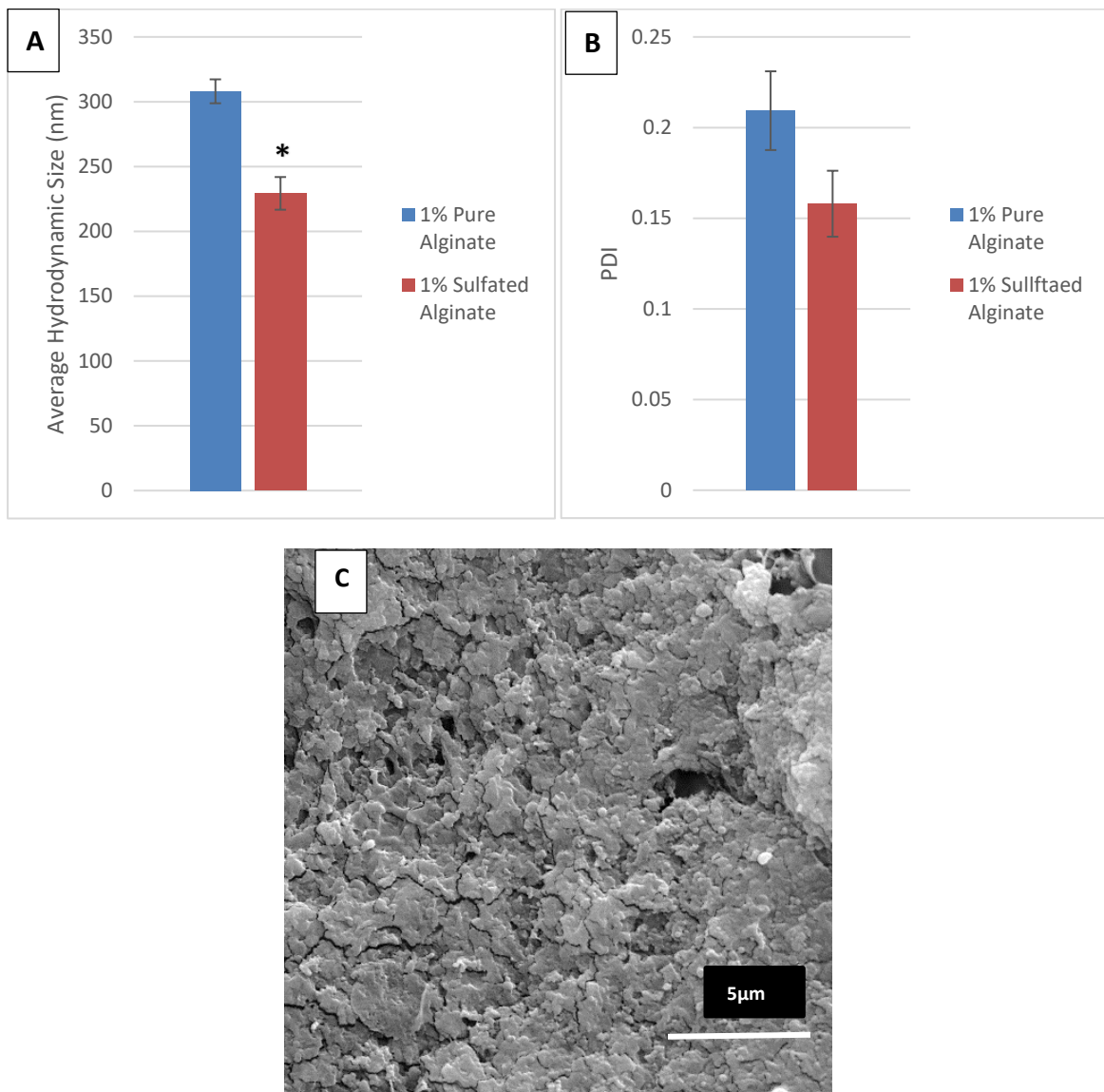


Figure 14 AlgSulf2.0 instead of pure Alg in the inner aqueous phase. (A) The average hydrodynamic size vs. pure or sulfated Alg in the inner core (* $P < 0.05$). (B) PDI of the particles vs. pure or sulfated alginate in the inner core. The size and PDI were measured by DLS. The data is reported as mean \pm SEM (n=3). (C) SEM image of AlgSulf_{2.0} PCL particles.

3.2 Modeling

3.2.1 Effect of energy

In order to generate consistent results when using different sonicators, there should be a parameter that is directly related to the morphology of the particles. For instance, sonication time and amplitude correspond to the energy delivered to the processed liquid; however, they lead to different outputs depending on the specifications of the instrument. On the other hand, acoustic energy is the main factor affecting the size and could be manipulated by the time and amplitudes has been shown in the previous experiments. Therefore, the aim of this section is to explore whether the morphology depends solely on the total magnitude of energy or on the rate of delivery as well. Furthermore, a calibration curve was generated to predict the size based on calculating the energy allocated for disruption of the particles in the second emulsification step after eliminating heat losses.

Step 2		1 st Phase		Oil Phase	2 nd Aqueous Phase									
Time (min)	T1 (°C)	T2 (°C)	Δ T (°C)	Q (J)	Q (J)	T1 (°C)	T2 (°C)	Δ T (°C)	Q (J)	Total Heat (J)	E 2 (J)	E of sonication (J)	Size (nm)	
5	34	36	2	8	13	25	36	11	459	480	1857	1377	352	
10	34	46	12	49	74	25	46	21	863	986	3645	2660	345	
15	34	58	24	98	149	25	58	33	1356	1602	7145	5543	248	
20	34	62	28	118	178	25	62	37	1549	1845	11129	9284	277	
Step 2				1 st Phase	Oil Phase	2 nd Aqueous Phase								
Amplitude (%)	T1 (°C)	T2 (°C)	Δ T (°C)	Q (J)	Q (J)	T1 (°C)	T2 (°C)	Δ T (°C)	Q (J)	Total Heat (J)	E 2 (J)	E of sonication (J)	Size (nm)	
65	34	46	12	49	74	25	46	21	863	986	3645	2660	345	
80	34	50	16	66	100	25	50	25	1032	1198	7486	6288	236	
95	34	60	26	108	164	25	55	30	1252	1524	9232	7707	260	

Table 2 Energy allocated for disrupting the spheres by eliminating heat losses.

Table 3.1 summarizes the energy calculations and was used to draw two curves, one based on energy from time and the other from amplitude. As illustrated in Fig., the curves based on the actual data are in unison. Hence, the magnitude of the delivered energy is the controlling factor rather than the rate of delivery. Subsequently, the curves were fitted into the two model equations shown below:

$$\text{Through Time Variation: } \bar{d} = 0.364 \times 10^{-5} E^2 - 0.0504 E + 428.6$$

$$R^2 = 0.8724$$

$$\text{Through Amplitude Variation: } \bar{d} = 0.939 \times 10^{-5} E^2 - 0.114 E + 582.1$$

$$R^2 = 1$$

where \bar{d} : Average Diameter (nm)

$$E = E_2 - Q$$

where E_2 : Energy displayed by the sonicator, Q is total heat losses.

The two equations were evaluated at different values of energy and the difference between the two was measured using paired sample T-test on SPSS. The difference between them was insignificant ($P=0.28$). Therefore, their average of the data obtained from both was employed to create an energy calibration curve:

$$\bar{d} = 0.703 \times 10^{-5} E^2 - 0.0862 E + 511.1$$

The size of the nanoparticles can be predicted despite the type of sonicator given that the value of the energy delivered to the sample is provided by the device.

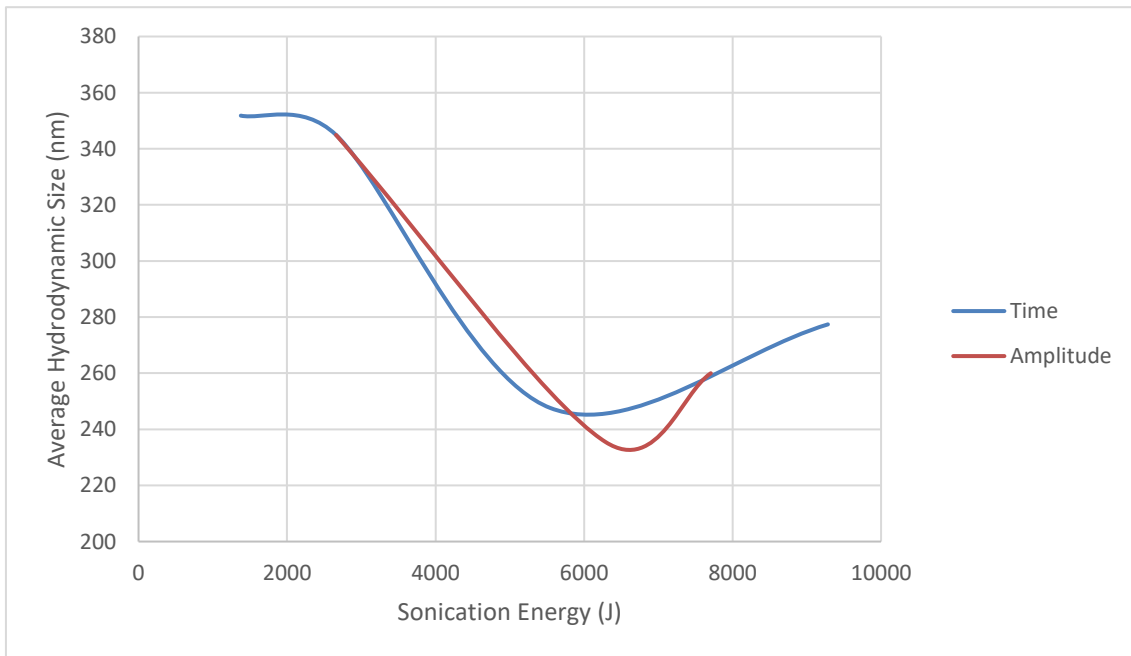


Figure 15 Effect of sonication energy released when processing time and amplitude were varied on the average hydrodynamic size based on actual data.

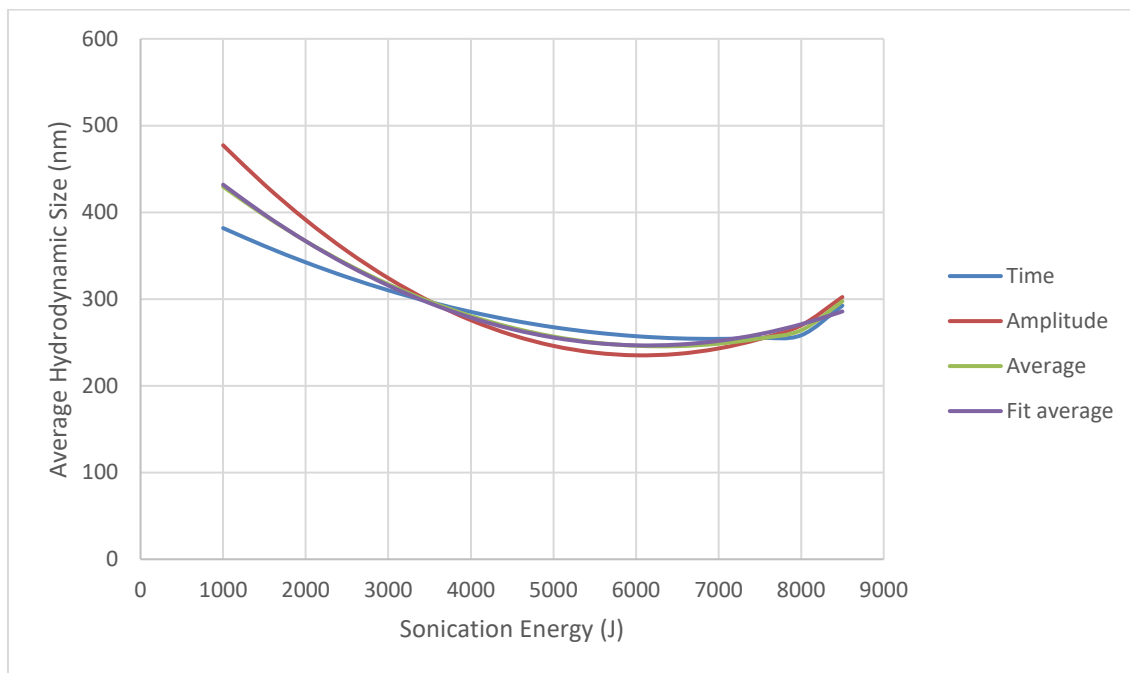


Figure 16 Curve-fitting based on the relation between the average hydrodynamic size and sonication energy.

3.2.2 Effect of sonication time, amplitude, and processing volume

Based on the results examined earlier, curve-fitting was applied to build a relationship between the size of NP's and sonication parameters.

Time

$$\bar{d} = 0.7355t^2 - 24.06t + 4$$

$$R^2 = 0.9038$$

where t: second step sonication exposure time (min)

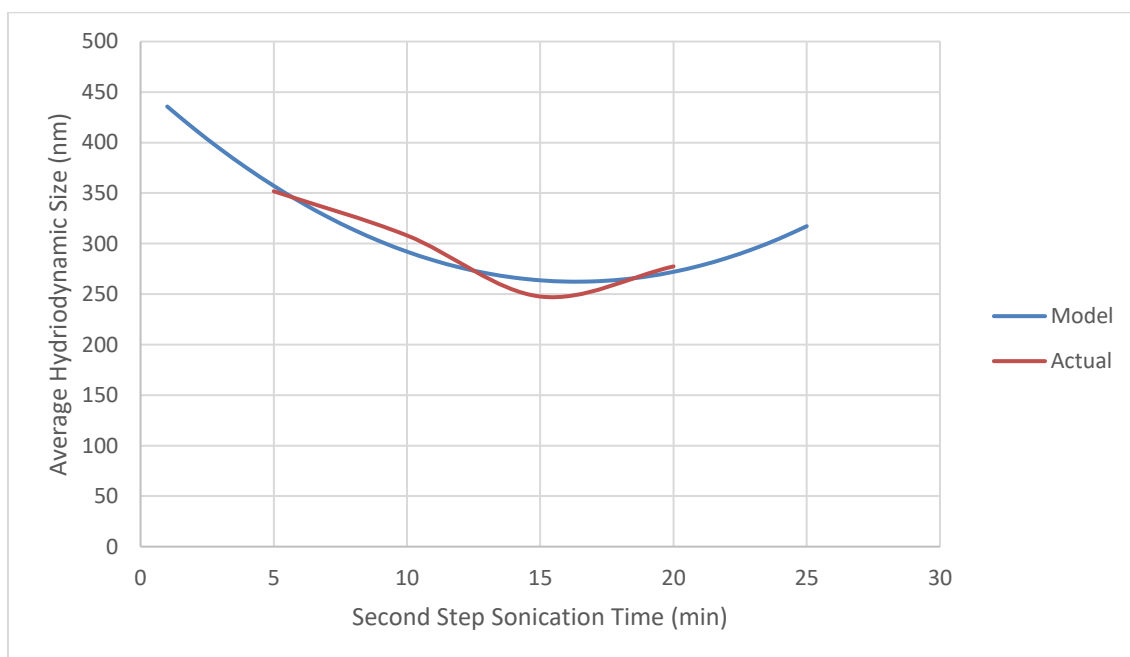


Figure 17 Modeling of the average hydrodynamic size based on second step sonication time.

Amplitude

$$\bar{d} = 0.2176A^2 - 36.4E + 1756$$

$$R^2=1$$

where A: second step sonication exposure amplitude (%)

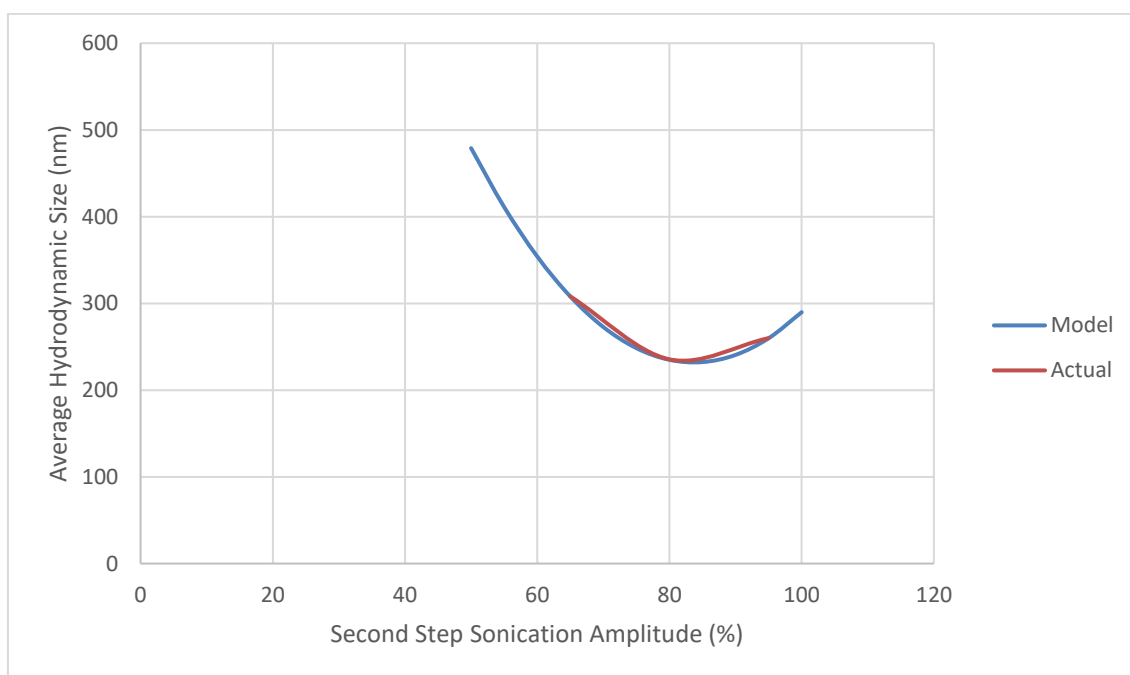


Figure 18 Modeling of the average hydrodynamic size based on second step amplitude.

Processing Volume

$$\bar{d} = 4.85V + 233.8$$

$$R^2=1$$

where V: total processing volume (ml)

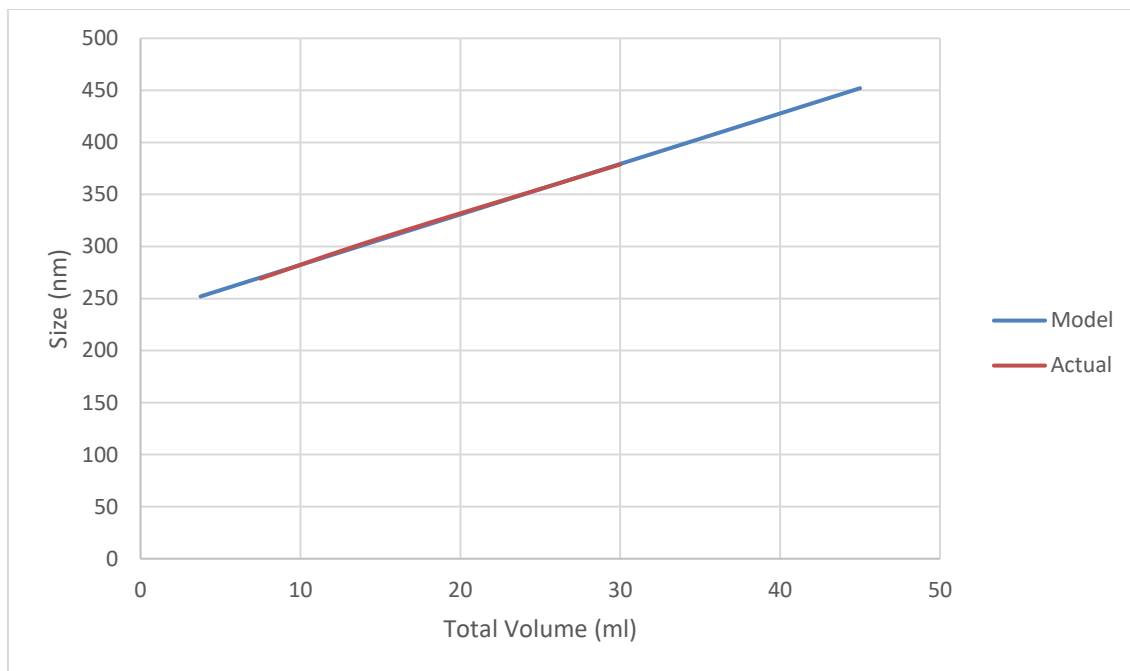


Figure 19 Modeling of the average hydrodynamic size based on total processing volume while keep phase ration constant.

Unlike energy, these models vary based on the specifications of the instrument itself in terms of type of the probe and power.

3.3 Effect of loading different amounts of BSA on size

Varying amounts of BSA (1, 5, and 10 mg) were loaded into (1%) Alg PCL. The different amounts did not affect the size of the resulting NP's as shown in Fig.21.

Therefore, entrapping relatively low amounts of the desired protein for different applications along with any amount of BSA within this range will not affect the size.

Therefore, in the following studies of encapsulation efficiency and release profile, 10 mg of BSA was dissolved in the inner aqueous phase.

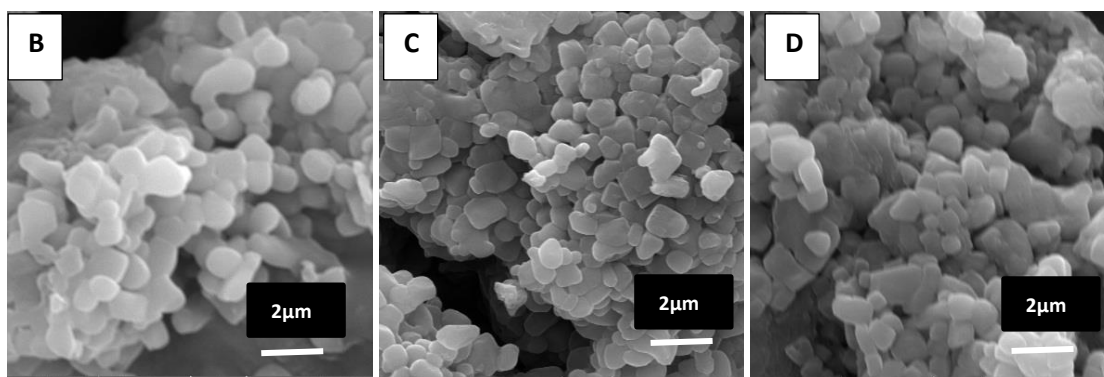
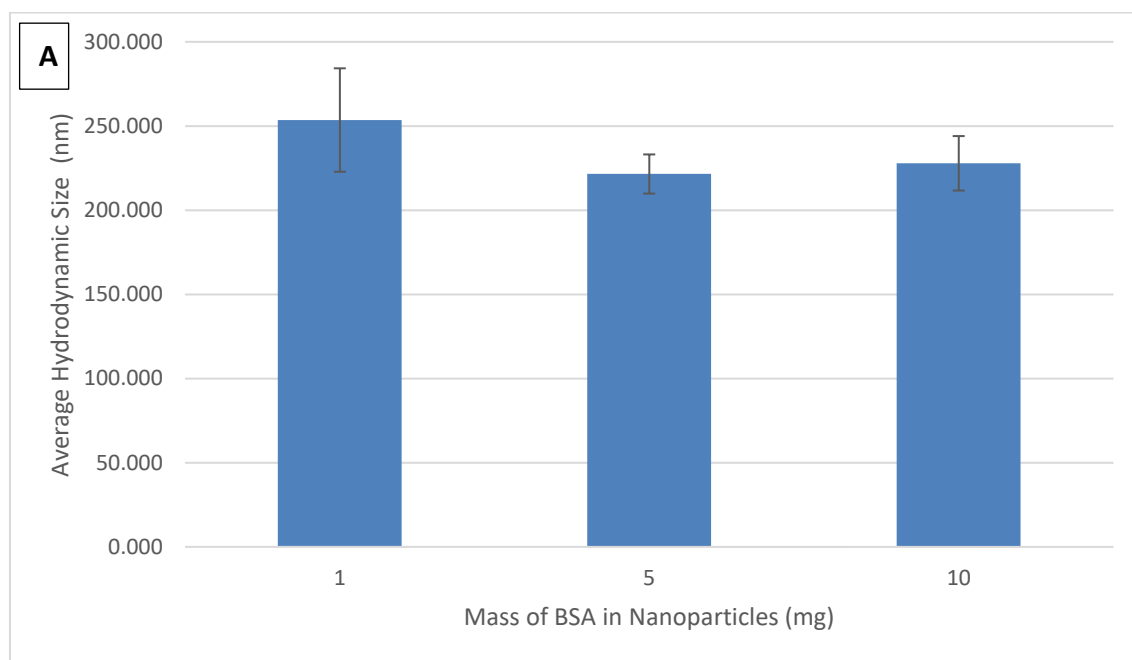


Figure 20 Effect of BSA amount in the inner aqueous phase on the average hydrodynamic size of the particles. (A) Relation between the amount of BSA on the size. The size was measured using DLS. The data is reported as mean \pm SEM ($P < 0.05$, One-Way ANOVA, $n = 3$). SEM images of (A) 1 mg, (B) 5mg, and (C) 10mg of BSA in the inner aqueous phase.

3.4 Encapsulation Efficiency

The optimal formulation for drug encapsulation is to be determined by the physiochemical properties of the different types of particles. In other words, by studying the size, PDI, zeta-potential, and EE% upon encapsulating BSA as a model drug. With regards to the preparation parameters, the faster the particles solidify, the higher the EE since proteins will not get enough time to diffuse into the continuous phase [3]. Therefore, the container with the largest surface area, 2463 mm², was used to accelerate evaporation rate. Increasing the concentration of pure alginate from 1% to 2% in the inner core of PCL particles increased its viscosity leading to a significantly higher EE% from 71.6 to 87.4%. Furthermore, including AlgSulf_{2.0} instead of pure alginate in the first aqueous phase significantly increased EE% from to 94.7%. This can be attributed to the fact that BSA has positively charged moieties of lysine and histidine [7] that can attach to the negatively charged sulfate groups in the alginate. Since the viscosity of the inner core affects the EE as shown when comparing PCL NPs containing 1% against 2% Alg in the inner, increasing the concentration of AlgSulf could increase the EE since it is known to be much softer than the pure ones.

The difference between PCL and PLGA in terms of EE was not significant as shown on Fig.22.A. since in both formulations 2% Alg was utilized. With respect to the size, the three formulations listed in Table 3.2 had approximately equal diameters of about 200nm. This specific size is within the optimal size range (100-200) to achieve efficient biodistribution and maximal residence time where 60% of the particles were retained. In contrast, about 20% of the particles out of that range remain in circulation. In other words, particles are more prone to be cleared by the body in case their diameter is less than 50 nm

or more than 250nm [8]. On the other hand, the PDI was lower in the case of PCL compared to PLGA indicating higher monodispersity.

Formulation	Average Size (nm)	PDI	Zeta Potential (mV)
(2%) Pure Alg PCL	205.88±12.9	0.125±0.045	-15.63±3.41
(2%) AlgSulf_{2.0} PCL	202.87±21.18	0.130±0.037	-18.26±1.88
(2%) Pure Alg PLGA	209.23±3.2	0.142±0.0048	-11.40± *1.47

Table 3 The average size, PDI and zeta potential of the three different formulations (*P<0.05 vs. AlgSulf2.0PCL).

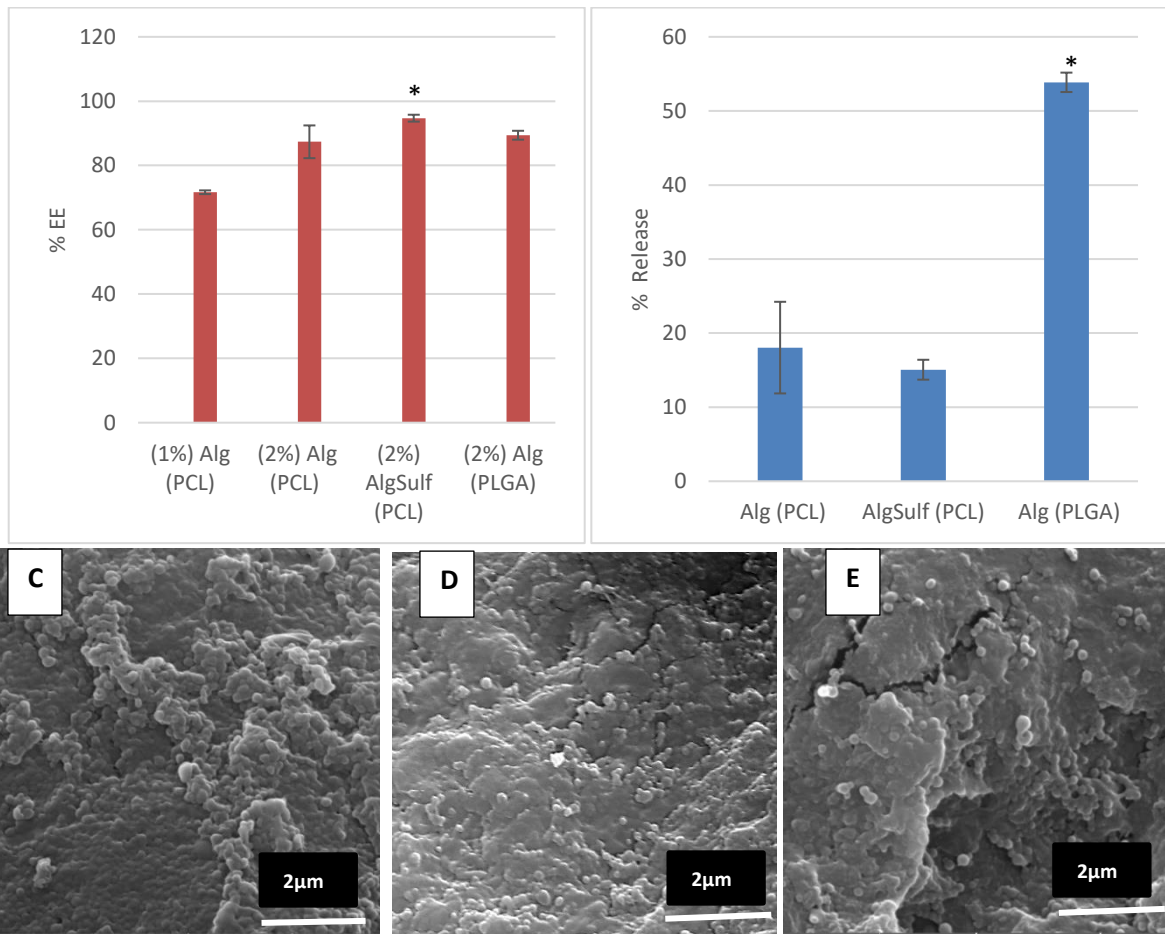


Figure 21 Comparing the encapsulation efficiency and the burst release of the different formulations. (A) The effect of the inner core and the intermediate phase polymer on the efficiency of BSA encapsulation (* $P \leq 0.05$ vs. 1% Pure Alginate PCL, $\Delta P < 0.05$ vs. 2% AlgSulf_{2.0} PCL, # $P = 0.05$ vs. 2% AlgSulf_{2.0} PCL). (B) The effect of the inner core and the intermediate phase polymer on the initial release after dispersion * $P < 0.05$ vs. 2% Pure Alginate PCL and 2% AlgSulf_{2.0} PCL). The data is reported as mean \pm SEM (n=3). SEM images of (C) 2% pure alginate PCL, (D) 2% AlgSulf_{2.0} PCL, and (E) 2% pure alginate PLGA.

The three formulations exhibited a negative surface charge implying colloidal stability. However, the zeta-potentials of PCL particles prepared with both pure alginates and sulfated alginates were lower compared to PLGA. The further are the values from 0mV, neutral, the higher the stability is. Although these particles are not highly charged

compared to the ones reported in literature [8] but them being in this range (-10 to -20mV) is considered an advantage. Highly charged particles, positively or negatively, have an exceptionally high colloidal stability but are subject to clearance [3,8-9]. For instance, particles with a size of 200nm and zeta potential of -15 mV remained for a longer time compared to particles with different specifications. In addition, highly negative or positive particles can contribute to the activation of mitogenic signaling pathways such as ERK or AKT [9].

3.5 *In Vitro* Release Studies

The accumulative release from the different formulations is illustrated in Fig.23 The amount of released BSA into PBS was quantified using Lowry assay at different time points. The initial one being at 0hr which represents the burst release. Particles covered with PLGA released a significant amount of BSA ($\approx 50\%$) upon dispersion into PBS (pH 7.0) compared to other formulations. This amount was reduced to 44.4% when PLGA particles were dispersed into PBS at high pH (8.00). This can be due to the increased concentration of salts and, thus, osmotic pressure decreases solute diffusion from the particles. A very high burst release can lead to cytotoxicity due to increased drug dose and the target.

PLGA elucidated the most rapid release profile. This is due to its amorphous structure against the crystalline structure of PCL [10]. Hence, the amorphous sites serve as targets for water molecules leading to hydration and relaxation of the polymer chains. As a result, faster diffusion of the drug through the polymer matrix takes place [11].

As for the release profiles of AlgSulf_{2.0} and pure Alg with PCL, the results showed that they did not have significant differences in burst release (<25%). Therefore, this confirms

the previous finding regarding PLGA being the responsible factor of the high initial release. With time, the AlgSulf_{2.0} released more of the drug due to the swelling of the gel compared to pure Alg. Either profiles can be preferable depending on the delivery application. However, in case of wound healing applications, faster release is desired during early treatment days [12]. The obtained results might vary based on the encapsulated drug. Namely, if heparin-binding growth factors such as CTGF or IGF were encapsulated, they might bind to AlgSulf_{2.0} affecting the release rates. Moreover, to further control the release profile, pure Alg can be mixed with AlgSulf to tune the mechanical properties of the inner core.

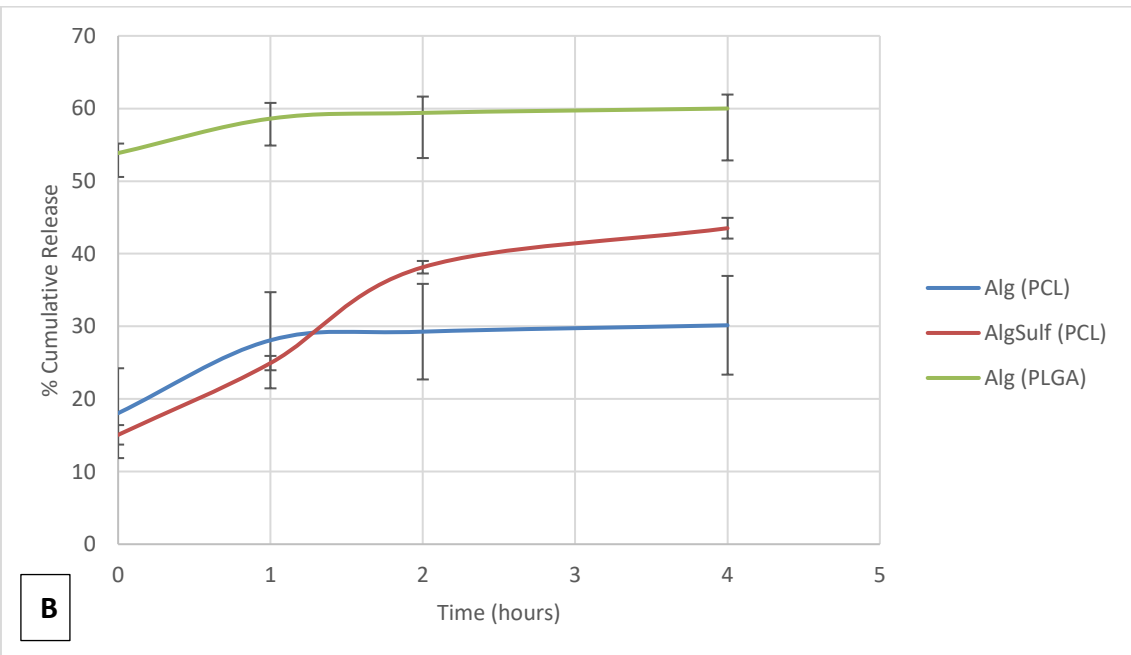
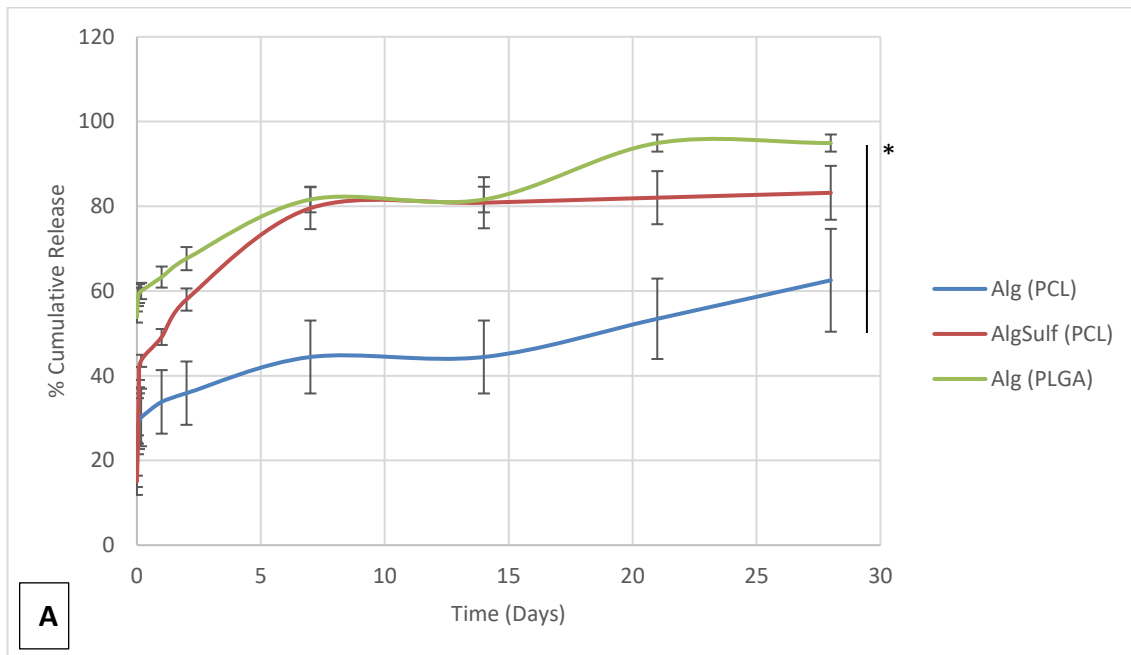


Figure 22 Cumulative release profile of BSA from the three different formulations, 2% Alg PCL, 2% AlgSulf2.0 PCL, and 2% Alg PLGA. (A) The release measured over 28 days. (B) The release during the first 4 hours. The data is reported as mean \pm SEM. (* $P < 0.05$ between the three samples, Two-Way ANOVA, $n=3$).

With respect to the release conditions, particles that experienced shaking while incubation had a significantly higher BSA release rates as illustrated in Fig.24. Hence, it also depends on the ultimate aim of the carrier.

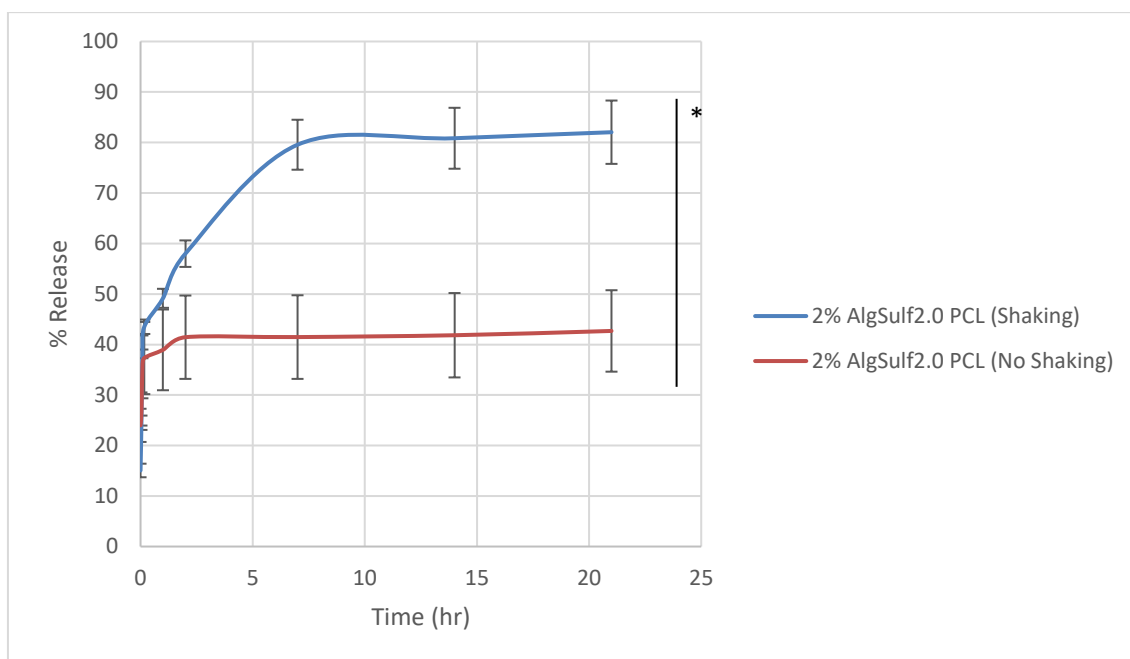


Figure 23 Cumulative release profile of BSA from the 2% AlgSulf2.0 with or without shaking during incubation. The data is reported as mean \pm SEM. ($P < 0.05$, Two-Way ANOVA, $n=3$).

3.6 Thermal and Colloidal Stability of the Nanoparticles

NP's are considered as a colloidal system that can cause cytotoxic effects if becomes unstable (i.e. Aggregation) when dispersed in different types of media or placed at elevated temperatures. Therefore, the thermal stability was investigated by monitoring the size and PDI of the particles with time upon incubation at 37°C. As results show Fig.3.25 the size and PDI did not change over time implying the absence of aggregations and the stability of the high stability of the system. The colloidal

stability was also determined upon dispersing the particles in cell culture medium. Their size and PDI did not change significantly indicating their stability in biological fluids.

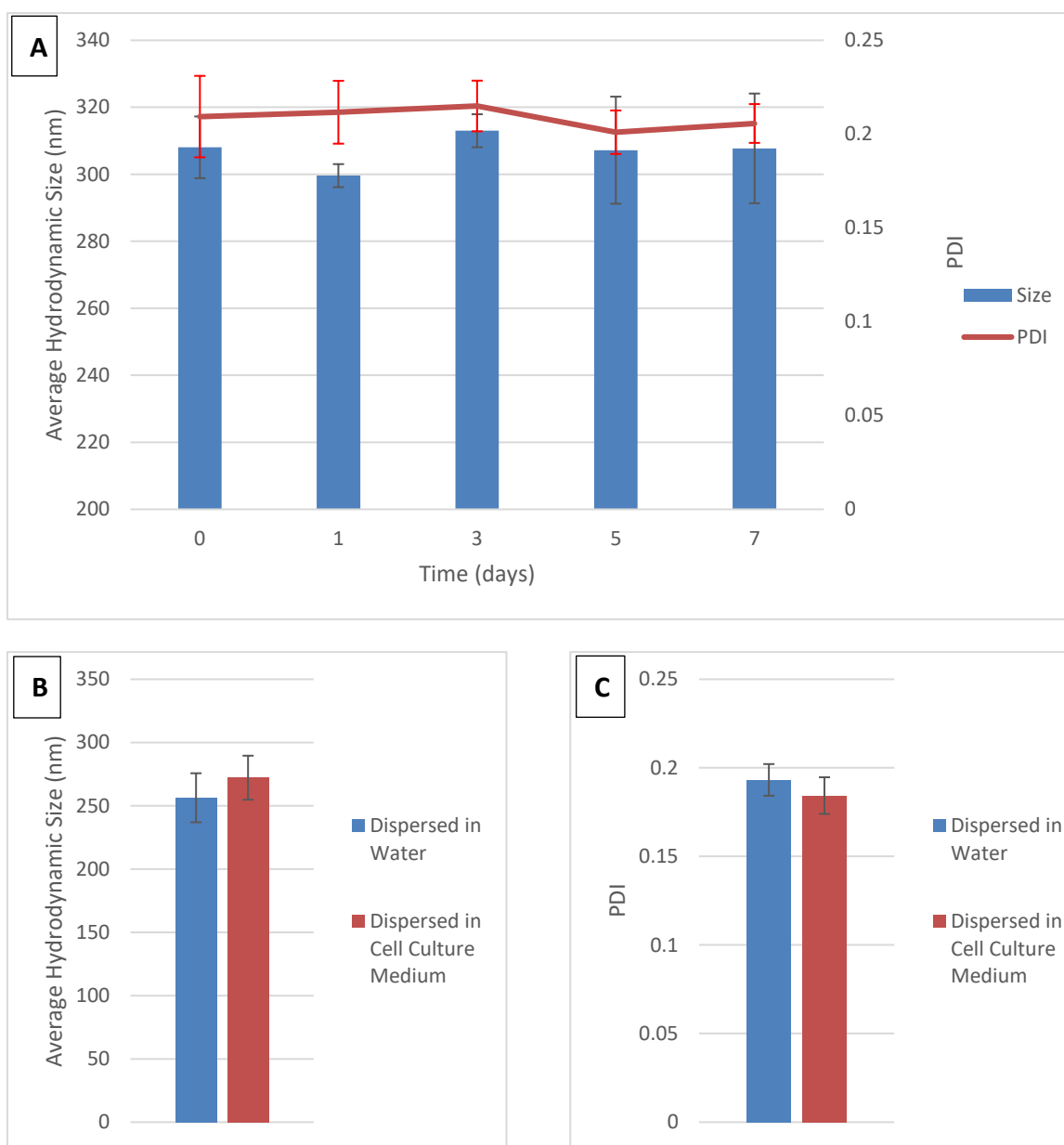


Figure 24 NP's thermal and colloidal stability studies. (A) The change in the average hydrodynamic size and PDI of the NP's over time while incubated at 37°C ($P>0.05$, One-Way ANOVA). (B) The average hydrodynamic size and (C) PDI of the NP's after dispersing them in water vs. in cell culture medium ($P>0.05$, T-test). The data is reported as mean \pm SEM (n=3).

3.7 Cytotoxicity studies

The toxic effects of the Alg/PCL NPs were tested against HaCat cell line through three different approaches. These approaches included Trypan-Blue exclusion, MTT, and immunoblotting assays.

3.7.1 Trypan-Blue exclusion assay

HaCat cells were incubated with varying concentration of NP's (5, 25, 50, and 100 $\mu\text{g/ml}$) for different time points (24, 48, and 72 hr). The viability decreased as a function of increasing concentration (Fig.3.16). Based on Two-Way ANOVA the interaction parameter between concentration and time was not significant ($P=0.165$). At concentrations of 50 and 100 $\mu\text{g/ml}$, the significance value was $P<0.05$. However, at these two concentrations, the viability increased significantly after 72 hr indicating a decrease in toxicity with time. In addition, the lowest value attained was 80.2% at the highest concentration, implying the low toxicity of the particles.

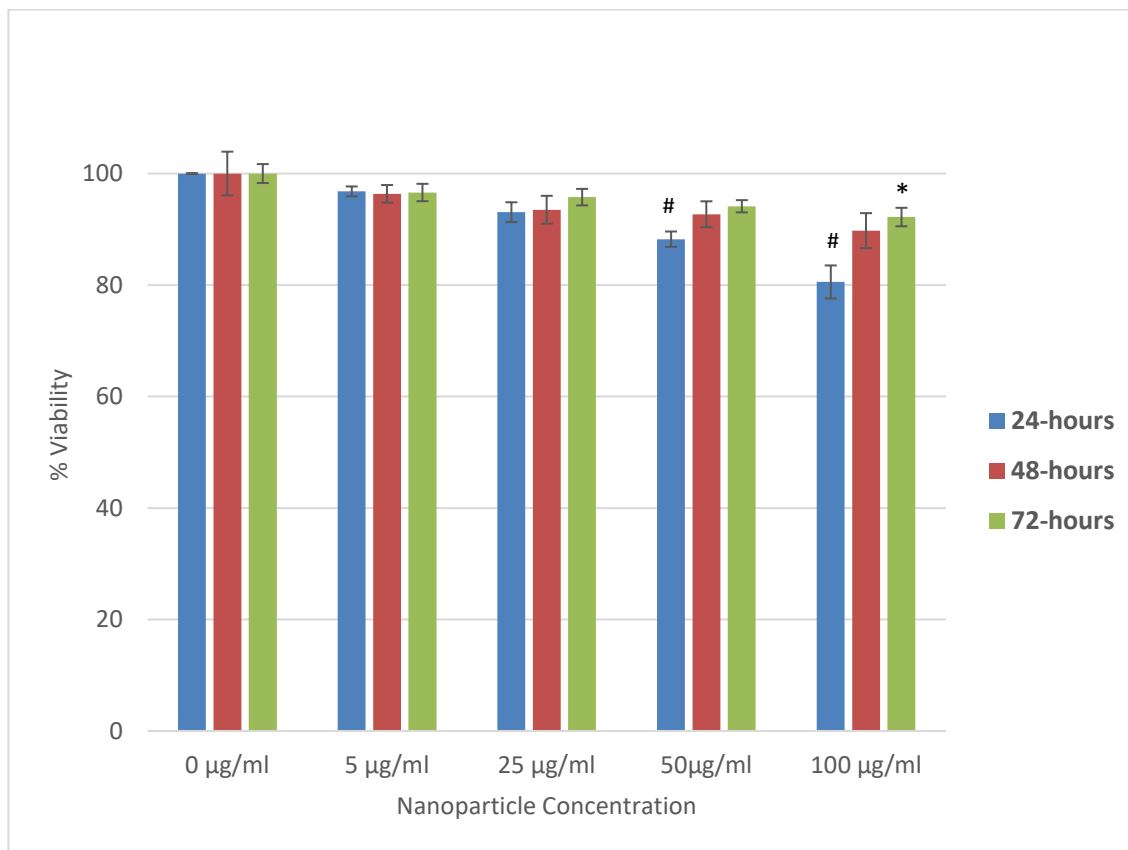


Figure 25 % Viability of HaCaT cells using Trypan Blue as a function of NP's concentration. The interaction parameter between concentration and time was not significant $P=0.165$ as shown by a Two-Way Anova, particle concentration was a significant factor $P<0.05$ with significant differences for concentrations $\geq 25\mu\text{g/ml}$ (# non-significant compared to $0\mu\text{g/ml}$). However, for 72h cultures significant differences were only found at $100\mu\text{g/ml}$ as show by One-Way Anova $*P<0.05$, and for 24h cultures significant differences were found at 50 and $100\mu\text{g/ml}$. The data is reported as mean \pm SEM (n=3).

3.7.2 MTT assay

The MTT assay was performed at different concentrations of the particles for 24 hr only based on the Trypan-Blue exclusion assay results (viability was lowest at 24 hr). However, the amount of particles corresponded to the ones in the previous assay in terms the area of the well rather than concentration. As illustrated in Fig.27, no cytotoxicity was observed regardless of the

concentration. This could be because MTT assay does not directly reflect viability. In fact, the endocytosis process by which polymeric nanoparticles enter the cells is energy dependent [14]. Thus, more energy could have been consumed as the concentration increased.

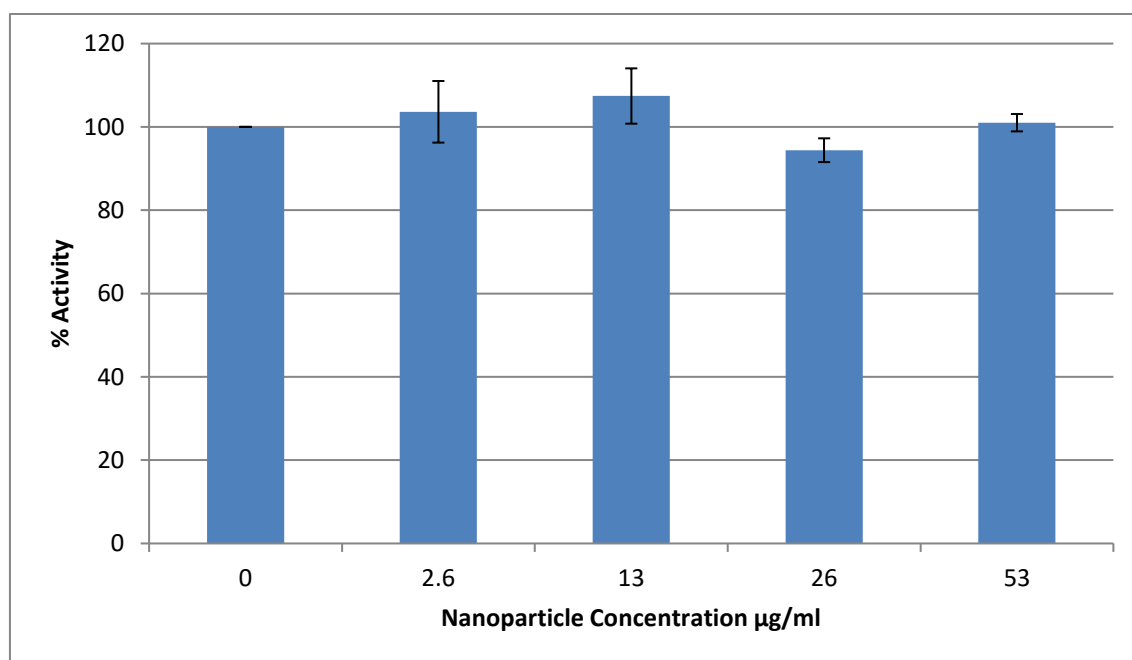


Figure 26 % Activity of HaCaT cells using MTT assay as a function of NP's concentration. The data is reported as mean \pm SEM. ($P > 0.05$, One-Way ANOVA, $n=3$).

3.7.3 Immunoblotting

To determine whether the particles are inert or not, HaCat cells were incubated with increasing concentration of the particles (5, 25, 50, and 100 $\mu\text{g/ml}$) for 15 minutes. In response, P-ERK and P-AKT which are usually activated due to extracellular signals to regulate proliferation, migration, and growth were not activated. According to the results in Fig.28 A and Fig.28 B, there was no significant difference between the bands at different concentrations for both kinases. Therefore, due to the optimal size and surface charge discussed earlier, no cytotoxic effects were

elucidated. Furthermore, the decreased viability at high concentrations measured by Trypan Blue is probably due to the stress on the cells rather than the presence of cytotoxic constituents.

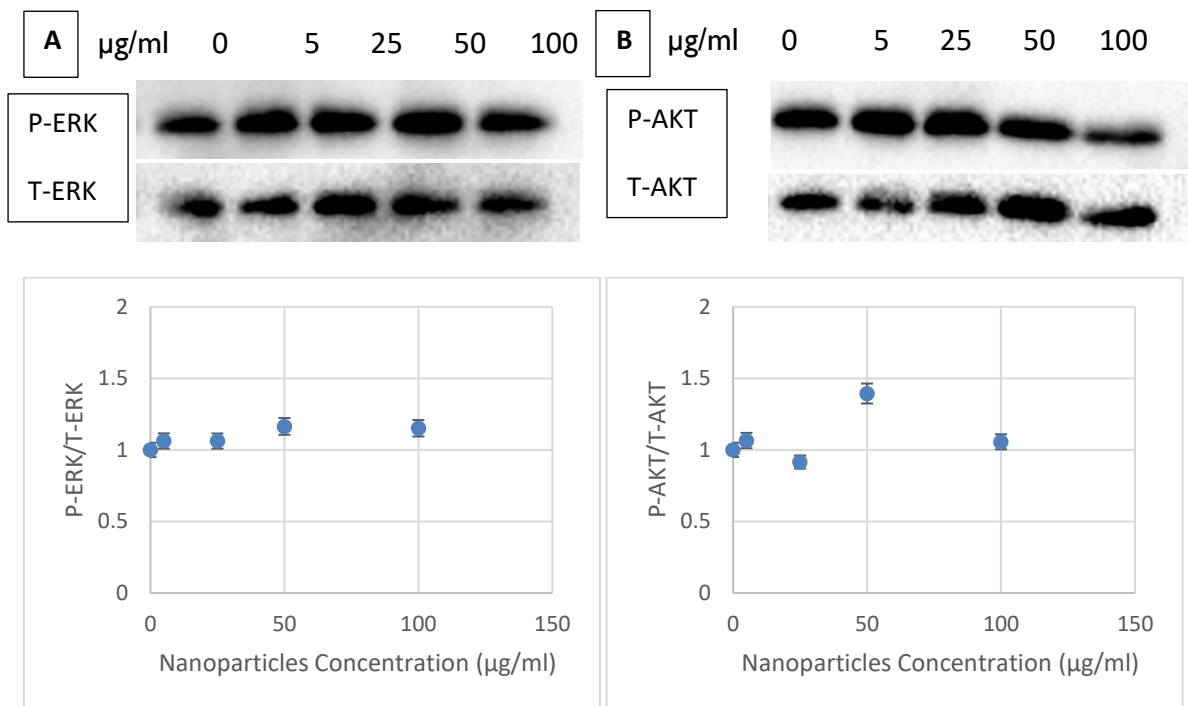


Figure 27 Regulation of ERK and AKT signaling by NP's in HaCat cells. Activation of (A) ERK and activation of (B) AKT was assessed after 15 minutes by immunoblotting. The data is reported as mean \pm SEM. ($P > 0.05$, One-Way ANOVA, $n=3$).

3.8 References

- [1] M. Iqbal *et al*, "Preparation of biodegradable PCL particles via double emulsion evaporation method using ultrasound technique," *Colloid and Polymer Science*, vol. 293, (3), pp. 861-873, 2015.
- [2] Y. Yoon and K. Park. "Control of encapsulation efficiency and initial burst in polymeric microparticle systems." *Archives of Pharmacal Research*, vol. 27, (1), 2004.
- [3] B. Taghipour *et al*, "The effects of technical and compositional variables on the size and release profile of bovine serum albumin from PLGA based particulate systems," *Research in Pharmaceutical Sciences*, vol. 9, (6), pp. 407-420, 2014.
- [4] Mark, H. F. (Herman Francis) and Wiley InterScience (Online service), *Encyclopedia of Polymer Science and Technology*. (4th ed.) Hoboken, N.J: Wiley-Interscience, 1999;2003;.
- [5] L. M. S. Loura *et al*, "Effects of fluorescent probe NBD-PC on the structure, dynamics and phase transition of DPPC. A molecular dynamics and differential scanning calorimetry study," *BBA - Biomembranes*, vol. 1778, (2), pp. 491-501, 2008.
- [6] C. E. Pinguet *et al*, "PEO-b-PPO star-shaped polymers enhance the structural stability of electrostatically coupled liposome/polyelectrolyte complexes," *PloS One*, vol. 14, (1), pp. e0210898-e0210898, 2019.
- [7] H. T. M. Phan *et al*, "Investigation of Bovine Serum Albumin (BSA) Attachment onto Self-Assembled Monolayers (SAMs) Using Combinatorial Quartz Crystal Microbalance with Dissipation (QCM-D) and Spectroscopic Ellipsometry (SE)," *PloS One*, vol. 10, (10), pp. e0141282-e0141282, 2015.
- [8] C. He *et al*, "Effects of particle size and surface charge on cellular uptake and biodistribution of polymeric nanoparticles," *Biomaterials*, vol. 31, (13), pp. 3657-3666, 2010.
- [9] J. Rauch, W. Kolch and M. Mahmoudi, "Cell type-specific activation of AKT and ERK signaling pathways by small negatively-charged magnetic nanoparticles," *Scientific Reports*, vol. 2, (1), pp. 868-868, 2012.

- [10] S. Chou and K. A. Woodrow, "Relationships between mechanical properties and drug release from electrospun fibers of PCL and PLGA blends," *Journal of the Mechanical Behavior of Biomedical Materials*, vol. 65, pp. 724-733, 2017.
- [11] N. Kamaraj *et al.*, "Fabrication, characterization, in vitro drug release and glucose uptake activity of 14-deoxy, 11, 12-didehydroandrographolide loaded polycaprolactone nanoparticles," *Asian Journal of Pharmaceutical Sciences*, vol. 12, (4), pp. 353-362, 2017.
- [12] R. Gary Sibbald and K. Y. Woo, "The biology of chronic foot ulcers in persons with diabetes," *Diabetes/Metabolism Research and Reviews*, vol. 24, (S1), pp. S25-S30, 2008.
- [13] Ø. Arlov and G. Skjåk-Bræk, "Sulfated Alginates as Heparin Analogues: A Review of Chemical and Functional Properties," *Molecules (Basel, Switzerland)*, vol. 22, (5), pp. 778, 2017.
- [14] I. Rivolta, Panariti, and Miserocchi, "The effect of nanoparticle uptake on cellular behavior: disrupting or enabling functions?," *Nanotechnology, Science and Applications*, p. 87, 2012.

Chapter IV

IN VITRO ASSESSMENT OF ALGINATES AND GROWTH FACTORS ON WOUND HEALING

4.1 Introduction

Different GFs and cytokines are involved in the consecutive and overlapping steps of wound healing as discussed in the first chapter. However, many of these factors becomes deficient in chronic wounds specifically diabetic ones. These factors include CTGF, IGF, VEGF, TNF- α , and interleukin-6 (IL-6). Accordingly, migration and proliferation processes of keratinocytes and fibroblasts become dysregulated leading to non-healing wounds [1].

4.1.1 Growth factors and cytokines

CTGF

The normal wound healing cascade of events requires both systemic and local factors that induce and enhance the occurrence of the different phases. One of these discovered factors is CTGF that belongs to the cysteine rich CNN2 family with highly conserved dilsulfide bonding patter; it has been proven to be deficient in diabetic wounds. CTGF is usually overexpressed in profibrotic conditions and is involved in fibroblast proliferation and matrix deposition which accelerates wound healing. It acts with other biological agents including (TGF- β), collagen, and FN that play critical roles in the wound

repair process. The activities of these agents are known to be modulated by the presence of CTGF as it binds to cytokines and proteins serving as an extracellular adapter. It is known for its high binding affinity to the sulfated GAGs such as heparan sulfate to the extent that it can displace the other heparin binding GFs; it binds via its C-terminal domain to perform its functions. As a result, CTGF becomes available for the cell and dimerization of the receptor takes place to activate the signaling pathway. When CTGF was applied topically, either directly or using an acellular dermal scaffold, on chronic wounds induced in diabetic rats; consequently, it boosted the process wound repair. Wounds with CTGF had increased collagen and its regeneration that is caused by FN through the protein kinase C (pkc) pathway [2-4].

IGF

IGF is a cytokine composed of 70 amino acids and is similar to insulin. It is known to induce mitogenic effects in keratinocytes and fibroblasts. Because it has a critical role in promoting wound healing, its expression usually gets elevated in wounds. Accordingly, it enhances migration, proliferation, angiogenesis, and transformation of fibroblasts into myofibroblasts. Like CTGF, its expression is decreased in chronic and diabetic wounds. It is a HBGF that was also proven to bind to AlgSulf [5-7].

Inflammatory cytokines

Although chronic wounds remain in an inflammatory phase, but the dysregulation of cytokines release causes the deficiency in the expression of TNF- α and IL-6. These two cytokines act in unison with other GFs to promote wound healing and build the wound bed.

They are also known to bind to heparin; however, only IL-6 was proven to bind to AlgSulf as well [7-9]. Furthermore, they are among the inflammatory cytokines that their expression is elevated among the application of alginates. In other words, alginates induce the release of TNF- α and IL-6.

Ras homologous protein

The Ras superfamily of proteins comprises small GTPases such as the Ras homologous proteins (Rho). These proteins play crucial roles in cell migration, adhesion, and polarization. For instance, RhoA, a member from the Rho family, was found to be an integral regulator in wound healing through actin polymerization. It was also found to be an inducer of the matricellular protein, CTGF, where it regulates its expression in various tissues such as fibroblasts [10-12].

4.1.2 Wound dressing

For a chronic wound to heal effectively, it must be covered with a dressing that can provide protection, moisture, and deliver bioactive molecules. In other words, a wound dressing must be capable of mimicking the natural skin. For instance, an ideal dressing should be moist and absorbent to speed up re-epithelization and collagen synthesis. This can be achieved by using hydrocolloid system that contains alginate that are known to have high water absorption capacity. Another important characteristic is biocompatibility which is available in PVA, PCL and alginate. In addition, dressings with long wear time and that are easily removed when needed reduce costs and physical trauma; this can be

accomplished by utilizing the features of the different elements of the particles. Firstly, the sustained release and prolonged delivery can be achieved by including PCL in the formulation due to its slow degradation. Furthermore, the anticoagulant/antifouling property of AlgSulf can extend the life of the dressing. Secondly, GF stimulation can enhance the process; hence, AlgSulf can be used to bind to the CTGF entrapped within and other GFs present in the ECM. Thirdly, protease sequestration is one of the desired characteristics where diabetic wounds have increased protease activity. Since heparin can sequester proteases, which could be a possible property of SA. In addition, using more than one polymer does not merely lead to additive advantages; it also allows the creation of an optimum hydrophobic and hydrophilic balance for better cell adhesion and proliferation and a stable degradation rate [12-23].

4.1.3 Objective

For a chronic wound to heal effectively, the several intricately processes must be well regulated. This can be achieved by delivering the proper factors that contribute to the process. This includes CTGF and IGF which are among the key players in the process which become suppressed in chronic wound and specifically DFUs. Therefore, in this section the effect of these factors on the healing process will be studied. Furthermore, the results of combining them with alginates, either pure or sulfated will be investigated.

The three main elements of wound healing are cellular migration, proliferation, and matrix deposition. Therefore, the effects of GFs and alginates on these three outcomes will be examined by scratch assay, MTT assay, and western blot.

4.2 Materials and methods

4.2.1 Measurement of cell migration in vitro

HaCat cells were seeded in 6-well plates at a density of 10^6 cells/well in complete medium and cultured at 37°C until they formed a confluent monolayer. A sterile plastic 1 ml pipette tip was used to create a cell-free zone in each well. The medium was immediately aspirated, and the wells were washed with PBS to remove any cellular debris due to the scratch. The complete culture medium was replaced with (a) fresh serum-free DMEM, medium containing (b) $10\mu\text{g/ml}$ of pure alginate, (c) $10\mu\text{g/ml}$ of AlgSulf_{2.0}, (d) 250ng/ml rhCTGF, (e) 250ng/ml rhIGF, and combinations of growth factors and Algs at the same concentrations (i.e. CTGF+pure Alg, CTGF+AlgSulf_{2.0}, IGF +pure Alg, and IGF-I+ AlgSulf_{2.0}). The area of the gaps at different time points (0,2,4,6,20, and 24 hr) was measured using ImageJ software from images taken through Lieka to observe cell migration and proliferation. The same experiment was then repeated, however, at a lower concentration of the growth factors. Similar treatment groups were applied but at a 100ng/ml instead of 250ng/ml of the growth factors (Appendix). To account for the variability in the size of the scratch between the wells, the calculations were based the total area as below:

$$\% \text{ Wound} = \frac{\text{Area Scratched}}{\text{Total Area}} \times 100$$

4.2.2 Bioactivity assay for CTGF

HaCat cells were seeded in 96-well plate at 50,000 cell/well in complete medium at 37°C for 24 hr. The medium was replaced with different treatment groups listed below. Then the cells were cultured for 72 hr. The activity of the samples was evaluated by MTT assay. After 72 hr, the medium was aspirated from the wells and they were washed with PBS and 10µl of MTT solution with 90µl of serum free medium were added and incubated for 3 hr at 37°C. 150 µl of MTT stop solution was added to each well and the absorbance was read at 595nm.

- 1.Serum-Free Medium (SFM)
2. Complete Medium (CM)
- 3.Alg in SFM (10ng/ml)
5. AlgSulf in SFM (10ng/ml)
- 7.Alg in CM (10ng/ml)
- 9.SulfAlg in CM (10ng/ml)
- 11.CTGF in SFM (100ng/ml)
12. CTGF in SFM (250ng/ml)
- 13.CTGF (100ng/ml) +Alg(10ng/ml) in SFM
- 14.CTGF (250ng/ml) +AlgSulf(10ng/ml) in SFM
- 15.CTGF (250ng/ml) +AlgSulf (10ng/ml) in SFM
- 16.CTGF (250ng/ml) +Alg(10ng/ml) in SFM
- 17.Heparin in SFM (10ng/ml)
18. Heparin in CM (10ng/ml)

19.CTGF (100ng/ml) +Heparin(10ng/ml) in SFM

20. CTGF (250ng/ml) +Heparin(10ng/ml)

4.2.3 Role of Rho-GTPase signaling in the effects of CTGF, IGF, and alginates on HaCat cells

To observe the role of RhoA in cellular migration upon treating with CTGF and IGF, HaCat Cells were seeded in 6-well plates at a density of 10^6 cell/well. Each treatment group was added to two wells, one of them was pretreated with Rho-specific inhibitor (30 μ M) for 2 hr. Subsequently, the scratch was created in the wells and 250ng/ml of either CTGF or IGF was applied and then cell migration was observed as described earlier.

4.2.4 Role of Alginates in protecting FN from degradation

HaCat cells that were used in the wound healing assay were then collected after two different time intervals, 24 and 72 hr, to quantify the amount of FN. This was implemented by western blot using anti-fibronectin (Abcam, 1:3000). The expression of FN in the different treatment groups at both time points was then compared.

4.3 Results and Discussion

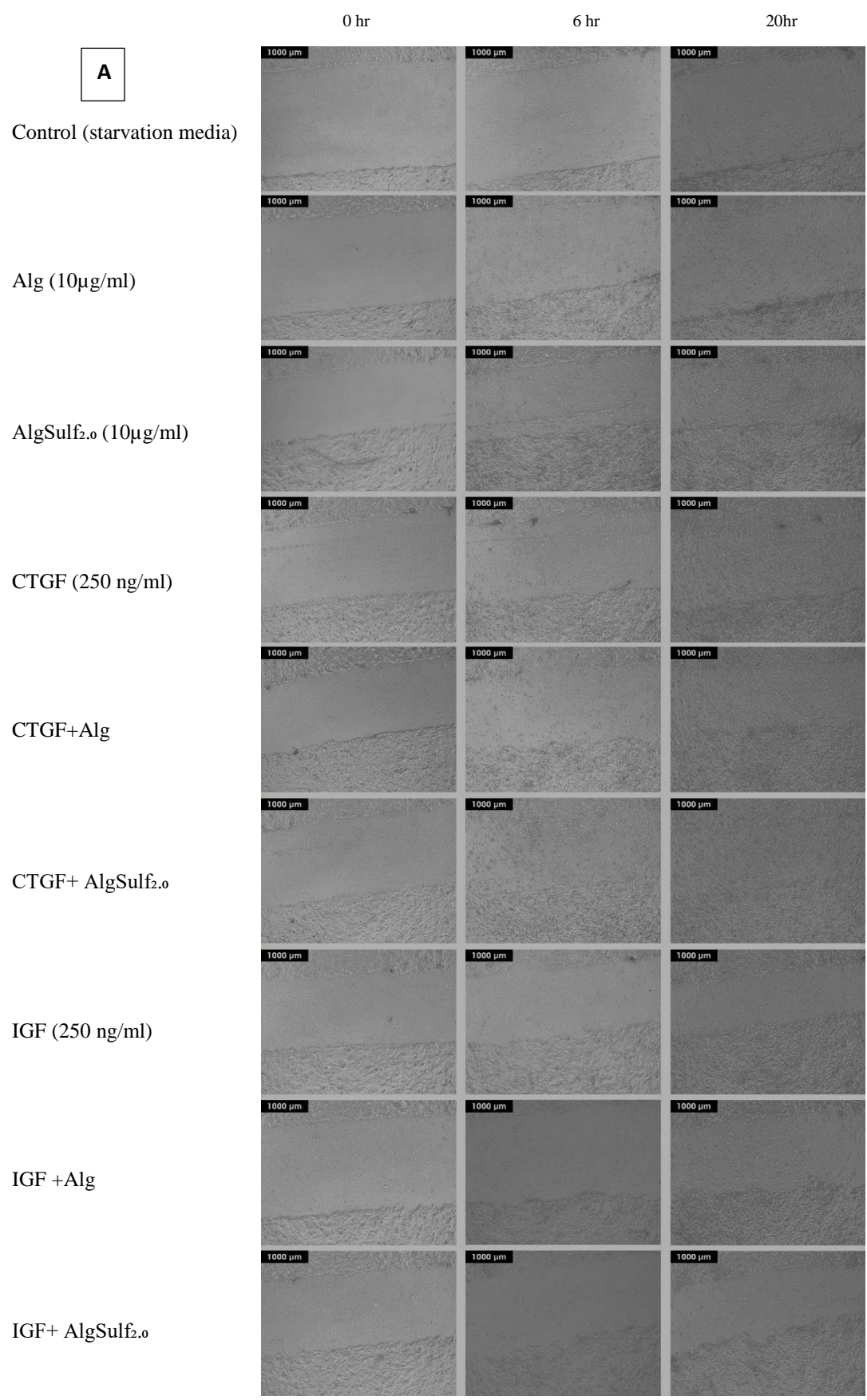
4.3.1 Effect of Alginates and Growth Factors on HaCat Cells Migration *in Vitro*

As illustrated in Fig.29, after treatment with pure and sulfated alginates, CTGF, IGF, and their combinations, the area of the wound decreased at different rates depending on the treatment. A profile analysis to assess if there is treatment and time effects, and interaction effect between time and treatment was carried. The results showed that there was a time effect (P-value<0.0001), treatment effect (P-value < 0.0001) and no interaction between time and treatment. In specific, a significant difference in the percentage of wound area was detected between all the groups compared to the control after 6hr. This indicates that treatments yielded an improvement in healing. Significant differences in means of empty areas between the treatments and the control were detected at various time points following injury and are detailed below:

Treatment/Time	Alg	AlgSulf	CTGF	CTGF+Alg	CTGF+AlgSulf	IGF	IGF+Alg	IGF+AlgSulf
2	ns	ns	ns	ns	ns	ns	ns	ns
4	ns	ns	ns	p<0.032	p<0.016	ns	ns	p<0.022
6	p<0.01	p<0.01	p<0.012	p<0.012	p<0.001	p<0.033	p<0.043	p<0.013
20	ns	p<0.028	p<0.009	p<0.007	p<0.006	p<0.019	p<0.022	P<0.018
24	ns	ns	p<0.037	p<0.032	p<0.03	p<0.035	p<0.026	p<0.053

Table 4 Summary of the longitudinal statistical analysis with the P-values of each treatment against the control. (ns: not significant).

The optimal treatment was found to be CTGF (250 ng/ml) combined with AlgSulf_{2.0} (10 µg/ml) since it had the smallest wound area after 6 hr compared to the other treatments (One-Way ANOVA, P<0.05). Adding alginates alone to the cell culture medium upon the scratch enhanced cellular migration. This is probably due to the fact that the (G) block of the alginates induces the production of cytokines [1-2] that in turn plays a crucial role in regulating cell migration [3]. The effect of the growth factors, CTGF and IGF, was expected since they are well-known to regulate cellular migration. However, combining them with AlgSulf_{2.0} improved their effect as Algs tend to mimic heparin when sulfated and, thus, binds to heparin binding proteins. Accordingly, it aided in protecting the GFs from degradation and presented them to their receptors.



B

Condition/Time(hr)	t=0	t=2	t=4	t=6	t=20	t=24
Control	55.7±15.8	54.8±16.5	53.8±16.1	52.8±15.1	33.8±18.4	26.2±8.29
Alg (10µG/ml)	57.0±9.5	55.2±9.4	43.5±23.0	28.5±18.7	12.8±2.9	8.7±3.6
AlgSulf _{2.0} (10µg/ml)	50.3±13.1	47.5±11.9	36.7±21.9	22.0±23.1	7.3±2.6	5.9±3.7
CTGF (250ng/ml)	49.6±11.9	46.9±13.6	34.5±19.4	22.2±19.3	2.3±0.7	0.9±0.34
CTGF+Alg	47.4±18.2	44.6±18.0	27.9±22.2	22.4±25.7	1.0±0.26	0.3±0.54
CTGF+ AlgSulf _{2.0}	51.7±13.5	44.7±18.0	24.6±22.5	13.8±18.1	0.1±0.21	0
IGF (250ng/ml)	45.2±12.2	43.7±13.1	28.1±20.4	24.4±21.6	8.3±4.5	6.2±4.8
IGF+Alg	51.9±11.6	48.5±14.1	29.3±18.4	25.1±20.4	6.9±4.15	5.3±5.23
IGF+ AlgSulf _{2.0}	49.6±7.63	44.4±12.2	26.0±26.4	22.7±21.0	5.2±3.4	2.8±2.80

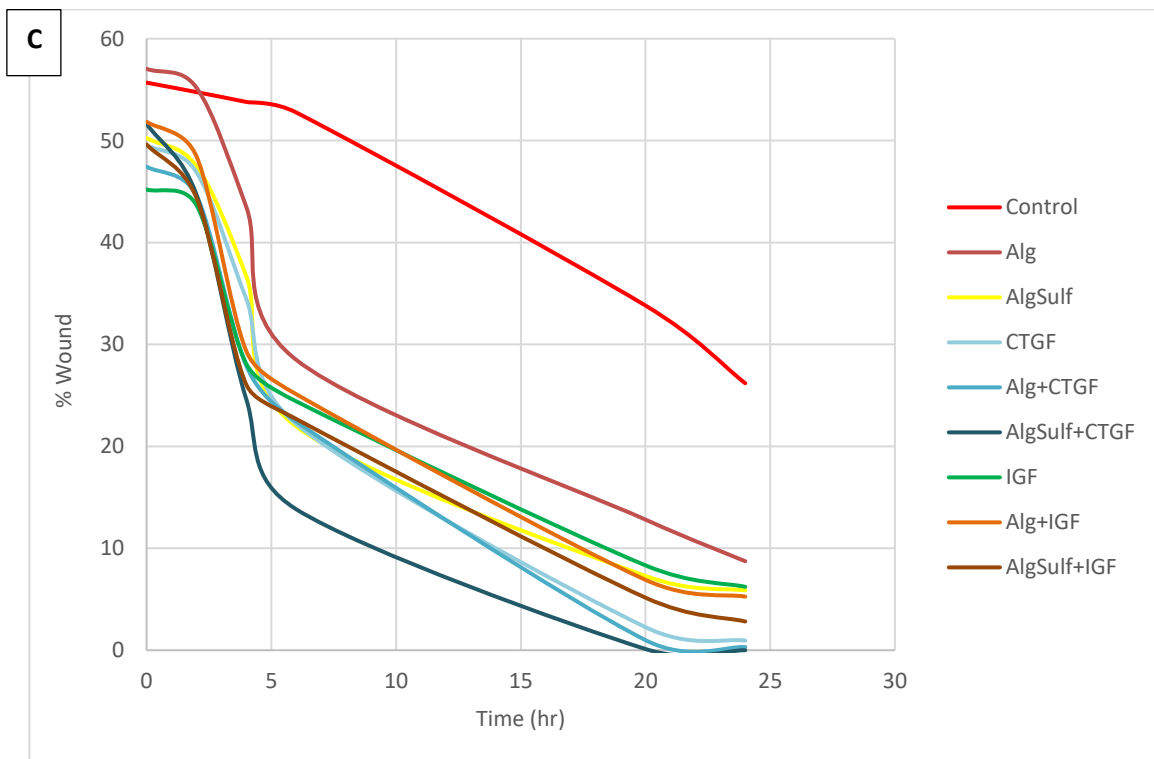


Figure 28 The *in vitro* wound healing upon the application of CTGF and IGF at a concentration of 250ng/ml. (A) Images of the different treatment groups taken at times 0, 6, and 20 hr (Scale bar = 1000 µm). (B) The data presented in C is reported as mean ± SEM, n=3. (C) Representation of the wound closure during the experiment.

4.3.2 Effect of CTGF and AlgSulf on Cellular Activity and Proliferation

Different Concentrations of CTGF with or without Alg and AlgSulf

As illustrated in Fig.30, the activity was higher at a lower concentration of CTGF, 100ng/ml, but it was not significantly different compared to the higher concentration, 250ng/ml. On the other hand, there was no significant difference between CTGF (100ng/ml) with AlgSulf_{2.0} (10ng/ml) and the FBS supplemented medium (P=0.128). Therefore, the effect of CTGF on the activity of the cells is comparable to FBS indicating that it has proliferative effects on keratinocytes.

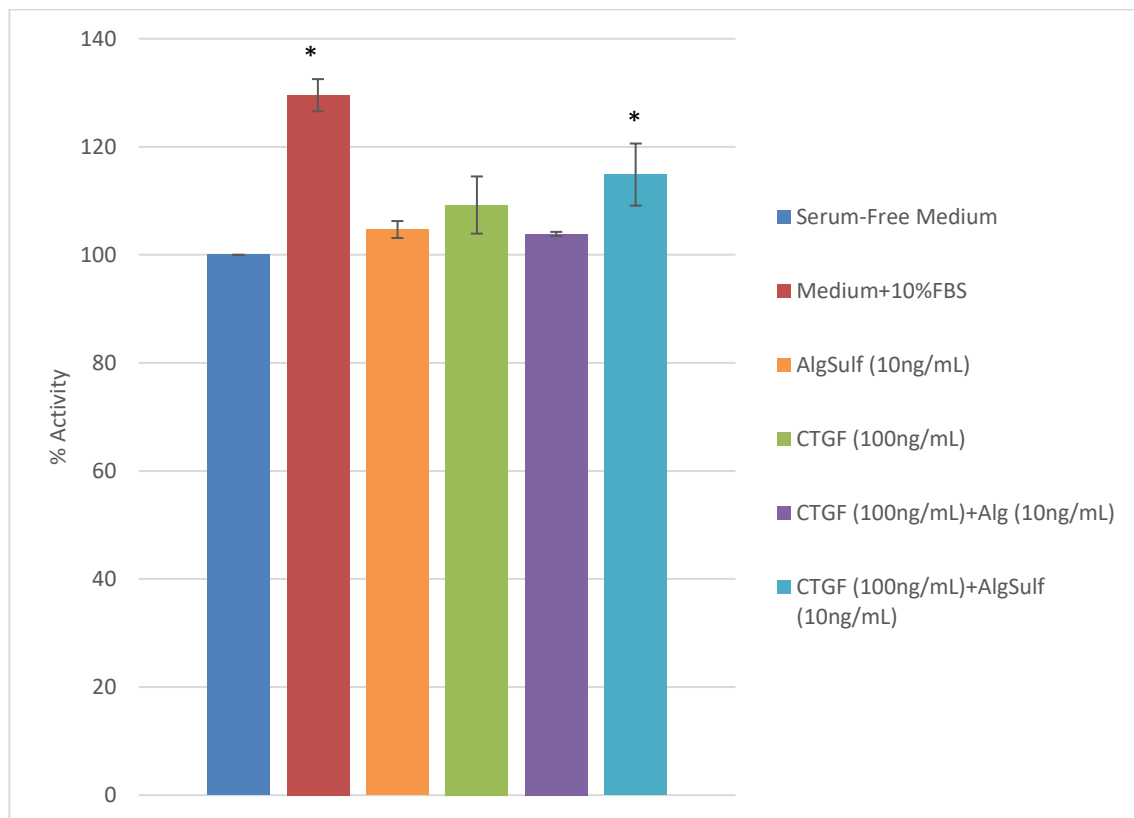


Figure 29 The effect of different treatments on the activity of the cells. The data is reported as mean ± SEM. Serum free medium was considered 100%. (One-Way ANOVA *P<0.05, n=3).

AlgSulf_{2.0} Mimics Heparin

The results in Fig.31 show that the effect of AlgSulf_{2.0} was similar to that of heparin with regard to cellular activity. That is mainly due to the resemblance in the chemical structure and presence of sulfate groups on the polysaccharide chains [7,24]. In fact, at certain concentrations, AlgSulf outperformed heparin.

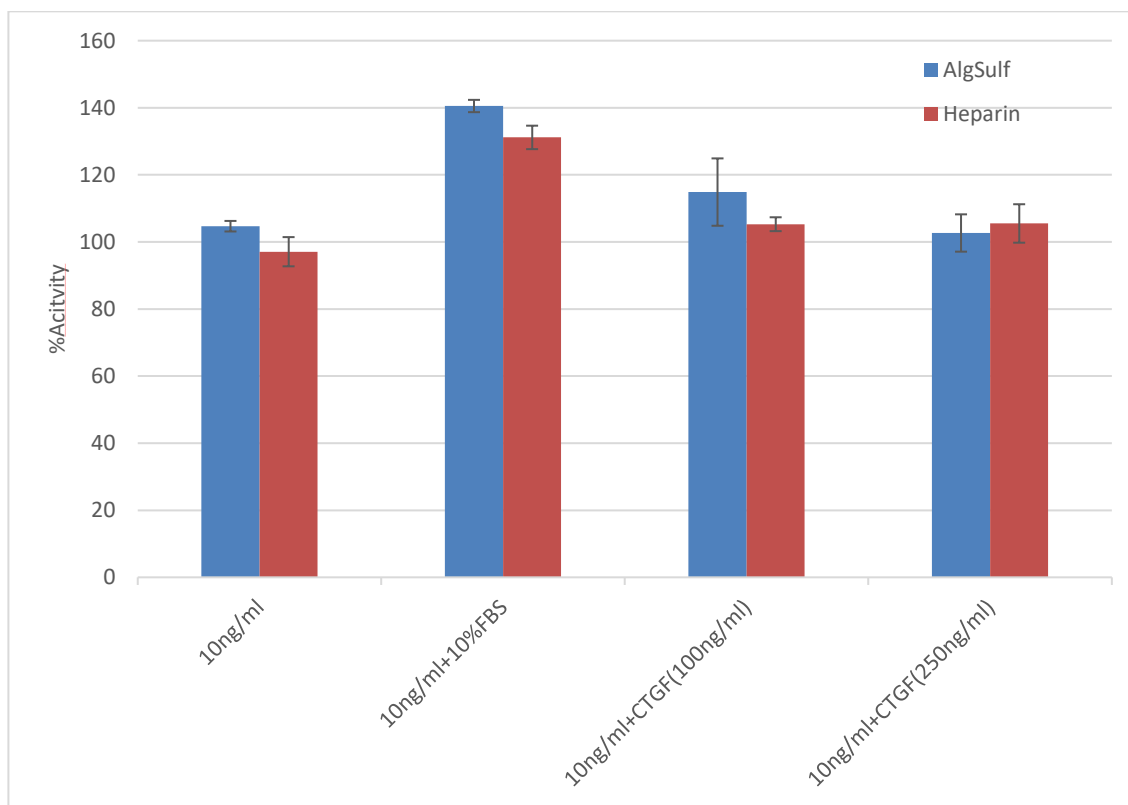
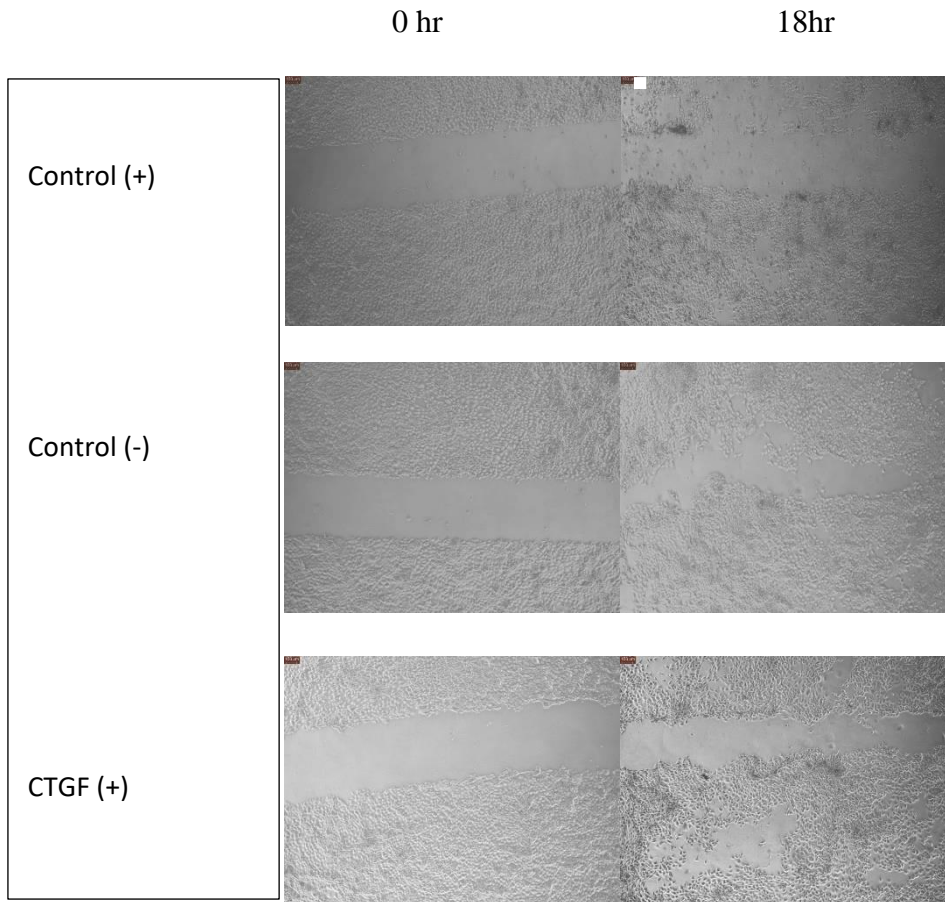


Figure 30 Comparison between the effect of AlgSulf and heparin with and without CTGF at different concentrations. The data is reported as mean \pm SEM. Serum free medium was considered 100%. (Paired sample t-test * $P < 0.05$, $n = 3$).

4.3.3 RhoA is involved in the cellular migration during wound healing

When RhoA signaling pathway was inhibited, the wound did not heal completely after 18 hrs compared to their uninhibited counterparts (Fig.32). This indicates that both CTGF and IGF induce cellular migration through the RhoA pathway. It was shown before that RhoA stimulates the expression of CTGF [11]. However, based on these results, it can be inferred that CTGF activates RhoA to enhance cellular migration.



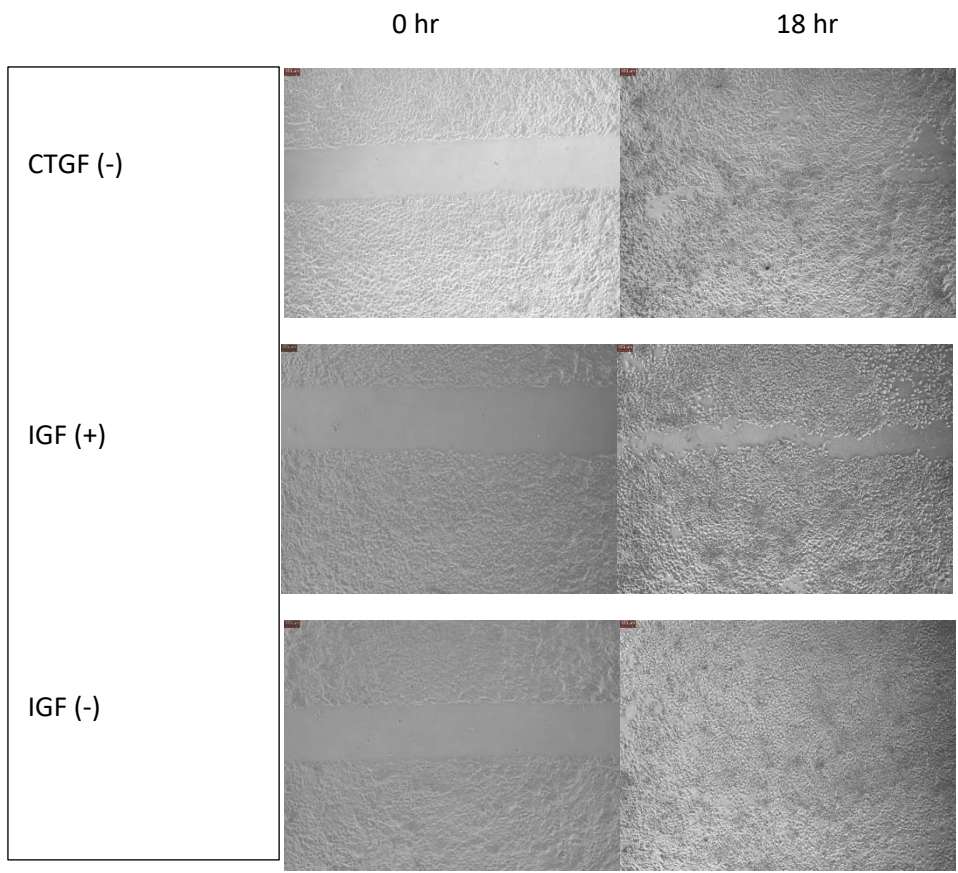
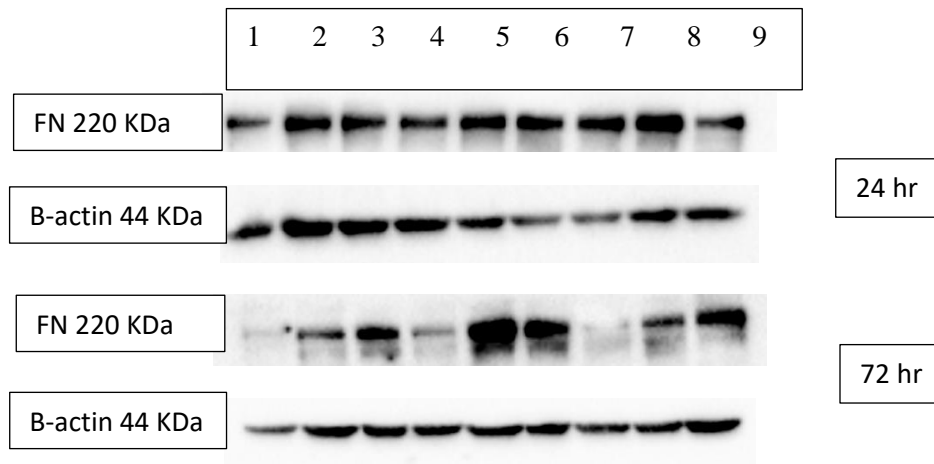


Figure 31 RhoA signal transduction involved in cell migration. (-) indicates the absence of the GTPase inhibitor (n=3). Scale bar=150 μ m.

4.3.4 Alginates protects matrix proteins from degradation

Immunoblotting was utilized to figure out the expression of matrix proteins such as FN upon treatment of HaCat cells after the scratch as described earlier. FN was produced 24 hr post-treatment, however, it started deteriorating after that in case of control and CTGF and IGF alone, i.e. in the absence of alginates (Fig. 33). This result was expected in the case of AlgSulf since it binds to HBGF but not in the case of Alg. This can be attributed to the fact that FN constitute adhesive domains that usually binds to ECM components and alginates are polysaccharides that imitates these components [25-26]. Therefore, it can be concluded that alginates in general exhibit a binding affinity towards FN which protects it from denaturation. Accordingly, FN enhances the healing process by regulating cellular functions such migration, growth, and spreading [25]. Furthermore, this aids in explaining the results of the scratch assay where healing was evident in the case of merely adding the alginates without the GFs.



Condition/Time(hr)
1.Control
2.Alg (10 μ G/ml)
3.AlgSulf _{2.0} (10 μ g/ml)
4.CTGF (250ng/ml)
5.CTGF+Alg
6.CTGF+ AlgSulf _{2.0}
7.IGF (250ng/ml)
8.IGF+Alg
9.IGF+ AlgSulf _{2.0}

Figure 32 Immunoblotting results after the scratch assay (24 and 72 hr). Algs, pure and sulfated, protected FN from degradation with time (n=3).

4.5 References

- [1] H. Brem and M. Tomic-Canic, "Cellular and molecular basis of wound healing in diabetes," *Journal of Clinical Investigation*, vol. 117, no. 5, pp. 1219–1222, Jan. 2007.
- [2] R. A. N. Achar *et al*, "Use of insulin-like growth factor in the healing of open wounds in diabetic and non-diabetic rats," *Acta Cirurgica Brasileira*, vol. 29, (2), pp. 125-131, 2014.
- [3] K. E. Lipson *et al*, "CTGF is a central mediator of tissue remodeling and fibrosis and its inhibition can reverse the process of fibrosis," *Fibrogenesis & Tissue Repair*, vol. 5, (Suppl 1), pp. S24-S24, 2012.
- [4] X. Shi-Wen, A. Leask and D. Abraham, "Regulation and function of connective tissue growth factor/CCN2 in tissue repair, scarring and fibrosis," *Cytokine and Growth Factor Reviews*, vol. 19, (2), pp. 133-144, 2008.
- [5] B. Zuhaili MD *et al*, "Gene transfer of insulin-like growth factor (IGF-1) improves wound healing in diabetic full-thickness porcine wounds," *Journal of the American College of Surgeons*, vol. 205, (3), pp. S55-S55, 2007.
- [6] R. A. N. Achar *et al*, "Use of insulin-like growth factor in the healing of open wounds in diabetic and non-diabetic rats," *Acta Cirurgica Brasileira*, vol. 29, (2), pp. 125-131, 2014.
- [7] I. Freeman, A. Kedem and S. Cohen, "The effect of sulfation of alginate hydrogels on the specific binding and controlled release of heparin-binding proteins," *Biomaterials*, vol. 29, (22), pp. 3260-3268, 2008.
- [8] M. Kenig *et al*, "Identification of the heparin-binding domain of TNF-alpha and its use for efficient TNF-alpha purification by heparin–Sepharose affinity chromatography," *Journal of Chromatography B*, vol. 867, (1), pp. 119-125, 2008.
- [9] S. Patel, S. Srivastava, M. R. Singh, and D. Singh, "Mechanistic insight into diabetic wounds: Pathogenesis, molecular targets and treatment strategies to pace wound healing," *Biomedicine & Pharmacotherapy*, vol. 112, p. 108615, 2019.
- [10] Y. Nagai, D. Kawanami, K. Matoba, Y. Takeda, T. Akamine, S. Ishizawa, Y. Kanazawa, T. Yokota, and K. Utsunomiya, "Rho-Kinase Induces CTGF Expression through Actin Dynamics in Mesangial Cells," *Diabetes*, vol. 67, no. Supplement 1, 2018.

- [11] C. Ott, A. Graness, K. Giehl, and M. Goppelt-Struebe, "Modulation of the expression of connective tissue growth factor (CTGF) by alterations of the cytoskeleton," *International Journal of Experimental Pathology*, vol. 85, no. 1, 2008.
- [12] L. P. Desai, A. M. Aryal, B. Ceacareanu, A. Hassid, and C. M. Waters, "RhoA and Rac1 are both required for efficient wound closure of airway epithelial cells," *American Journal of Physiology-Lung Cellular and Molecular Physiology*, vol. 287, no. 6, 2004.
- [13] T. N. Tozer and M. Rowland, *Introduction to Pharmacokinetics and Pharmacodynamics: The Quantitative Basis of Drug Therapy*. Baltimore MD: Lippincott Williams & Wilkins, 2006.
- [14] A. Bhattacharyya *et al*, "Development of pH sensitive polyurethane–alginate nanoparticles for safe and efficient oral insulin delivery in animal models," *RSC Advances*, vol. 6, (48), pp. 41835-41846, 2016.
- [15] M. Iqbal *et al*, "Preparation of biodegradable PCL particles via double emulsion evaporation method using ultrasound technique," *Colloid and Polymer Science*, vol. 293, (3), pp. 861-873, 2015.
- [16] L. I. F. Moura *et al*, "Recent advances on the development of wound dressings for diabetic foot ulcer treatment—A review," *Acta Biomaterialia*, vol. 9, (7), pp. 7093-7114, 2013.
- [17] R. Mhanna *et al*, "Sulfated Alginate as a Mimic of Sulfated Glycosaminoglycans: Binding of Growth Factors and Effect on Stem Cell Behavior," *Advanced Biosystems*, vol. 1, (7), pp. 1700043-n/a, 2017.
- [18] M. A. Fonder BS *et al*, "Treating the chronic wound: A practical approach to the care of nonhealing wounds and wound care dressings," *Journal of the American Academy of Dermatology*, vol. 58, (2), pp. 185-206, 2008.
- [19] F. R. Henshaw *et al*, "Topically Applied Connective Tissue Growth Factor/CCN2 Improves Diabetic Preclinical Cutaneous Wound Healing: Potential Role for CTGF in Human Diabetic Foot Ulcer Healing," *Journal of Diabetes Research*, vol. 2015, pp. 1-10, 2015.
- [20] U. Lindahl *et al*, "Structure of the antithrombin-binding site in heparin," *Proceedings of the National Academy of Sciences of the United States of America*, vol. 76, (7), pp. 3198-3202, 1979.

- [21] T. B. McNeely and M. J. Griffith, "The anticoagulant mechanism of action of heparin in contact-activated plasma: inhibition of factor X activation," *Blood*, vol. 65, (5), pp. 1226, 1985.
- [22] Y. Liang and K. L. Kiick, "Heparin-functionalized polymeric biomaterials in tissue engineering and drug delivery applications," *Acta Biomaterialia*, vol. 10, (4), pp. 1588-1600, 2014.
- [23] B. Mordorski and T. Prow, "Nanomaterials for Wound Healing," *Current Dermatology Reports*, vol. 5, (4), pp. 278-286, 2016.
- [24] Ø. Arlov *et al*, "Heparin-like properties of sulfated alginates with defined sequences and sulfation degrees," *Biomacromolecules*, vol. 15, (7), pp. 2744-2750, 2014.
- [25] D. C. Roy, S. J. Wilke-Mounts and D. C. Hocking, "Chimeric fibronectin matrix mimetic as a functional growth- and migration-promoting adhesive substrate," *Biomaterials*, vol. 32, (8), pp. 2077-2087, 2010;2011.
- [26] S. Yanagisawa *et al*, "Improving cell-adhesive properties of recombinant Bombyx mori silk by incorporation of collagen or fibronectin derived peptides produced by transgenic silkworms," *Biomacromolecules*, vol. 8, (11), pp. 3487-3492, 2007.

CHAPTER V

CONCLUSION

DFUs are classified as chronic wounds that requires a prolonged time period to heal. However, if these ulcers do not heal effectively this will lead to partial or complete lower limb amputations. CTGF and IGF are both essential proteins that become deficient at the wound site in diabetic patients and can be applied to improve healing. However, these factors have a very short-half life and should be applied continuously at high doses. Therefore, to circumvent the side effects of high dosage and biological inactivation that accompanies direct application or delivery of the drugs, controlled delivery can be utilized. Encapsulating bioactive molecules in biocompatible and biodegradable in DDSs mitigates cytotoxic effect and improves drug efficiency. In this research, a novel multifunctional drug carrier for chronic wounds and DFUs applications was developed.

In chapter 3, the process of preparing the alginate-PCL NPs was optimized to generate the best formulation based on size, zeta-potential, and drug release profile that will encapsulate the drug of interest. The morphology and the size of the particles were studied upon variations in the processing parameters. A minimum average hydrodynamic size of 247.6 and 235.5 nm were attained by varying the sonication exposure time and amplitude, respectively. The organic solvent evaporation rate had a linear negative effect on the size. That is, the higher the evaporation rate, the smaller the resulting NPs. As for the ratio of the oil to the aqueous phase, it was found that although increasing the volume of the outer phase significantly increased the size and PDI; however, it helped in stabilizing the

particles. Including AlgSulf_{2.0} instead pure alginate led to the formation of significantly smaller NPs with a lower PDI due to its gelling and swelling properties.

This versatile process, EEM, was shown to be scalable in terms of volume, thus, can be transformed simply to industries to produce mass amounts. The relation between the volume and the size was linear. It was also shown that the size was merely affected by the magnitude of the delivered energy rather than the rate. In other words, it does not matter whether the energy delivered increased by sonication exposure time or amplitude. Accordingly, a calibration curve that is device independent and based on energy was created.

The NPs were then loaded with BSA as a model drug and their release profile was studied. The formulation that attained the highest %EE of 94.6 % was the 2% Alg Sulf_{2.0} PCL. In addition, compared to PLGA, PCL had a slower release of BSA with time. Based on cytotoxicity studies, the NPs showed a relatively high viability compared to the control at different concentrations using trypan blue, MTT, and immunoblotting assays.

In chapter 4, the efficiency of the drugs to be entrapped was investigated by *in vitro* wound healing assays and, subsequently, measurement of matrix deposition that assists in healing. It was shown that the optimal treatment that caused the most rapid wound closure was the combination of CTGF (250 ng/ml) and AlgSulf_{2.0} (10µg/ml). Alg as also shown binding affinity towards FN which protects it from degradation.

In conclusion, this DDS mimics the ECM and serves its role in chronic wounds where the processes are dysregulated. Namely, PCL and AlgSulf provide controlled delivery and protects the GFs, such as CTGF and IGF-I, from degradation. In future, the

system will be tested on diabetic *in vivo* models to verify healing efficacy. This novel system can also be employed to deliver other drugs in other applications especially if the drug has affinity towards affinity.

CHAPTER VI

APPENDIX

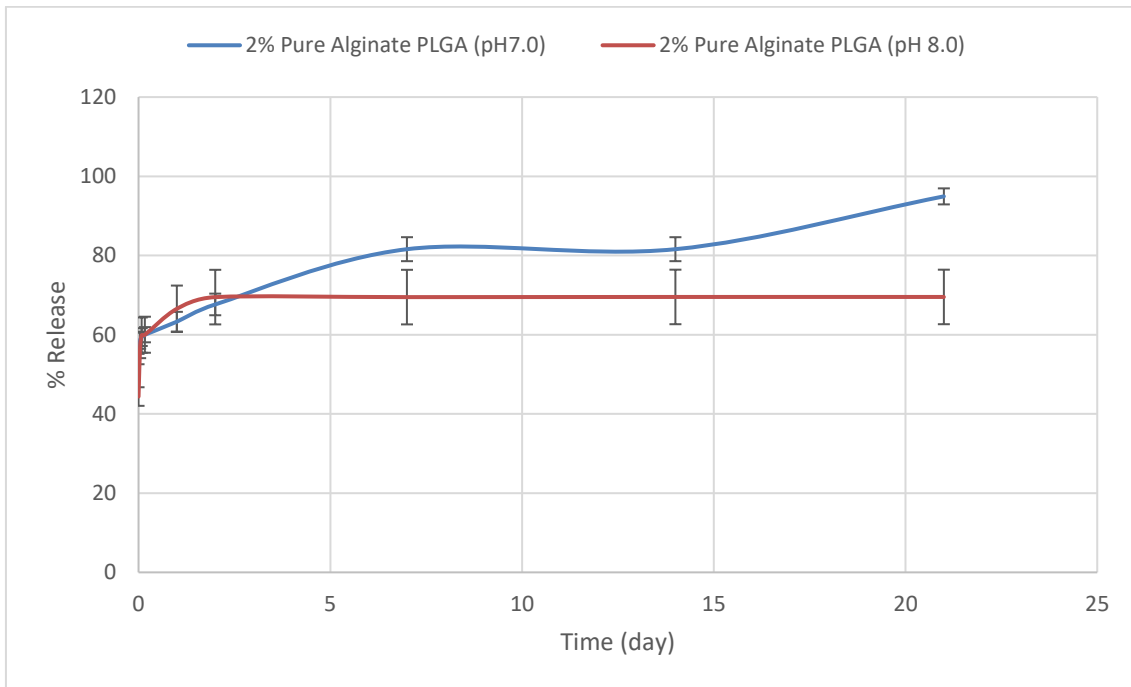


Figure 1A Effect of pH on the Cumulative release of BSA from 2% pure alginate PLGA (P<0.05).

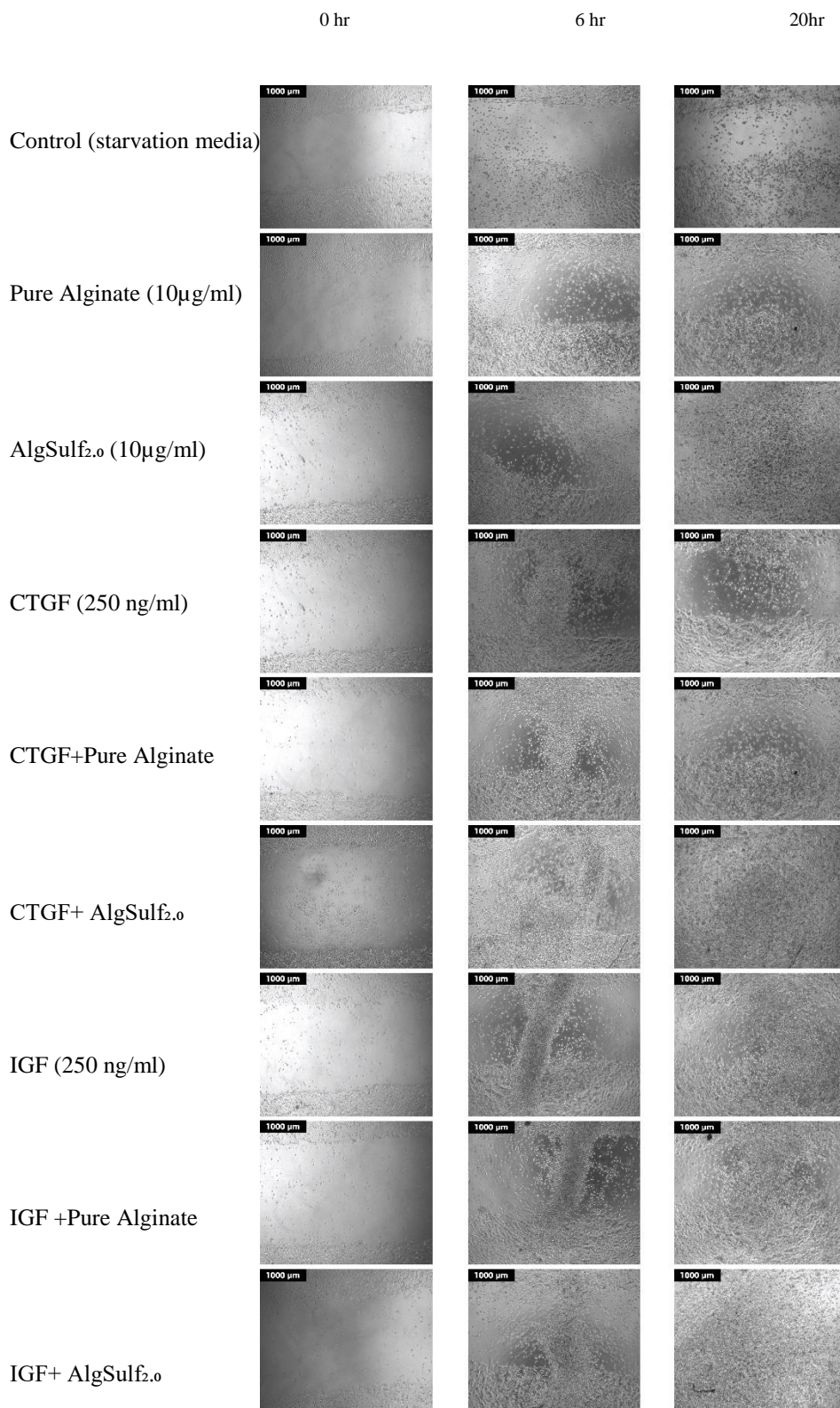
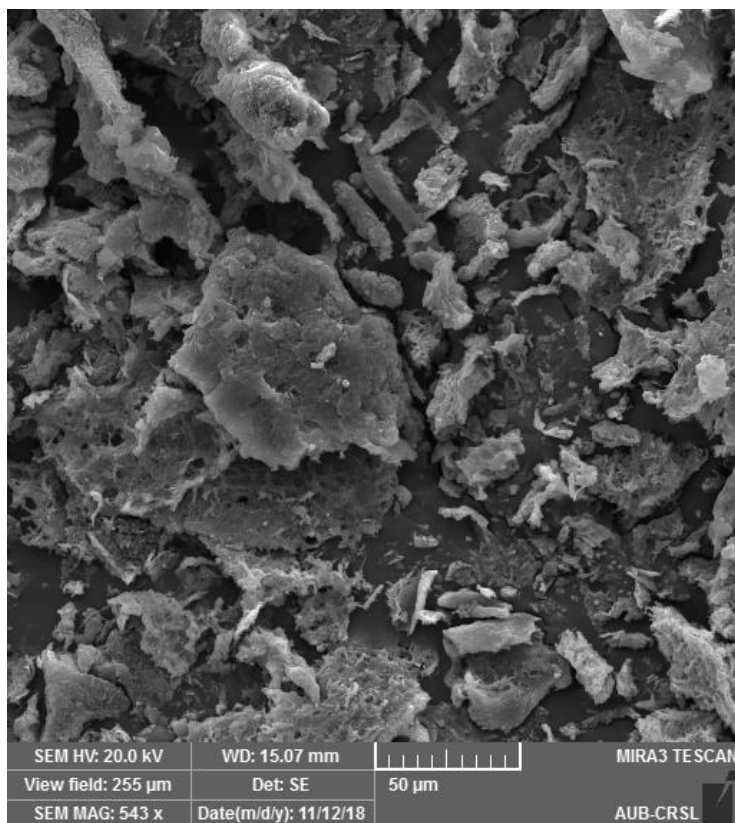


Figure 2A The *in vitro* wound healing upon the application of CTGF and IGF-I at a concentration of 100 ng/ml. Images of the different treatment groups taken at times 0, 6, and 20 hr (Scale bar = 1000 µm).

Type of Solvent

In all of the previous samples DCM was used as the organic solvent.

In this sample methoxy benzenes (Anisole) was used.



The vapor pressure of DCM and anisole are 46.5 and 0.472 Kpa, respectively. Accordingly, DCM is considerably more volatile compared to anisole. Therefore, when the evaporation rate became very low, the solidification process became very slow that the particles reaggregated and lost their morphology. Probably if the evaporation rate was increased by using a container with a larger surface area, better results can be achieved.

